IntechOpen

Advances in Functionally Graded Materials and Structures
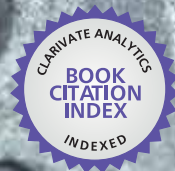
Edited by Farzad Ebrahimi

ADVANCES IN FUNCTIONALLY GRADED MATERIALS AND STRUCTURES

Edited by **Farzad Ebrahimi**

Advances in Functionally Graded Materials and Structures
Edited by Farzad Ebrahimi

Contributors

Arzum Uluköy, Muzaffer Topcu, Suleyman Tasgetiren, Emad Ewais, Dina H. A Besisa, Shubhankar Bhowmick, Vivek Gaba, Anil Kumar Tiwari, Yongsheng Zhang, Takahiro Kunimine, Hisashi Sato, Eri Miura-Fujiwara, Yoshimi Watanabe, Zhu Su, Guoyong Jin, Tiangui Ye

Notice

Statements and opinions expressed in the chapters are these of the individual contributors and not necessarily those of the editors or publisher. No responsibility is accepted for the accuracy of information contained in the published chapters. The publisher assumes no responsibility for any damage or injury to persons or property arising out of the use of any materials, instructions, methods or ideas contained in the book.

We are IntechOpen, the world's leading publisher of Open Access books
Built by scientists, for scientists

3,800+
Open access books available

116,000+
International authors and editors

120M+
Downloads

151
Countries delivered to

Our authors are among the
Top 1%
most cited scientists

12.2%
Contributors from top 500 universities

CLARIVATE ANALYTICS
BOOK CITATION INDEX
INDEXED

WEB OF SCIENCE™

Selection of our books indexed in the Book Citation Index
in Web of Science™ Core Collection (BKCI)

Interested in publishing with us?
Contact book.department@intechopen.com

Numbers displayed above are based on latest data collected.
For more information visit www.intechopen.com

Meet the editor

Dr. Farzad Ebrahimi was born in Qazvin, Iran, in 1979. He graduated in Mechanical engineering, from the University of Tehran, Iran, in 2002. He received his MSc and PhD in Mechanical engineering, with a specialization in applied design from the University of Tehran, Iran, in 2009. Since 2002, he has been working at the "Smart Materials and Structures Lab" Research Center of the Faculty of Mechanical Engineering at the University of Tehran, where he is a researcher of smart functionally graded materials and structures. He joined the department of mechanical engineering of Imam Khomeini International University as an assistant professor in 2010.

He is involved in several international journals as editor and reviewer. He serves on the editorial board of the SAGE Publication: "Journal of advances in mechanical engineering". He is the author of books "Smart Functionally Graded Plates" and "Progress in Analysis of Functionally Graded Structures", Nova Science Publishers, NY. He also served as the editor of the book "Nanocomposites - New Trends and Developments", InTech – Open Access Publisher. His research interests focus on areas of smart materials and structures, nanostructures, vibration nanocomposites, composite materials and structures, and he has published several researches in these fields. His research in these areas has been presented at international conferences and appeared in academic journals such as "Composite Structures", "Composites Part –B", "Journal of Mechanical Science and Technology", "Smart Materials and Structures", "European Journal of Mechanics" and "Archive of Applied Mechanics". Dr. Ebrahimi has also strong collaboration with Iranian industries on gas and oil projects, as well as serves as ad-hoc referee in several top academic journals.

Contents

Preface

Functionally graded materials (FGMs) are composite materials, microscopically inhomogeneous, in which the mechanical properties vary smoothly and continuously from one surface to the other. This is achieved by gradually varying the volume fraction of the constituent materials. An FGM is a two-component composite characterized by a compositional gradient from one component to the other. The properties of both components can be fully utilized. For example, the toughness of a metal can be mated with the refractoriness of a ceramic, without any compromise in the toughness of the metal side or the refractoriness of the ceramic side. FGMs were initially designed as thermal barrier materials for aerospace structures and fusion reactors and now they are also considered as potential structural materials for future high-speed spacecraft and now are being increasingly considered in various applications to maximize strengths and integrities of many engineering structures.

This book is a result of contributions of experts from international scientific community working in different aspects of FGMs and structures and reports on the state of the art research and development findings on this topic through original and innovative research studies. Through its six chapters, the reader will have access to works related to processing, sintering properties and applications of functionally graded ceramics and new processing routes for FGMs while it introduces some specific applications, such as functionally graded annular fins and the high-performance self-lubricating ceramic composites with laminated graded structure. Besides, it presents an experimental crack propagation analysis of aluminum matrix FGMs and a unified accurate solution for three-dimensional vibration analysis of functionally graded plates and cylindrical shells with general boundary conditions.

The book contains up-to-date publications of leading experts, and the edition is intended to furnish valuable recent information to the professionals involved in functionally graded materials and structure analysis and applications. The text is addressed not only to researchers but also to professional engineers, students and other experts in a variety of disciplines, both academic and industrial, seeking to gain a better understanding of what has been done in the field recently, and what kind of open problems are in this area.

I hope that readers will find the book useful and inspiring by examining the recent developments in FGMs and structures.

Lastly, I would like to thank all the authors for their excellent contributions in different areas covered by this book, and the InTech team, especially the process manager Ms. Iva Lipović, for their support and patience during the whole process of creating this book.

Dr. Farzad Ebrahimi
Department of Mechanical Engineering,
Imam Khomeini International University, Qazvin, Iran

Advances in Functionally Graded Ceramics – Processing, Sintering Properties and Applications

Dina H.A. Besisa and Emad M.M. Ewais

Additional information is available at the end of the chapter

Abstract

In multilayered structures, sharp interface is formed between the layers of dissimilar materials. At this interface, the large difference in thermal expansion coefficients of the two dissimilar materials generates residual thermal stresses during subsequent cooling. These stresses lead to cracking at the interface, and these cracks lead to the deterioration of mechanical properties, and finally crack propagation leads to the delamination of the multilayered structure. Scientific progress in the field of material technology, and the continuing developments of modern industries have given rise to the continual demand for ever more advanced materials with the necessary properties and qualities. The need for advanced materials with specific properties has brought about the gradual transformation of materials from their basic states (monolithic) to composites. Recent advances in engineering and the processing of materials have led to a new class of graded multilayered materials called Functionally Graded Materials (FGMs). These materials represent a second generation of composites and have been designed to achieve superior levels of performance. This chapter looks at the best processing technologies and the uses and applications of the advanced, high quality products generated, and also presents an extensive review of the recent novel advances in Functionally Graded Ceramics (FGCs), their processing, properties and applications. The manufacturing techniques involved in this work have involved many concepts from the gradation, consolidation and different sintering processes. Each technique, however, has its own characteristics and disadvantages. In addition, the FGC concept can be applied to almost all material fields. This chapter covers all the existing and potential application fields of FGCs, such as engineering applications in cutting tools, machine parts, and engine components, and discusses properties of FGCs such as heat, wear, and corrosion resistance plus toughness, and their machinability into aerospace and energy applications.

Keywords: Functionally graded ceramics (FGCs), Classification, Design and processing, Applications

1. Introduction

The result of scientific progresses in materials science and the continuing developments of modern industry, have given rise to the continual demand for advanced materials that can satisfy the necessary advanced properties and qualities. This requirement for advanced materials with specific properties brought about the gradual transformation of materials from their basic states(monolithic) to composites. Recent advances in engineering and the processing of materials have led to a new class of materials called Functionally Graded Materials (FGMs). These represent a second generation of composite materials and have been designed to achieve superior levels of performance.

FGMs are a type of composite material and are classified by their graded structure. Specifically, an FGM typically consists of a composite material with a spatially varying property and is designed to optimize performance through the distribution of that property. It could be a gradual change in chemical properties, structure, grain size, texturization level, density and other physical properties from layer to layer. FGMs have a graded interface rather than a sharp interface between the two dissimilar materials. Using a material with, for example, a graded chemical composition, minimizes the differences in that property from one material to another. No obvious change may take place in their chemical composition if the gradient is smooth enough, and if the transition is smooth, the mismatches in the property from one point in the material to another will be limited. Therefore, the ideal FGM has no sharp interfaces. Moreover, there will be no single location that is inherently weaker than the rest of the composite.

The aim of the production of FGMs is the elimination of the macroscopic boundary in materials in which the material's mechanical, physical and chemical properties change continuously and have no discontinuities within the material. Thus, these materials exhibit superior mechanical properties when compared to basic (monolithic) and composite materials.

In the past, the composition of FGMs typically included at least one metal phase. Recently, great attention has been devoted to ceramic-ceramic and glass-ceramic systems due to their attractive properties. Ceramic materials are designed to withstand a variety of severe in-service conditions, including high temperatures, corrosive liquids and gases, abrasion, and mechanical and thermal induced stresses. In this chapter, special attention will be given to the new advances in Functionally Graded Ceramics (FGCs), their processing and applications.

2. Origin of FG ceramics concept

The FGCs concept originated in Japan in 1984 during the space plane project of Niino and co-workers [1] in the form of a proposed thermal barrier material capable of withstanding a surface temperature of 2000K and a temperature gradient of 1000K in a cross-section of <10 mm. It is difficult to find a single material able to withstand such severe conditions. The researchers used the FGM concept to manufacture the body of a space plane using material with high refractoriness and mechanical properties resulting from gradually changing

compositions. They designed a ceramic material for the outer surface that is exposed to a high temperature environment and a thermally conductive metal for the inner surface. In 1987, the successful FGC research was accepted for use in a major project by the Ministry of Education and Science. During the period 1987–1991, a research project entitled "*Research on the generic technology of FGM development for thermal stress relaxation*" was conducted by Japanese scientists. In 1992, FGMs were selected as one of 10 most advanced technologies in Japan. Since then, FGM technology has grown in importance and has garnered the attention of many authors throughout the world. Although FGMs were invented fairly recently, these materials are not actually new. Gradual variations in the microstructure of materials have been explored for millions of years by the living organisms. FGMs have been long established in nature (bio-tissues of plants, bamboos, shells, coconut leaves and animals) and are even found in our bodies — such as in bones and teeth. [2].

3. Classification of FG ceramics

Future applications will demand materials that have extraordinary mechanical, electronic and thermal properties which can tolerate different conditions and yet are easily available at a reasonable price. As a result, it becomes necessary to reinforce at least one ceramic material in the functionally graded structure. FGM-based ceramic reinforcement is able to withstand high temperature environments due to the higher thermal resistance of the ceramic constituents and their attractive properties. Functionally graded ceramic compositions can be classified into:

3.1. Ceramic/metal

Due to the appearance of new industries that require high temperature and aggressive media, it became important to insert at least one ceramic material phase in any advanced FGM due to its attractive properties. In this type of FGC, the desirable properties of both metals and ceramics are combined. For example, we can use the high thermal conductivity and toughness of metals as an internal surface and combine it with the greater hardness and thermal insulation of ceramics as an external surface, thereby enabling the material to withstand high temperature environments. Examples of this type are the **(Ti-TiB$_2$) FGC** that is used as an armor material [3] and (Ni/Al$_2$O$_3$) **FGCs** which are used as lightweight armor materials with high ballistic efficiency [4].

In addition, ceramic/metal FGCs can be designed to reduce thermal stresses and to take advantage of both the heat and corrosion resistances of ceramics, and the mechanical strength, toughness, good machinability and bonding capability of metals — without severe internal thermal stresses.

3.2. Ceramic/ ceramic and glass/ ceramic

By exploiting the myriad possibilities inherent in the ceramic/ceramic FGCs concept, it is anticipated that the properties of materials will be optimized and new uses for them will be

discovered. Examples of these FGCs are **alumina/zirconia**, a material used in biomedical and structural applications, **mullite/alumina,** which is used as a protective coating for **SiC** components in corrosive environments [2, 5]. **Zirconia-mullite/alumina** FGCs can be used as refractory materials in high temperature applications, as well as being suitable for engineering and tribological applications [6, 7].

3.3. Ceramic/ polymer

An example of this type of FGC is the **boron carbide/polymer** FGC. Due to its light weight and flexibility, the BC/polymer FGC is used in lightweight armor and wears related applications [8]. The feature of this FGC is that the ceramic with graded porosity is fully dense on the front surface changing to open porosity on the back surface. The polymer is then infiltrated into the porous side of the ceramic plate to provide a lightweight energy-absorbing backing. A ballistic fiber weave, such as Kevlar, could also be embedded in the polymer to provide constraint and enhanced ballistic protection.

Ceramic/ polymer FGCs could also find applications in reducing the wear of automotive components. Additionally, they are used in many industrial applications requiring materials that are resistant to wear, corrosion, and erosion in hostile environments. Also, this type of FGC can be used in nuclear applications, such as the manufacture, handling and storage of plutonium materials [8].

Recently, the introduction of porosity in ceramic/polymer FGCs has broadened the scope of their application in the fields of biomedicine and tissue engineering [9, 10]. Due to the large surface area, high porosity, low thermal conductivity and high-temperature resistance of the porous ceramics, they were widely used in many fields, such as functioning as supports for ceramic filters, as artificial bones, high temperature insulators, and active cooling parts.

4. Design and processing of FG ceramics

The processing of advanced ceramics is a complex operation requiring several process control steps to achieve the ultimate product performance in the end. A successful forming technique leads to a ceramic product with an engineered microstructure which is characterized by a small defect size and by a well-distributed homogeneous grain boundary composition in order to achieve optimal performance and a high degree of reliability.

The manufacture of FGCs can be divided into two steps, namely gradation and consolidation. Gradation is the building of the spatially inhomogeneous graded structure, while consolidation is the transformation of this graded structure into the bulk material. The gradation process is usually classified into three main groups: constitutive, homogenizing, and segregating processes. The stepwise creation of a graded material from precursor materials is the basic constitutive process. In the homogenizing processes, the sharp interface between the two materials is converted to a gradient by material transport i.e. diffusion. In the segregating process, the macroscopically homogeneous material is converted into a graded material by an

external gravitational or electric field. The primary advantage of the homogenizing and segregating processes is the production of a continuous gradient. Following this, drying and sintering (or solidification) steps need to be adapted relevant to the particular material selected, and attention has to be paid to the different shrinkage rates during the sintering of FGCs [11].

The manufacturing process is one of the most important areas of FGC research. A large part of the research into FGCs has been dedicated to processing, and a large variety of production methods have been developed for use in the processing of FGCs. Most of the processes of FGC production are based on variations of conventional processing methods, which are already well-established. Methods that are capable of accommodating a gradation step include powder metallurgy [12-14], sheet lamination, chemical vapor deposition and coating processes. In general, the forming methods used include centrifugal casting [15-17], slip casting, tape casting [18], and thermal spraying [19, 20]. Which of these production methods is the most suitable? It depends mainly on the material combination, the type of transition function required, and the geometry of the desired component. However, it was found that powder metallurgy (PM) will be the most suitable method for the manufacture of FGCs in the future. It is believed that the main issue in the implementation of the PM method is the sintering process, which needs to be explored further in order to achieve improvements in the microstructure and mechanical properties of the resulting FGCs [21].

4.1. Powder metallurgy

Powder metallurgy (PM) is one of the most prevalent techniques due to its wide range control of composition, its microstructure and its ability to form a near net shape. It is a cost-effective technique and has the advantages of greater availability of raw materials, simpler processing equipment, lower energy consumption and shorter processing times. In powder processing, the gradient is generally produced by mixing different powders in variable ratios and stacking the powder mixtures in separate layers.

The thickness of the separate layers is typically between 0.2 mm and 1mm. Several techniques have been introduced for powder preparation, such as chemical reactions, electrolytic deposition, grinding or comminution. These techniques permit the mass production of powder form materials and usually offer a controllable size range of the final grain population. In powder processing, the main consideration focuses on the precision in weighing of amounts of individual powders and the dispersion of the mixed powders. These elements will influence the properties of the structure and need to be handled very carefully. In the subsequent processes, the forming operations are performed at room temperature, while sintering is conducted at atmospheric pressure as the elevated temperature used may cause further reactions that may affect the materials [22]. [23] studied the manufacturing method of another constituent, **ZrO$_2$/AISI316L FGCs** for use in joint prostheses. The mechanical and biotribological properties of the FGCs were evaluated through studies of their fracture toughness, bending strength, and wear resistance. It was found that FGMs with a layer thickness of less than 1.0 mm showed a low wear resistance. FGCs with a layer thickness of more than 2 mm, therefore, have mechanical and biotribological properties which are suitable for use in joint prostheses. [24] studied the relative density, linear shrinkage and Vickers hardness of each

layer of **8YSZ/Ni FGC**. The microstructure and the composition of these components were also studied. The results obtained showed that FGCs produced by spark plasma sintering exhibited a low porosity level and consequently fully dense specimens. There are no macroscopic distinct interfaces in **YSZ/Ni** FGM due to the gradual change in components. Another successful FGC prepared by the PM method is ZrO_2**/NiCr** FGC, as studied by [12].

4.2. Hot pressing

Yittria stabilized zirconia **(YSZ)** and nickel 20 chromium **(NiCr)** are the two materials combined using **YSZ-NiCr FGC** interlayer via the hot pressing method [25]. At the initial stage of processing, the powdered YSZ and NiCr were mixed in a ball milling machine for 12 hours before being stacked layer-by-layer in a graphite die coated with boron nitride. In this study, the concept of stepwise gradation was applied by arranging the composition of each layer to be a certain desired percentage. The preoccupation of each layer was performed at a lower pressure before stacking the adjacent layer under higher pressure (10 MPa) to ensure an exact compositional distribution within the layers.

A new composition profile of 15 layers with a crack-free joint of the Si_3N_4**-**Al_2O_3 **FGC** was proposed using the hot pressing technique [26]. Bulk SiC/C FGC is another pair successfully manufactured using the hot pressing process. In terms of thermal properties, the hot pressed SiC/C FGC was found to have a high effective thermal conductivity at the interface of the 1 mm SiC layer when compared to the specimens prepared using other methods. No cracks were found in the SiC/C coatings, as a result of the high thermal fatigue behavior of the FGC. The plasma-relevant performance also indicated that the specimen has excellent high temperature erosion resistance [27]. Moreover, hot pressed **hydroxyapatite/Ti (HA/Ti) FGC** showed a strong biocompatibility and a high bonding strength with the bone tissue of rabbits, as investigated by [28]. The study concluded that the HA/Ti FGC has a good potential for use in hard tissue replacement applications as it possesses a high bonding strength which could exceed the 4.73 MPs shear strength of new bone tissues when compared to pure Ti metal. Amongst the successfully manufactured hot pressed FGCs are the novel TiB_2**/**ZrO_2 and TiB_2**-**SiC**/**ZrO_2 **FGCs** which show excellent properties and have been identified for possible use in ultra-high temperature applications [29].

4.3. Cold pressing

A beam-shaped porous lead zirconia titanate-alumina **(PZT-**Al_2O_3**) FGC** actuator that exhibits the theoretically matched electric-mechanical response with a crack-free structure based on the pyrolyzable pore-forming agent (PFA) porosity gradient, has been successfully manufactured using a cold sintering method [25].

The binder addition is similarly applied in the manufacture of another FGC composed of Ni and Al_2O_3 in order to investigate the influence of the particle size used. In this study, the appropriate Ni, Al_2O_3 and Q-PAC 40 (organic binder) particle sizes were selected, based on the desired microstructure of the corresponding composition. After being mixed together in the blending process, the powder mixtures were cold pressed under 86 MPa pressure. This

was followed by pressureless sintering at 1350°C with specific sintering [30]. The titanium/ hydroxyapatite **(HA/Ti)** and other FGC implants with a gradually changing composition in the longitudinal direction of the cylindrical shape were also manufactured via cold isostatic pressing (800 to 1000 MPa) in order to optimize the mechanical and biocompatibility properties of the resultant structures [31]. Figure 1 shows the flow chart outlining the manufacturing process of the cold pressed Al_2O_3-ZrO_2 FGC used in the study [30]. Different elemental consideration under powder characteristic in terms of the addition of the space holder material was investigated on porous Ti-Mg (titanium-magnesium) FGM.

Most researchers working with this technique increasingly intend to use microscale particles in the manufacture of FGCs since nanoparticles need greater precision during processing. Only a small number of limited studies report using nano-sized composition particles [21]. **Co/α-Al_2O_3 FGC** composed of nano-sized powders was successfully manufactured using a high pressure torsion procedure [32]. This procedure is classified as a PM method, and cold pressing — as the consolidation or sintering process — is performed after compaction. The difference is only in the way of delivering the pressure in the torsional mode.
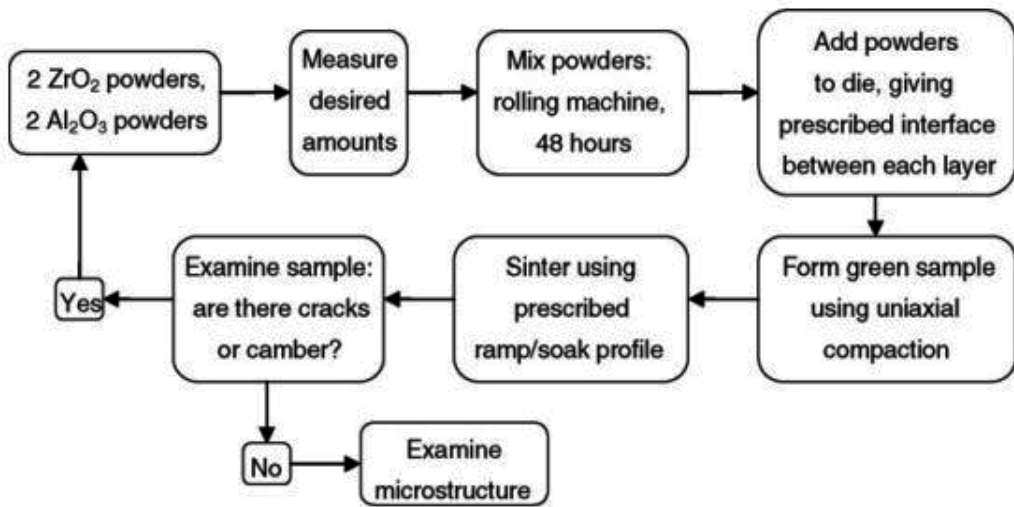
Figure 1. Flow chart detailing the manufacturing process of Al_2O_3/ZrO_2 FGC [30].

4.4. Sintering process

The sintering process is performed simultaneously with the compaction process if the FGC is prepared using a hot pressing process. However, in the cold pressing process, the sintering process is performed only after the powders have been compacted. The effectiveness of three different sintering methods, including electric furnace heating, high frequency induction heating, and spark plasma sintering (SPS) were investigated, [33]. SPS is a newly developed process which enables the sintering of high quality materials in short periods by charging the

intervals between powder particles with electrical energy. Their systems offer many benefits in terms of ease of operation, low cost, a more uniform and rapid sintering compared to the conventional systems using hot press sintering, hot isostatic pressing or atmospheric furnace processes applied to many advanced materials. Amongst the reported SPS FGCs are WC based materials **(WC/Co, WC/Co/steel, WC/Mo),** and **ZrO_2** based composites **(ZrO_2/steel, ZrO_2/TiAl, ZrO_2/Ni), Al_2O_3/TiAl**, etc. [34]. The influence of **ZrO_2** content and sintering temperature on microstructures and mechanical properties of the composites were investigated by [35].

In order to evaluate the sintering performances, one of the parameters that could be investigated is the porosity. As a result, some sintering models have been developed and analyzed to this end. These studies proved that the amount of porosity is directly related to the rate at which shrinkage occurs [36]. The changes in porosity and shrinkage in the theoretically sintered nickel/alumina **(Ni/Al_2O_3) FGC** have been studied [37]. This study shows how the porosity reduction model can be used to access the quality of particle-reinforced metal-ceramic FGCs formed by pressureless sintering and to predict the changes that can be achieved in porosity reduction through the engineering of the particle dispersion in the processing of FGCs. The influence of other sintering parameters including time, temperature, sintering atmosphere and the isostatic condensation on the performance of the resulting FGCs, was investigated [38]. During the manufacture of the sintered tool gradient materials — composed of **wolfram carbide** and cobalt — used in the study, the sintering parameters were changed in order to find their optimum values. The sequential concentration of the molding, with layers having an increasing content of carbides and a decreasing concentration of cobalt and sintering, ensures the acquisition of the required properties, including resistance to cracking. Another successful example of pressureless sintering is the functionally graded zirconia-mullite/alumina ceramics **(ZM/A FGC).** These exhibit a homogenous structure with highly improved and unique properties. The recorded value of each test of tailored FGZM/A was nearly equal to the average of the test values of its non-layered composites. This is good evidence of the strength of the interfacial bonding between subsequent layers of the composite as well as the homogeneity and uniformity of the powders in each layer [6, 7].

4.5. Infiltration process

Infiltration, or to give it the correct scientific terminology — hydrology —is the process by which fluid on the ground surface precipitates into the soil. This process is governed by the force of either gravity or capillary action. The rate of infiltration depends on soil characteristics such as storage capacity, transmission rate through the soil, and the ease of entry of the fluid.

The infiltration method was introduced in order to prepare certain complex FGCs shape. This manufacturing method needs little or no bulk shrinkage and more rapid reaction kinetics. As the common process for mold shaping is the heating of the powder to a temperature that is higher than the liquid phase, the demand of ensuring there is no bulk shrinkage is quite challenging.

A compositionally graded **Al-SiC FGC** was successfully manufactured using the pressureless infiltration method in the early part of the last decade. This indicated that the thermal conductivity of the FGC produced increased in a nonlinear manner, while the volume fraction of

the ceramic element decreased [39]. An innovative method of infiltration processing using microwave sintering and an environmental barrier coating (EBC) was subsequently developed for the manufacture of **Si$_3$N$_4$ FGC**. This FGC is composed of **α-Si$_3$N$_4$-Yb-silicate** green parts and porous β-Si$_3$N$_4$ ceramics as the substrates [40]. Figure 2 shows the successful manufacture of **YSZ/SiC FGC** via the infiltration method, as investigated by [41]. In addition, different compositions of porous **Ti/HAP FGCs** were also manufactured using the infiltration technique. The Young's Modulus of the manufactured FGCs was comparable to human cortical bone in the porosity range of 24 to 34%, [42]. The effect of glass infiltration was investigated on the **CaO-ZrO$_2$-SiO$_2$ system** in the development of **glass/alumina FGCs.** In order to obtain the final compositional gradient which is indicated by blue glass, the glass formulation of the system was doped with cobalt by adding a small molar percentage (0.1 mol %) of CoO. Characterization of the specimens proved that the cobalt-doped glass has interesting mechanical properties, including a high elastic modulus, good fracture toughness, and an acceptable coefficient of thermal expansion [43].
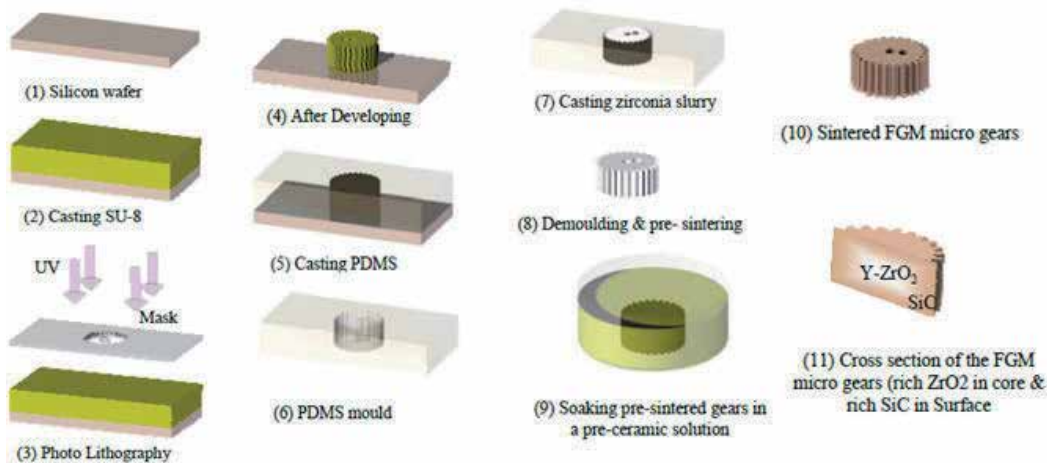
Figure 2. Schematic diagram of the infiltration process of YSZ/SiC FGM [41].

4.6. Centrifugal casting

Centrifugal casting is one of the most effective methods used in the processing of FGCs due to its wide range control on composition and microstructure. The microstructure and composition gradients in some aluminum based FGCs including **Al/SiC, Al/Shirasu, Al/Al$_3$Ti, Al/Al$_3$Ni,** and **Al/Al$_2$Cu** combinations have been made by evaluating the dispersion of the different phase particles within the FCM structures manufactured via different centrifugal casting processes [44]. The study found that **Al/SiC, Al/Shirasu** and **Al/Al$_3$Ti FGCs** can be manufactured using the centrifugal solid-particle method, while the centrifugal in-situ method is suitable for the manufacture of Al/Al$_3$Ni and Al/Al$_2$Cu FGMs. The combination of both processing methods is required for **Al/(Al$_3$Ti+Al$_3$Ni)** hybrid FGCs.

The phase compositions of FGCs manufactured using this approach depend strongly on the condition of the centrifugal sedimentation process. Relevant factors include the duration of the process, rotation speed, and solid and dispersive fluid contents [45]. A self-propagating high temperature synthesis reaction is added as one of the steps, followed by centrifugal casting, in the manufacture of TiC-reinforced iron base **(Fe-TiC) FCC**. Observation of the manufactured specimen indicated an increasing trend in the hardness profile from the outer surface to the TiC-rich inner surface. The wear performance of the TiC-rich inner face was found to be better when compared to the particle free outer surface of ferritic steel matrices [46].

The formation of gradient solidification is another aspect that was evaluated in the investigation into FGCs manufactured via centrifugation. In this study, **SiC, B$_4$C, SiC- graphite** hybrid, primary silicon, **Mg$_2$Si** and **Al$_3$Ni** reinforced aluminum based FGCs were prepared using centrifugal casting. The densities and the size of the reinforcements were found to be two major factors influencing the formation of the graded microstructure [47].

4.7. Slip casting

TZP/SUS304 FGC was developed using a slip casting technique [48]. The gradual distribution of the chemical composition and microstructure of the manufactured specimens eliminated the macroscopic FGC interface that occurs in a traditional ceramic/metal joint. Another FGC material that was successfully manufactured via the slip casting method is **Al$_2$O$_3$/W FGC**, which has the potential to be used as a conducting and sealing component in high-intensity discharge lamps (HiDLs) [49].

4.8. Thermal spraying

Thermal spraying has been frequently used to produce FGC coatings. Thermal spraying of FGCs offers the possibility of combining highly refractory phases with low-melting metals, and allows for the direct setting of the gradation profile. [50] studied the heat insulation performance of thermal barrier-type FGC coatings under a high heat flux. The FGC coatings with thicknesses varying from 0.75 to 2.1 mm were designed and deposited onto a steel substrate using plasma spraying. [51] studied and investigated the different properties, microstructure and chemical composition of FG 20 wt.% **MgO-ZrO$_2$/ NiCrAl** thermal barrier coatings that were obtained using the plasma spraying process. Scanning Electron Microscope (SEM) observations of the fractured surface revealed that the intermediate graded layer had the compositional mechanical properties of strength and toughness, due to improvement of the microstructure and relaxation of the residual stress concentration. In another study, the spark plasma technique used in the thermal spraying process was employed in the manufacture of an FGC composed of Hydroxyapatite **(HAp)** and titanium nitride **(TiN)** [52]. In order to improve the adhesion between the adjacent graded layers of the FGC, a proper bond coat should be introduced. It is thought that by arranging the smooth change of the mismatch between the thermal expansion coefficients of the composition, the delamination within the FGC structure could be addressed. Other FGCs manufactured using this technique are **HAp/TiO$_2$, Yttria stabilized zirconia (YSZ)/mullite** coats deposited on **SiC** substrates [53] and tungsten carbide/cobalt **(WC/Co) FGC** [54].

4.9. Laser cladding

In the laser cladding process, two or more dissimilar materials are bonded together using laser intercession. During the process, the material which is in powdered form is injected into the system — which is purpose-built for the cladding process — while the laser, which causes melting to occur, is deposited onto the substrate. Although the technique has become the best method for coating various shapes and has been declared to be the most suitable process for applications with graded material, limitations still exist because the setup of the high technology system processes is very expensive and is unsuitable for mass production as a result of the layer-by-layer process. The Nd:YAG type of laser was also being used in the manufacture via selective laser melting (SLM) of super **nickel alloy and zirconia FGC**, Figure 3. The resulting materials contained an average porosity of 0.34% with a gradual change between the layers, and without any major interface defects [55]. The final **WC-NiSiB alloy FGC** product manufactured by this method was found to be suitable for use in high-temperature tribological applications. The study mentioned that the surface roughness and the geometrical properties of the synthesized FGCs can be controlled by adjusting the heat input during the laser cladding process [56].
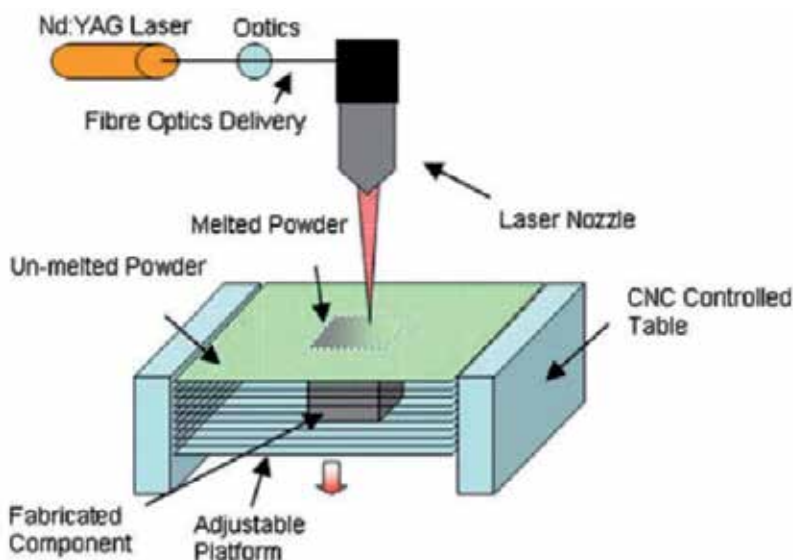
Figure 3. Experimental setup used for laser assisted processing using an Nd:YAG laser power source [55].

4.10. Vapor deposition method

Vapor deposition is a process by which materials in the vapor phase are condensed to form a solid material. This process is generally employed to make coatings for the alteration of the properties of the substrates such as mechanical, electrical, thermal, and wear etc. Basically, vapor deposition is classified into two categories, namely chemical vapor deposition (CVD)

and physical vapor deposition (PVD). C-based materials that have an excessive chemical sputtering which yields at 600 to 1000 K and exhibits irradiation with enhanced sublimation at >1200 K when exposed to plasma erosion conditions, were successfully manufactured via the CVD method in 2002. The problem of serious C-contamination of the plasma was solved by using chemically deposited SiC coatings on the surface of the C-substrate. C-based FGCs such as **SiC/C, B$_4$C/Cu, SiC/Cu and B$_4$C/C bulk FGC** were also successfully manufactured using this method [57].

5. Advanced applications of FGC ceramics

The use of FGCs has rapidly gained popularity in recent years, especially in high temperature environments and aggressive media, as illustrated in Figure 4. The FGCs concept is applicable to almost all material fields. Examples of a variety of real and potential applications of FGCs in the field of engineering are cutting tools, machine parts, and engine components, while incompatible properties such as heat, wear, and corrosion resistance, plus toughness and machinability are incorporated into a single part. For example, throwaway chips for cutting tools made of graded tungsten carbide/cobalt **(WC/Co)** and titanium carbonitride **(TiCN)-WC/ Co** that incorporate the desirable properties of high machining speed, high feed rates, and a long life have been developed and commercialized. Various combinations of these ordinarily incompatible functions can be applied to create new materials for the aerospace industry, chemical plants, optoelectronic applications, bio-medical applications, solar cells, and nuclear energy reactors.

5.1. FG Ceramics for aerospace, military and automotive applications

Thermal barrier coating FGCs are used for military and commercial aero engines as well as in gas turbine engines for automobiles, helicopters, marine vehicles, and electric power genera-tors. They are also used in augmentor components, e.g. tail cones, flame holders, heat shields and duct liners, and in the nozzle section they are being used experimentally in the verging/ diverging flaps and on seals where hot gases exit the engine [58, 59].

Space vehicles flying at hypersonic speeds experience extremely high temperatures from aerodynamic heating due to friction between the vehicle surface and the atmosphere. One of the main objectives of investigating FGCs deposited by chemical vapor deposition (CVD-FGCs) was the development of thermal barrier coatings (TBCs) for a space plane. It was found that sheets of **SiC/C FGCs** produced by CVD provide excellent thermal stability and thermal insulation at 1227°C, as well as excellent thermal fatigue properties and resistance to thermal shock [60]. A combustion chamber with a protective layer of SiC/C FGC has been developed for the reaction control system engine of HOPE, a Japanese space shuttle. These FGCs produced for rocket combustors have undergone critical tests with nitrogen tetroxide and monomethyl hydrazine propellants at firing cycles of 55 seconds with subsequent quenching by liquid nitrogen. The maximum outer wall temperature of these model combustors was 1376°C to 1527°C, while the inner wall temperature reached 1677°C to 2027°C. No damage to the
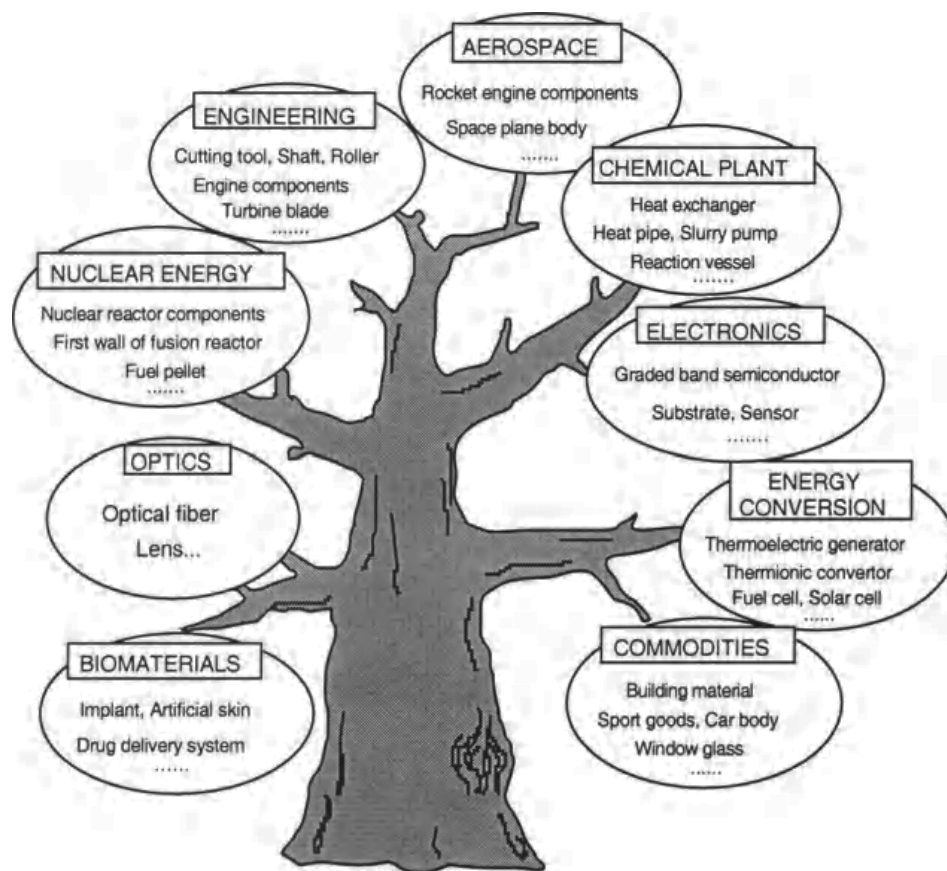
Figure 4. Areas of potential application of FGCs.

combustors was observed after two test cycles [61]. It is expected that the Si-based ceramics, **SiC** and **Si$_3$N$_4$**, will be introduced in the hot-sections of the next generation of gas turbines operating at higher temperature. **Mullite/SiC** TBC FGC exhibited excellent adhesion and corrosion resistance as shown in the study by [62].

Graded zirconia/nickel **ZrO$_2$/Ni** and **Al$_2$O$_3$/ZrO$_2$ FGC** TBCs have also been considered for other rocket engines, such as in the small regeneratively cooled thrust chambers in orbital maneuvering systems [63, 64]. These chambers are prepared using a combination of galvano-forming and plasma spraying. No delamination of ZrO$_2$ was observed after 550 seconds of combustion.

Nowadays it is necessary to reduce the weight of army systems in order to cope with the rapidly developing requirements of military contingencies. Ultralight weapons will be the cornerstone of future battlefield domination. Military strategists have asked for radical weight reductions in future military equipment, which will need new materials in new structures and designs. The concept of FGCs is one of the material technologies identified for this purpose [65].

Stealth missiles are now a required component of a modern weapons system. Parts made from specific materials can be used to absorb the electromagnetic energy emitted in order to minimize waves reflected in the direction of the enemy radar receiver. The most promising new materials for use in these applications are ceramic matrix composites reinforced with ceramic woven fabrics. The use of long, continuous ceramic fibers embedded in a refractory ceramic matrix creates a composite material with much greater toughness than basic (mono-lithic) ceramics, and which has an intrinsic inability to tolerate mechanical damage without brittle fracture. **Nicalon SiC fibers**, which have semiconducting properties, and **Nextel mullite ($3Al_2O_3$- $2SiO_2$- 0.1 B_2O_3) fibers**, which are completely dielectric, are used in the preparation of graded oxide matrix ceramic composites [66].

Some structural ceramics such as **B_4C, SiC, Al_2O_3,** AlN, TiB_2 and Syndie (synthetic diamond) FGCs [67–70] are viewed as potential materials for use in armor applications for both personnel and vehicle protection, owing to their low density, reliability, superior hardness, compressive strength and greater energy absorption capacity, which enable effective protection from projectiles.

Moreover, spark plasma sintered **Ti/TiB_2, TiB_2/$MoSi_2$** [71] and Ni/Al_2O_3 [4], FGCs are used as lightweight armor materials with high ballistic efficiency.
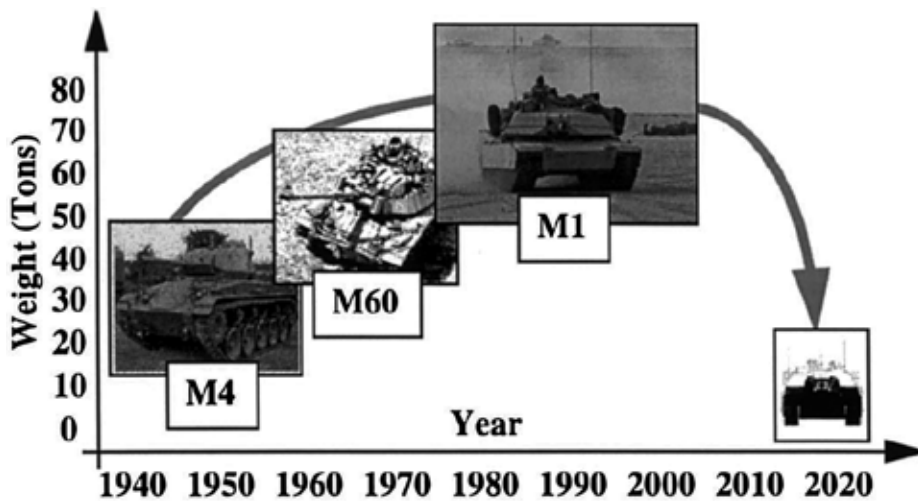
Figure 5. Radical weight reduction for future ground vehicles [65].

At present, the braking system is one of the most important part of the world's transportation systems. The traditional disc brake rotors in use today are manufactured from gray cast iron [72]. Up until very recently, the best candidate material for the future generation replacement of car brake rotors in terms of the relationship between high speed and lower coefficients of friction had not been identified.

The new advances in functionally graded ceramics allows them to be utilized in car braking systems as brake discs. It is anticipated that aluminum titanate **(Al_2TiO_5) FGCs** may replace

conventional gray cast iron as a result of its better thermal performance when used in car brake rotors. Moreover, due to its low density compared to gray cast iron, Al_2TiO_5, it is a fuel saving option for use in car brake rotors [73].

Nowadays, [74] it is known that functionally graded Al_2O_3/ Al_2TiO_5 ceramics can be used successfully in car brake rotor systems due to the excellent properties and behaviors they exhibit.

5.2. FG ceramics for energy applications

The majority of today's power stations still burn conventional fuels. By optimizing combustion techniques and combining stationary gas turbines with steam turbines, efficiencies close to 60 % have been achieved. The incorporation of advanced material concepts such as FGCs could further improve the efficiency of these systems [75].

Turbine blades made from **titanium aluminide** with gradients in Cr content have been produced by hot isostatic pressing. Measurement of the mechanical properties of machined pieces cut from tested $Ti_{48}Al_2Cr_2Nb/Ti_{46}Al_3Cr_5Nb_2Ta$ **FGC** turbine blades were evaluated after heat treatment at 1350°C for 2 hours, and confirm the presence of the expected microstructural and mechanical gradients [76].

Porous **SiC** FG ceramics are proving to be the most promising materials for use as liquid fuel evaporator tubes in gas turbine combustors with premix burners which can significantly reduce the probability of failure **[77, 78]**. FGCs can also be used as components for integrated thermionic/thermoelectric systems. Figure 6 shows a schematic of a hybrid direct energy conversion system proposed in the second Japanese FGC program [79]. Thermionic conversion is based on the principle that electrons discharged from a hot emitter will move to a low temperature collector located on the opposite side [80]. By applying the FGC concept **(TiC/Mo – MoW – WRe) FGCs**, the performance of the thermionic converter can be optimized by decreasing the energy loss between the emitter and the converter (the barrier index) [79].

Thermoelectric materials with a FGM structure show a higher performance than basic materials. FGC joining is also a useful technique for use in setting an electrode in order to relax thermal stress and suppress inter diffusion. SiGe is one of the materials under consideration for use in thermoelectric conversion at high temperatures. Dense graded SiGe units with electrodes have been manufactured by a one-step sintering process using hot isostatic pressing (HIP) with glass encapsulation, as shown in Figure 7 [81]. Materials with low electrical resistivity, including tungsten, molybdenum disilicide, and titanium diboride **(W, MoSi$_2$, and TiB$_2$)** were selected for the electrodes. They were blended with silicon nitride **(Si$_3$N$_4$)** in order to reduce the thermal expansion mismatch of the joints between the electrodes and the thermoelectric conversion unit.

It has recently been found that the tellurium compound**s Bi$_2$Te$_3$** and **Sb$_2$Te$_3$** having ZT > 2 and PbTe based FGCs are well established thermoelectric materials suitable for use in the future [82].
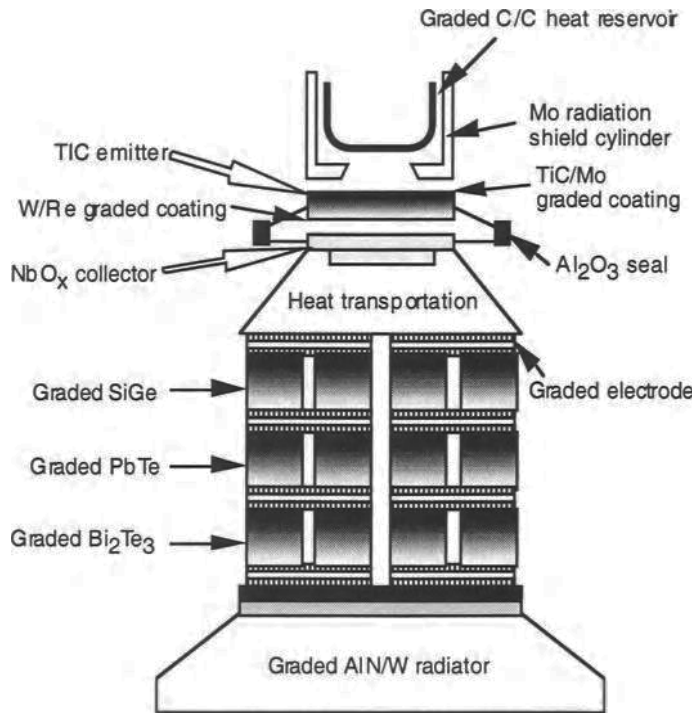
Figure 6. A hybrid direct energy conversion system consisting of thermionic and thermoelectric converters.
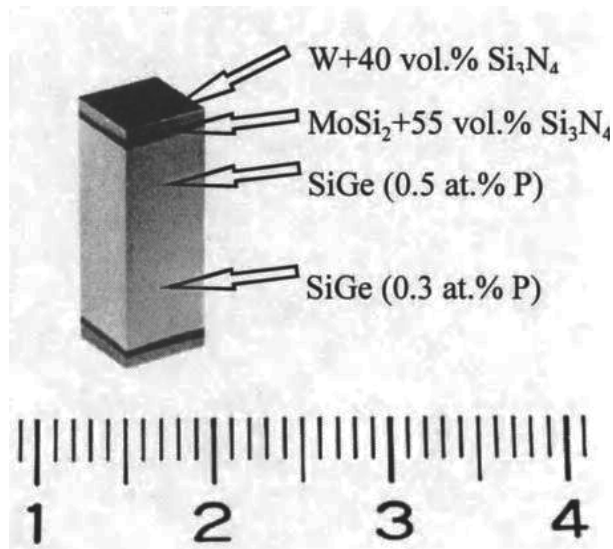

Figure 7. A dense, graded n-type (SiGe) conversion unit produced by HIP [81].

FGCs are also promising candidates for use in the manufacture of technological components in solid oxide fuel cells (SOFC). [83] has successfully manufactured nano-structured and functionally graded **LSM–LSC–GDC FGC** cathodes to have about 240 μm thick YSZ electrolyte supports using a combustion CVD method. Moreover, FGCs are used as components in the fusion and nuclear reactor field. Chemical vapor deposited FGC coatings of 1 mm thick **TiC/C** were evaluated at a surface heat flux of up to 70 MW/m^2 for several seconds. The FGC film sustained temperature differences as high as 1500°C without cracking or melting [84].

5.3. FG ceramics for electronic and optoelectronic applications

Ceramic/metal and ceramic/ceramic FGMs are showing great promise as both specialized electrical materials, and thermal barrier materials, due to their high temperature properties.

Functionally graded ceramics have become widely and commonly used in many advanced optical and electrical applications such as semi-conductor devices, anti-reflective layers, sensors, fibers, GRIN lenses and other energy applications [85]. In semi-conductors, concentration, carrier mobility, diffusion length, built-in electric field and other properties exert a strong influence on the parameters of electronic and optoelectronic devices. Functionally graded **AlN/GaN** ceramics can be used as a buffer layer for heteropitaxy that is able to distribute strain in the buffer layer and reduce cracking in the active layer [86].

In addition, in conventional edge lasers applied to fiber telecommunications, there are several factors that influence the quality of a device. Two most important are the low threshold current and the numerical aperture of the light beam. It is possible to decrease the numerical aperture, but also to increase the threshold current through increasing the thickness of the active region. One possible solution is the use of a graded-index separate-confinement heterostructure (GRINSCH). In such a structure, the FGC is used as a waveguide cladding layer, and as a barrier to carriers [87].

On the other hand, the substantial shortfall in the efficiency of silicon solar cells is due to the constant band gap width of the bulk material. In such cells, high radiation is absorbed in a shallow layer under the surface. As a result, it is important to initiate an electric field in close vicinity to the surface. A successful way to overcome this limitation is through the use of graded materials [88]. Functionally graded **Al$_x$Ga$_{1-x}$N (n)/GaN (p)** ceramics can be used as high efficient photodetectors and in solar cells [89].

Piezoelectrics have been used extensively in the design of actuators and sensors in many fields due to their versatility and efficiency in the mutual transformation between mechanical and electrical energy. The piezoelectric actuator has many excellent properties, such as low energy consumption, a compact size, quick response and high resolution. Therefore, piezoelectric actuators and sensors are seen as promising candidates for use in microelectro-mechanical systems and smart material systems. Functionally graded piezoelectric ceramics are novel devices, which can successfully overcome the inherent structural defects in conventional piezoelectric bending-type actuators that result from the use of epoxy binder.

Functionally graded piezoelectric ceramics with a ceramic backing of **(1-x) Pb(Ni$_{1/3}$Nb$_{2/3}$)O/ xPb(Zr$_{0.3}$Ti$_{0.7}$)O$_3$** are used as highly efficient ultrasonic transducers [90]. These ultrasonic

transducers are widely used in ultrasonic measurement systems such as nondestructive testing and medical diagnosis.

Another advanced FGC is porous lead zirconate titanate **(PZT)**, which is manufactured by aqueous tape casting technology and is used in pyroelectric applications [91].

5.4. FG ceramics in biomedical applications

Over the past 30–40 years, there have been major advances in the development of medical materials and this has seen the innovation of ceramic materials for use in skeletal repair and reconstruction. Bioceramics are now used in a number of different applications throughout the body. However, the increase in biomedical applications of bioactive ceramics is occurring simultaneously with the growth of interest in tissue engineering.

The use of FGCs in biomaterial applications is growing in importance. Over 2500 surgical operations undertaken to incorporate graded hip prostheses have been successfully performed in Japan over the past twelve years. These graded hip implants enable a strong bond to develop between the titanium implant, bone cement, hydroxyapatite (HAp), and bone. The bone tissue penetrates HAP granules inserted between the implant and the bone forming a graded structure. Hence, FGCs have enabled the development of this promising approach to bone tissue repair [92].

Biomaterials must simultaneously satisfy various requirements and possess certain properties such as being non-toxic, having good mechanical strength, and they need to be biocompatible [93, 94]. Natural tissues often possess FGMs which enable them to satisfy multiple requirements [95]. Human tissues have evolved to be best adapted to their multiple functional requirements. For instance, the perfect design of natural bone with a dense, stiff external structure (cortical bone) and a porous internal structure (cancellous bone) demonstrates that functional gradation has been utilized for biological adaptation [96].

A functionally graded carbon fiber (CF) reinforced poly-lacticacid (PLA)/nanometer hydroxyapatite (HA) biomaterial has been prepared by [97]. CF was used as the reinforcement to improve mechanical properties, while at the same time the advantages of PLA and nano-HA were retained. [31] developed a dental implant with functionally graded titanium (Ti) and HA. [98, 99] developed a functional gradient HA composite containing glass-coated Ti and studied its microstructures, mechanical and thermal properties. [100] proposed a **HA–glass–titanium (HA–G–Ti)** composite and implanted it in the femur of a dog to evaluate its bonding strength. However, metal and polymer-based implants usually lead to stress shielding, wear debris, delayed osseointegration, resorption, degradability or other biological complications. Therefore, new bone tissue implants should aim to avoid these disadvantages and instead meet the multiple functional requirements of bone tissue [101, 102].

It was found that calcium phosphate ceramics, especially the bioactive nano-structured hydroxyapatite, have received considerable attention in recent years [103–105]. In vitro and in vivo experiments have demonstrated that the nano-HA has an excellent biological performance when compared with conventional micro-grain HA [106, 107]. Nano-HA possesses exceptional biocompatibility and bioactivity with respect to bone cells and tissues. Hence,

[108] prepared a successful nine layers of laminated and functionally graded HA/ yttria stabilized zirconia (Y-TZP) for orthopedic applications, using an SPS technique.

In addition, [92] presented a novel FGC with both micro-grain and nano-grain HA crystals that is able to satisfy the mechanical and biological property requirements of bone implants. It was concluded that a biologically functionalized nano-rough surface contributed better bioactive functionality to the HA ceramics. By applying the concept of FGM, bio-inspired multifunctional biomaterials open the door to a promising approach to bone tissue repair.

Other functionally graded ceramics that are used in biomedical applications are **ZrO_2/ AISI316L** as artificial joints and hip prostheses, and **ZrO_2/Al_2O_3** FGCs as teeth implants [109]. Nowadays, structure grading technology is also used in cancer prevention research. One of them, for instance, is a study on collagen structure reinforcement using grading technology. In such a type of graded structure, the graded material should not only possess excellent hardness, wear and corrosion resistance, but should also have high biological compatibility and harmlessness.

5.5. FG ceramics in structural and tribological applications

FGCs offer great promise for use in applications where the operating conditions are severe, for example, in cutting tools and wear resistant linings for handling large heavy abrasive ore particles. These applications require graded ceramics with high corrosion and wear resistance. This type of FGC can also be used as protective coatings in the form of an **alumina/mullite FGC** that is used to protect SiC components from corrosion, and act as a thermal barrier coating, improving the efficiency of turbine engines by providing the capability to sustain a significant temperature gradient across the coating **ZrO_2/Al_2O_3** FGC, which also improves thermal resistance and resistance to oxidation [110].

Moreover, a novel functionally graded **Al_2O_3/lanthanum hexaaluminate (LHA)** ceramic with a gradient in composition and porosity was developed using the PM method as a high temperature thermal barrier coating, protecting the components from a corrosive and severe thermal environment [111]. Graded **WC/Co FGCs** are used as abrasive cutting tools and in mining equipment, where a high wear resistance and toughness are both required [112].

In addition, the WC/Co FGC is coated with a layer of titanium nitride **(TiN)**, a layer of alumina **(AI$_2$O$_3$)**, and a layer of titanium carbonitride **(TiCN)** by chemical vapor deposition. These graded and multiple coated WC/Co FGC cutting tool chips are very resistant to flank wear. Furthermore, they have the advantage of a high machining speed combined with a high feed rate. Their graded composition can also control the internal stresses arising from the mismatch in thermal expansion. A simple, asymmetric gradient in composition such as in a ceramic/metal FGM can reduce thermal stress, while a symmetrical or radial gradient can induce a sizable compressive stress at the outer ceramic layer, resulting in stress reinforcement similar to that of tempered glass or pre-stressed concrete [113]. Graded cutting tools have also been made for interrupted cutting from cermets of **TiC-NiMo FGC** in which the percentage of TiC in the graded layer ranged from 95 wt. % at the top surface to 86 wt % at the site of

transition to plain steel [114]. Recently, **Al$_2$O$_3$/TiC** and **Al$_2$O$_3$/(W-Ti) C** FG ceramics have been investigated as highly efficient ceramic tools with excellent thermal shock resistance [115].

FGCs are also used as engineering components, machine parts and in joints for gas and steam turbines as well as in coatings and wear resistant materials [116]. For example, **SiC/C** FGC acts as a structural part of the heat collector for an energy conversion system, and also provides thermal stress relaxation, heat conduction, and protection from oxidation.

Another FGC application that involves thermal stress relaxation and a low coefficient of friction, is in welding apparatus. For example, **Si$_3$N$_4$-Cu FGC** is used in automated electric arc welding of the large aluminum sheets used in building huge ships such as liquid natural gas (LNG) tankers [117]. Other suggested applications included use as filters, catalysts, mufflers, heat exchangers, self-lubricating bearings, silencers, vibration dampers, and shock absorbers [118].

Silicon nitride Si$_3$N$_4$, and silicon aluminum oxynitride **SiAlON** are a special class of high temperature ceramic and refractory materials. Moreover, they represent a vital and unique class of structural ceramics. They can be used in many industrial and structural applications that require chemical stability, high heat resistance and specific mechanical properties [119].

Previously, [120] developed graded in situ SiAlON ceramics by embedding **β-SiAlON** green compacts in **α-SiAlON** powder. The compositions, microstructures and properties of the graded SiAlON ceramic change gradually from the hard α-SiAlON with spherical morphology on the surface, to the tough and strong β-SiAlON with elongated grains in the core. [121] developed a technique for the in situ formation of an α-SiAlON layer on a β-SiAlON surface. In another study, [122] obtained a gradual change of α-SiAlON content from the surface through to the core using the rapid cooling method. Recently, [123] have manufactured a twin layer FGC of **α-SiAlON (100 wt%)/AlN-BN (50:50 wt%)** for advanced structural applications.

5.6. Other applications of functionally graded ceramics

In addition to the above mentioned applications, FGCs can be used in the lining of thermal furnaces and other ultra-high temperature applications:

- Novel **zirconia-mullite/alumina** FGC tailored by the reaction sintering method and used in refractory materials that line furnaces, and high temperature applications [6, 7].

- **ZrB$_2$/ZrO$_2$** FGC prepared using spark plasma sintering for ultra-high temperature applications and in severe environments [124].

- **ZrO$_2$/Fe** FGC with excellent thermal and mechanical properties, used for high temperature engineering applications [125].

- A crack-free **Si$_3$N$_4$/Al$_2$O$_3$** FGC suitable for high temperature structural applications [26].

- Multi-layered Zircon/yttria **(ZrO$_2$.SiO$_2$/Y$_2$O$_3$)** FGC with high thermal shock resistance, used as crucibles for the induction melting of TiAl based alloys with zero contamination [126].

6. Future direction

Functionally graded ceramics are excellent advanced materials with unique properties and characteristics that have entered into the manufacturing world in the 21st century. The major success of FGCs is due to the fact that the irreconcilable properties on each side of a FGC can be fully utilized. FGCs can be tailored according to the application requirements by controlling the appropriate components in order to achieve some specific tailored applications and to overcome the problems of laminated composites. However, there are some obstacles to the realization of this success. The high costs that are entailed during the manufacturing process and powder processing are considered to be a crucial issue. The technology of powder metallurgy can offer a vital solution to this problem, however, there are a lot of issues relevant to this technology that need to be considered. In addition, an extra effort in different axes should be exerted in order to generate a predictive model for proper process control. This will improve the execution of the process and so reduce the cost of FGC production. Another issue that needs to be taken into consideration is that of determining the residual stresses resulting from the inhomogeneous cooling of the graded layers of the FGC body. The values of these residual stresses are an important indication to both the success of FGC preparation and to their subsequent properties. Because one of the main purposes when designing FGCs is to decrease or prevent the residual stress formed at the interface of the two dissimilar materials, and thereby prevent crack propagation and ultimately the delamination of these materials by having smooth transitions between layers.

Author details

Dina H.A. Besisa and Emad M.M. Ewais[*]

*Address all correspondence to: dr_ewais@hotmail.com

Refractory & Ceramic Materials Division (RCMD), Central Metallurgical R&D Institute (CMRDI), Cairo, Egypt

References

[1] Koizumi M., "The concept of FGM", in second International Symposium on function-ally gradient materials (ed. Holt, J. B., Koizumi, M., Hirai, T. and Munir, Z. A.), J. Am. Ceram. Soc. 3-10, (1992).

[2] Kaya C., "Al_2O_3-Y-TZP/Al_2O_3 functionally graded composites of tubular shape from nano-sols using double-step electrophpretic deposition," J. Eu.Ceram. Soc., 23, 1655-1660, (2003).

[3]   Pettersson A., Magnusson P., Lundberg P. and Nygren M., "Titanium-titanium diboride composites as Part of a gradient armour material," Int. J. Impact Eng., 32, 387-399, (2005).

[4]   Panda K.B., and Chandran K.S.R., "Titanium-titanium boride (Ti-TiB) functionally graded materials through reaction sintering: synthesis, microstructure, and properties", Metallurgical and Mater. Trans. A., 34 [9], 1993-2003 (2007).

[5]   Sotirchos S.V., "Functionally graded alumina/mullite coatings for protection of silicon carbide ceramic components from corrosion", semi-annual report provided by university of Rochester, department of chemical engineering, Rochester, New York 14627, (1999). Special contribution to the book "Functionally graded materials; design, processing and applications", 1999.

[6]   Ewais E.M.M., Besisa D.H.A., Zaki Z.I., Kandil A.T., "Tailoring of functionally graded zirconia-mullite/alumina ceramics, " J Eur Ceram Soc., 32, 1561-1573, (2012).

[7]   Ewais, E. M. M., Besisa, D. H. A., & Zaki, Z. I., "Influence of MgO addition on the properties of new tailored FGZM/A ceramics," J Mater Sci and Eng. A, 578, 197–206, (2013).

[8]   Petrovic J.J., and McClellan K.J., "Ceramic/Polymer functionally graded material (FGM) lightweight armor system," DOE office of scientific and technical information (OSTI), 96510, (1997).

[9]   Rice, R.W., "Fabrication of ceramics with designed porosity", Ceram. Eng. Sci. Proc., 23, 149–160, (2002).

[10] Werner, J.P., Linner-Krcmar, B.; Friess, W.; Greil, P. "Mechanical properties and in vitro cell compatibility of hydroxyapatite ceramics with graded pore structure, Biomaterials", 23, 4285–4294, (2002).

[11] Kieback B., Neubrand A., and Riedel H., "Processing techniques for functionally graded materials," J. Mater. Sci. Eng.,A, 362, 81-105, (2003).

[12] Jin X., Wu L., Guo L., Yu H., and Sun Y., "Experimental investigation of the mixed-mode crack propagation in ZrO_2/NiCr functionally graded materials," Eng. Fracture Mechanics, vol. 76[12], pp. 1800-1810, (2009).

[13] Shahrjerdi A, Mustapha F, Bayat M, Sapuan SM, Majid DLA.," Fabrication of functionally graded hydroxyapatite-titanium by applying optimal sintering procedure and powder metallurgy", Int. J. Phys. Sci. 6[9],2258-2267, (2011).

[14] He Z., Ma J., Tan G., J All and Comp. 54, 459, (2009).

[15] Watanabe Y., Yamanaka N., Fukui Y., "Control of Composition Gradient in a Metal-Ceramic Functionally Graded Material Manufactured by the Centrifugal Method. Composites Part A," 29 A, 5-6, 595- 601, (1998).

[16] Duque N B., Melgarejo Z H., Suarez M O., "Functionally graded aluminum matrix composites produced by centrifugal casting", J Mater Charact., 55[2]: 167–171, (2005).

[17] Torii S., Tanaka S., Yano, T., Watanabe, Y., J Trans. Phenomena, 6, 189, (2004).

[18] Yeo JG; Jung YG; Choi SC.,, "zirconia-stainless steel functionally graded material by tape casting", J Eur Ceram Soc., 18[9], 1281-1285, (1998).

[19] Cannillo V., Lusvarghi L., Siligardi C., Sola A., "Prediction of the elastic properties profile in glass-alumina functionally graded materials", J Eur Ceram Soc., 27, 2393-2400, (2007).

[20] Belmonte M., Gonzalez-Julian J., Miranzo P., Osendi M.I., "Continuous in situ Functionally Graded Silicon Nitride Materials", Acta. Mater. 57, 2607-2612, (2009).

[21] Jamaludin S N S., Mustapha F., Nuruzzaman D M. and Basri S N., " A review on the fabrication techniques of functionally graded ceramic-metallic materials in advanced composites", Sci Res and Essays, 8[21], 828-840, (2013).

[22] El-wazery M., El-Desouky A.," A review on functionally graded ceramic-metal materials", Mater. Environ. Sci., 6 [5], 1369-1376, (2015).

[23] Mishina H, Inumaru Y, Kaitoku K., "Fabrication of ZrO_2/AlSl316L functionally graded materials for joint prosthesis", Mater Sci Eng A., 475, 141–147,(2008).

[24] El-Wazery M., El-Desouky A.,"Fabrication and characteristics of 8YSZ/Ni functionally graded materials by applying spark plasma sintering procedure", J Appl. Sci. & Eng.,12, 313, (2014).

[25] Li JQ., Zeng XR., Tang JN., Xiao P., "Fabrication and thermal properties of a YSZ-NiCr joint with an interlayer of YSZ-NiCr functionally graded material", J. Eur. Ceram. Soc. 23:1847-1853, (2003).

[26] Lee S., Lemberg A., Cho, G., Roh Y., and Ritchie O.. "Mechanical properties of Si_3N_4–Al_2O_3 FGM joints with 15 layers for high-temperature applications",. J Eur Ceram Soc., 30, 1743–1749, (2010).

[27] Wu AH., Cao WB., Ge CC., Li JE., Kawasaki A., "Fabrication and characteristics of plasma facing SiC/C functionally graded composite material", Mater. Chem. Phys. 91(2-3), 545-550, (2005).

[28] Chu C., Xue X., Zhu J., Yin Z., "In vivo study on biocompatibility and bonding strength of Ti/Ti-20 vol.% HA/Ti-40 vol.% HA functionally graded biomaterial with bone tissue in the rabbit". Mater. Sci. Eng. A, 429, 18-24, (2006).

[29] Ming Lv,Wenlin Chen b, Chuanrang Liu, "Fabrication and mechanical properties of TiB_2/ZrO_2 functionally graded ceramics" Int. J of Ref. Metals and Hard Mater., 46, 1–5, (2014).

[30] Sun L, Sneller A, Kwon P. "Fabrication of alumina/zirconia functionally graded material: from optimization of processing parameters to phenomenological constitutive models". Mater. Sci. Eng. A, 488, 31-38, (2008).

[31] Watari, F., Yokoyama, A., Saso, F., Uo, M., Kawasaki, T., "Fabrication and properties of functionally graded dental implant". Compos. B-Eng., 28, 5–11, (1997).

[32] Menéndez E, Salazar-Alvarez G, Zhilyaev AP, Suriñach S, Baró MD, Nogués J, Sort J., " Cold consolidation of metal–ceramic nanocomposite powders with large ceramic fractions". Adv. Funct. Mater.,18, 3293-3298, (2008).

[33] Watari F, Kondo H, Matsuo S, Miyao R, Yokoyama A, Omori M, Hirai T, Tamura Y, Uoa M, Ohara N, Kawasaki T., "Development of functionally graded implant and dental post, for bio-medical application". Mater. Sci. Forum, 423-425:321-326, (2003).

[34] Tokita M., "Development of large-size ceramic/metal bulk functionally graded materials by spark plasma sintering", Mat Sci Forum, 308-311, 83-88, (1999).

[35] Menga, F., Liua, C., Zhangb, F., Tiana, Z., and Huanga, W., "Densification and mechanical properties of fine-grained Al_2O_3–ZrO_2 composites consolidated by spark plasma sintering". J of Alloys and Comp., 512, 63–67, (2012).

[36] Pines M, Bruck H., "Pressure-less sintering of particle-reinforced metal-ceramic composites for functionally graded materials: Part I. Porosity reduction models". Acta Mater., 54(6), 1457-1465, (2006a).

[37] Pines M, Bruck H. "Pressure-less sintering of particle-reinforced metal-ceramic composites for functionally graded materials: Part II. Sintering model. " Acta Mater. 54(6), 1467-1474, (2006b).

[38] Dobrzanski LA, Dolzanska B, Golombek K, Matula G., "Characteristics of structure and properties of a sintered graded tool materials with cobalt matrix". Arch. Mater. Sci. Eng., 47(2), 69-76, (2011).

[39] Cho K-M, Choi I-D, Park I. "Thermal properties and fracture behavior of compositionally graded Al-SiC composites. Designing, Processing and Properties of Advanced Engineering Materials", Mater. Sci. Forum, 449:621-624, (2004).

[40] Willert-Porada M, Grosse-Berg J, Sen I, Park H-S. "Microwave sintering and infiltration of highly porous silicon nitride ceramics to form dense ceramics". J. Key Eng. Mater. 287:171-176, (2005).

[41] Hassannin H, Jiang K. "Infiltration-processed, functionally graded materials for microceramic components". Micro Electro Mechanical System (MEMS) 2010 IEEE 23rdInternational Conference, 368-371, (2010).

[42] Nomura N, Sakamoto K, Takahashi K, Kato S, Abe Y, Doi H, Tsutsumi Y, Kobayashi M, Kobayashi E, Kim W-J, Kim K-H, Hanawa T. "Fabrication and mechanical proper-

ties of porous Ti/HA composites for bone fixation devices". Mater. Trans. 51(8): 1449-1454, (2010).

[43] Cannillo V, Mazza D, Siligardi C, Sola A. "Cobalt doped glass for the fabrication of percolated glass-alumina functionally graded materials". Ceram. Int. 34:447-453, (2008).

[44] Watanabe Y, Kim IS, Fukui Y. "Microstructures of functionally graded materials fabricated by centrifugal solid-particle and in-situ methods". Met. Mater. Int. 11(5): 391-399, (2005).

[45] Jaworska L, Rozmus M, Królicka B, Twardowska A. "Functionally graded cermets". J. Aci. Mater. 17(1-2):73-76, (2006).

[46] El-Hadad S, Sato H, Miura-Fujiwara E, Watanabe Y. "Review fabrication of Al-Al$_3$ Ti/Ti$_3$ Al functionally graded materials under a centrifugal force". Materials, 3, 4639-4656, (2009).

[47] Rajan TPD, Pai BC. "Formation of solidification microstructures in centrifugal cast functionally graded aluminum composites". T. Indian I. Metals 62(4-5):383-389, (2009).

[48] He X, Du H, Wang W, Jing W, Liu C. "Fabrication of ZrO$_2$-SUS functionally graded materials by slip casting". Key Eng. Mater. 368-372:1823-1824, (2008).

[49] Katayama T, Sukenaga S, Saito N, Kagata H, Nakashima K. "Fabrication of Al2O3-W functionally graded materials by slip casting method". Conf. Ser.: Mater. Sci. Eng. 18(20):20-23, (2011).

[50] Xiong, H.-P., Kawasaki, A., Kang, Y.-S., and Watanabe, R., "Experimental study of heat insulation performance of functionally graded Mmetal / ceramic coatings and their behavior at high surface temperature," Surf. Coat. Technol., vol.194, 203–214, (2005).

[51] Pan C., Xu X., "Microstructural characteristics in plasma sprayed functionally graded ZrO$_2$/NiCrAl coatings," Surf & Coat. Technol. 162, 194, (2003).

[52] Kondo H, Yokoyama A, Omori M, Ohkubo A, Hirai T, Watari F, Uo M, Kawasaki T. "Fabrication of titanium nitride/apatite functionally graded implants by spark plasma sintering". Mater. Trans. 45(11):3156-3162, (2004).

[53] Cojocaru CV, Wang Y, Moreau C, Lima RS, Mesquita-Guimara˜es J, Garcia E, Miranzo P, Osendi MI. "Mechanical behavior of air plasma-sprayed YSZ functionally graded mullite coatings investigated via instrumented indentation". J. Therm. Spray Technol. 20:100-108, (2010).

[54] Eriksson M, Radwan M, Shen Z. "Spark plasma sintering of WC, cemented carbide and functional graded materials". Int. J. Refract. Met. H. Mater. In press, P. 7, (2012).

[55] Mumtaz KA, Hopkinson N. "Laser melting functionally graded composition of waspaloy and zirconia powders". J. Mater. Sci. 42:7647-7656, (2007).

[56] Ouyang JH, Mei H, Kovacevic R. "Rapid prototyping and characterization of a WC-(NiSiB alloy) cermet/tool steel functionally graded material (FGM) synthesized by laser cladding". Proceedings of the Symposium on Rapid Prototyping of Materials in Proceedings of the TMS Fall Meeting, Columbus OH, 77-93, (2002).

[57] Ge CC, Wu AH, Ling YH, Cao WB, Li JT, Shen WP. "New progress of ceramic-based functionally graded plasma-facing materials in China". Key Eng. Mater. 224(2): 459-464, (2002).

[58] Mendelson, M., "Thermal protection systems for high heat flux environments" (1995).

[59] Rickerby, D.S. and Winstone, M.R. "Coatings for gas turbine engines", Materials and Manufacturing Processes, 7(4) 495-526, (1992).

[60] Sasaki, M. and Hirai, T. "Fabrication and properties of functionally gradient materials", J of Ceram Soc of Japan, 99, 1002-1013, (1991).

[61] Sohda, Y., "Carbon/carbon composites coated with SiC/C functionally gradient compositions," Ceram Trans., 34, Proc. of The Second Int'!. Symp. on FGM'92, (eds. J.B. Holt, M. Koizumi, T. Hirai, and Z.A. Munir), American Ceramic Society, Westerville,OH, 125-132, (1993).

[62] Basu S.N., Kulkarni T., Wang H.Z., Sarin V.K., "Functionally graded chemical vapor deposited mullite environmental barrier coatings for Si-based ceramics" J of Europ Ceram Soc., 28, 437–445, (2008).

[63] Kuroda, Y., "Evaluation tests of ZrO_2 /Ni", Ceram Trans., 34, Proc. of the second Int'l. symp. on FGM'92, (eds. J.B. Holt, M. Koizumi, T. Hirai, and Z.A. Munir), American Ceramic Society, Westerville, OH, 289-296, (1991).

[64] Leushake, U., "Al_2O_3/ZrO_2 graded thermal barrier coatings by EB-PVD concept, microstructure and phase stability", in Proc. of the fourth Int'l. symp. On FGM'96, (eds. I. Shiota and Y. Miyamoto), Elsevier Science B.V., Amsterdam, 263-268, (1997).

[65] Ernest S.C., "Army focused research team on functionally graded armor composites", Mater Sci and Eng, A259, 155–161, (1999).

[66] Mouchon, E. and Colomban, PH. "Microwave absorbent, preparation, mechanical properties and r.f-microwave conductivity of SiC (and/or mullite) fiber reinforced Nasicon matrix composites, J Mater Sci., 31, 323-34, (1996).

[67] Tarry, United States, Patent no. 5443917, 22, 3. Aug (1995).

[68] Homlmquist, T.J.; Rajendran, A.M.; Templeton, D.W. 4. & Bishnoi, K.D. "A ceramic armor database". TARDEC Technical Report, Jan (1999).

[69] Kumar, K.S. & DiPietro, M.S. "Ballistic penetration response of intermetallic matrix composites". Scripta Metallurgica et Materialia,31(5), 793-98, (1995).

[70] Madhu, V., Ramanjaneyulu, K.; Bhat T B., & Gupta, N.K. "An experimental study of penetration resistance of ceramic armour subjected to projectile impact". Int. J. Impact Eng. 32(1-2), 337-50. (2005).

[71] Gupta N, Bhanu Prasad V V., Madhu V., and Basu B., " Ballistic studies on TiB_2/Ti functionally graded armor ceramics", Def. Sci, J., 62 [6], 382-389, (2012).

[72] Borgioli, E., Galvanetto, E., Fossati, A., & Pradelli, G.. "Glow-Discharge and Furnace Treatments of Ti-6Al-4V, Surface Coating Technology", 184, 255-262, (2004).

[73] Sujan, D., Oo, Z., Hahman, M. E., Maleque, M. A., & Tan, C. K.. "Physio-mechanical Properties of Aluminium Metal Matrix Composites Reinforced with Alumina and Silicon Carbide". Int J of Eng and Applied Sci., 6, 288-291, (2012).

[74] Kimberly R.,.and Sujan, D." Microstructure analysis, physical and thermal properties of Al_2O_3- Al_2TiO_5 functionally graded ceramics for the application of car brake rot" Pertanika J. Sci. & Technol. 23 (1): 153 – 161, (2015).

[75] Parks, W.P., The advanced turbine systems program in the U.S.A., presented COST/98, Liege, Belgium, (1998).

[76] Rosler, J. and Tonnes, C., "Processing of Ti Al components with gradient microstructures, in Proc. of the third Int 'I. symp. on structural and functional gradient materials, (eds. B. Ilschner and N. Cherradi), Presses Polytechniques et Universitaires Romandes, Lausanne, 41-46, (1995).

[77] Drochel, M., "Tailored porosity gradient by FEM calculations for silicon carbide evaporator tubes", ibid., 820-825, (1998).

[78] Drochel M., Oberacker R., and Hoffmann M.J., "Processing of silicon carbide evaporators with porosity gradients by pressure filtration", in functionally graded materials 1998, ed.W.A.Kaysser, Mater. Sci. Forum, vols. 308-311, Trans Tech

[79] Niino, M. and Koizumi, M. "Projected research on high-efficiency energy conversion materials", ibid, 601-605, (1994).

[80] Eguchi, K., Hoshino, T., and Fujihara, T. "Performance analysis of FGM-based direct energy conversion system for space power applications", in Proc. of the third Int 'I. symp. on structural and functional gradient materials, (eds. B. Ilschner and N. Cherradi), Presses Poly techniques et Universitaires Romandes, Lausanne, 619-625, (1995).

[81] Lin J S., "One-step sintering of thermoelectric conversion units in the W/TiB_2/SiGe and W/$MoSi_2$/SiGe systems, in Functionally Graded Materials 1998, ed.W.A.Kaysser, Mater. Sci. Forum, 308-311, Trans Tech Publications Ltd., Zurich, 760-765, (1998).

[82]   Bharti I., Gupta N., and Gupta K. M., "Novel applications of functionally graded nano, optoelectronic and thermoelectric materials" Int. J of Mater, Mech and Manuf., 1[3], 221-224, (2013).

[83]   Liu Y., Compson C., and Liu M., "Nanostructured and functionally graded cathodes for intermediate temperature solid oxide fuel cells" J of Power Sources, 138, 194–198, (2004).

[84]   Itoh, Y., Takahashi, M., and Takano, H. "Design of tungsten/copper graded composite for high heat flux components", Fusion Eng. and Design, 31,279-289, (1996).

[85]   Muller E., Drasa R C., Schilz J., Kaysser W A., "Functionally graded materials for sensor and energy applications", Mater. Sci. and Eng. A., A 362 [1-2], 17-39, (2003).

[86]   Wosko M., Paszkiewicz B., Piasecki T., Szyszka A., Paszkiewicz R., and Tlaczala M., "Application of functionally graded materials in optoelectronic devices," optical Application, 35 [3], 663-667, (2005).

[87]   Baumeister H., Veuhoff E., Popp M., Hernecke H., "GRINSCH Ga In as PMQW laser structures grown by MOMBE", J. Cryst. Growth, 188 [1-4], 266-74, (1988).

[88]   Malachowski M J., "Impact of energy band-gap grading on responsivity of an $Al_xGa_{1-x}N$ ultraviolet p-n detector, Solid State Electro., 42 [6], 963-7, (1998).

[89]   Yamaguchi M., "III-V compound multi-junction solar cells: present and future", Solar Energ. Mater. And solar cells, 75 [1-2], 261-9, (2003).

[90]   Ichinose N., Miyamoto N., Takahashi S., "Ultrasonic transducers with functionally graded piezoelectric ceramics" J. Europ. Ceram. Soc., 24, 1681–1685, (2004).

[91]   Navarro A, whatmore R W. and Alcock J R. "Preparation of functionally graded PZT ceramics using tape casting" J. of Electroceramics, 13, 413–415, (2004).

[92]   Zhou C., Dengb C., Chena X., Zhaob X., Chena Y., Fana Y., Zhang X., "Mechanical and biological properties of the micro-/nano-grain functionally graded hydroxyapatite bioceramics for bone tissue engineering" J. Mech. Behav. of Biomed. Mater., 4 8, 1-11, (2015).

[93]   Lavine, M., Frisk, M., Pennisi, E., "Biomaterials introduction". Science, 338, 899, (2012).

[94]   Mehrali, M., Shirazi, F.S., Mehrali, M., Metselaar, H.S., Kadri, N.A., Osman, N.A., "Dental implants from functionally graded materials". J. Biomed. Mater. Res. Part A, 101, 3046–3057, (2013).

[95]   Zhang, Y., Sun, M.J., Zhang, D., "Designing functionally graded materials with superior load-bearing properties". Acta Biomater. 8, 1101–1108, (2012).

[96] Pompe, W., Worch, H., Epple, M., Friess, W., Gelinsky, M., Greil, P., Hempel, U., Scharnweber, D., Schulte, K., "Functionally graded materials for biomedical applications". Mater. Sci. Eng. A-Struct. 362, 40–60, (2003).

[97] Liao, X.L., Xu, W.F., Wang, Y.L., Jia, B., Zhou, G.Y., "Effect of porous structure on mechanical properties of C/PLA/nano-HA composites scaffold". Trans. Non ferr. Metals Soc. China 19, S748–S751, (2009).

[98] Maruno, S., Imamura, K., Hanaichi, T., Ban, S., Iwata, H., Itoh, H., "Characterization and stability of bioactive HA–G–Ti composite materials and bonding to bone". Bioceramics, 7, 249–254, (1994).

[99] Maruno, S., Itoh, H., Ban, S., Iwata, H., Ishikawa, T., "Micro- observation and characterization of bonding between bone and Ha–glass–titanium functionally gradient composite". Biomaterials, 12, 225–230, (1991).

[100] Kumar, R.R., Maruno, S., "Functionally graded coatings of HA–G–Ti composites and their in vivo studies". Mater. Sci. Eng. A-Struct., 334, 156–162, (2002).

[101] Campo, R.D., Savoini, B., Munoz, A., Monge, M.A., Garces, G., "Mechanical properties and corrosion behavior of Mg–HAP composites". J. Mech. Behav. Biomed. Mater. 39C, 238–246, (2014).

[102] Kraaij, G., Zadpoor, A.A., Tuijthof, G.J., Dankelman, J., Nelissen, R. G., Valstar, E.R., "Mechanical properties of human bone- implant interface tissue in aseptically loose hip implants". J. Mech. Behav. Biomed. Mater. 38, 59–68, (2014).

[103] Dorozhkin, S.V., "Nanosized and nanocrystalline calcium orthophosphates". Acta Biomater. 6, 715–734, (2010).

[104] Kandori, K., Kuroda, T., Togashi, S., Katayama, E., "Preparation of calcium hydroxyapatite nanoparticles using microreactor and their characteristics of protein adsorption". J. Phys. Chem. B 115, 653–659, (2011).

[105] Zhou, C.C., Hong, Y.L, Zhang, X.D., "Applications of nanostructured calcium phosphate in tissue engineering". Biomater. Sci. 1, 1012–1028, (2013).

[106] Balasundaram, G., Sato, M., Webster, T.J., "Using hydroxyapatite nanoparticles and decreased crystallinity to promote osteoblast adhesion similar to functionalizing with RGD". Biomaterials 27, 2798–2805, (2006).

[107] Kim, D.W., Cho, I.S., Kim, J.Y., Jang, H.L., Han, G.S., Ryu, H.S., Shin, H., Jung, H.S., Kim, H., Hong, K.S., "Simple large-scale synthesis of hydroxyapatite nanoparticles: in situ observation of crystallization process". Langmuir: ACS J. Surf. Colloids 26, 384–388, (2010).

[108] Guo, W.G., Qiu, Z.Y., Cui, H., Wang, C.M., Zhang, X.J., Lee, I.S., Dong, Y.Q., Cui, F.Z., "Strength and fatigue properties of three-step sintered dense nanocrystal hydroxyapatite bioceramics". Front. Mater. Sci. 7, 190–195, (2013).

[109] Leong K.F., Chuna C.K., Sudaramadji N., and Yeong W.Y., "Engineering functionally graded tissue engineering scaffolds," J. Mech. Behav. of Biomed. Mater., 1, 140-152, (2008).

[110] Limarga A.M., Widjaja S., and Yip T.H., "Mechanical properties and oxidation resistance of plasma-sprayed multilayered Al_2O_3/ZrO_2 thermal barrier coatings," Surface &coatings Tech., 197, 93-102, (2005).

[111] Negahdari Z., Willert-Porada M., Scherm F., "Development of novel functionally graded Al_2O_3-lanthanum hexaaluminate ceramics for thermal barrier coatings", Mater. Sci. Forum, 631-632, 97-102, (2010).

[112] Cherradi N., Kawasaki A., Gasik M., "Worldwide trends in functional gradient materials research and development", Compos. Eng., 4[8], 883-894, (1994).

[113] Miyamoto, Y. "Development of symmetric gradient structures for hyper functional materials by SHS /HIP compaction", in Proc. 8'h CIMTEC, Intelligent Materials and Systems, Florence, 87-98, (1995).

[114] Cline, C.F. "Preparation and properties of gradient TiC cermet cutting tools, in proc the third Int'/. symp. on structural and functional gradient materials, (eds. B. Ilschner and N. Cherradi), Presses Poly techniques et Universitaires Romandes, Lausanne, 595-595, (1995).

[115] Zhao J., Ai X., Deng J., Wang J., "Thermal shock behaviors of functionally graded ceramic tool materials, "J. Europ. Ceram. Soc., 24 847–854, (2004).

[116] Kaysser, W.A. and IIschner, B. FGM research activities in Europe, MRS Bull., 20(1) 22-6, (1995).

[117] Gasik, M. Principles of functional gradient materials and their processing by powder metallurgy, Acta Polytechnica Scand., Ch. 226, (1995).

[118] Shapovalov, V I., Porous metals, MRS Bull. 19(4) 24-8, (1994).

[119] Ekstrorm T. and Ingelstorm I., "Characterization and properties of SiAlON materials". In proc. Int. conf. non-oxide technical and engineering ceramics, ed. S. Hampshire. Elsevier Applied Science, London, UK, 231–253, (1986).

[120] Chen L., Kny E. and Groboth G., "SiAlON ceramic with gradient microstructures". Surface and Coating Technology, 100–101, 320–323, (1998).

[121] Jiang, X. and Kang, L., "Formation of -sialon layer on -sialon its effect on mechanical properties". J. Am. Ceram. Soc., 81, 1907–1912, (1998).

[122] Mandal, H., Thomson, D. P. and Ekstrom, T., "Reversible α- β SiAlON transformation in heat-treated SiAlON ceramics". J. Eur. Ceram. Soc., 12, 421–429, (1993).

[123] Calis N., Kushan R S., Kara F., Mandal H., "Functionally graded SiAlON ceramics", J. Europ. Ceram. Soc., 24, 3387–3393, (2004).

[124] Zhang X., Li W., Hong C., Han W. andHan J., "A novel development of ZrB_2/ZrO_2 functionally graded ceramics for ultrahigh-temperature application", Scripta Materialia, 59. 1214–1217, (2008).

[125] Atiyah A A., and Aziz A T., "Design and Modelling of (Fe /ZrO_2) functionally graded materials (Part I)"., Eng. & Tech. Journal,Vol.32, Part (A), No.7, (2014).

[126] Gnomes F., Barbosa J. and Ribeiro C S., "Evaluation of Functionally Graded Ceramic Crucible for Induction Melting of TiAl Based Alloys," Mater. Sci. Forum., 730-732, 769-774, (2012).

New Processing Routes
for Functionally Graded Materials
and Structures through Combinations
of Powder Metallurgy and Casting

Takahiro Kunimine, Hisashi Sato, Eri Miura-Fujiwara and
Yoshimi Watanabe

Additional information is available at the end of the chapter

http://dx.doi.org/10.5772/62393

Abstract

New processing routes for metal-matrix functionally graded materials (FGMs) and structures through combinations of powder metallurgy and casting are described in this chapter. Centrifugal mixed-powder method is introduced as a processing method for metal-matrix FGMs at first. The centrifugal mixed-powder method is a developed technique of centrifugal casting by setting predesigned mixed powder in a spinning mold in advance. As an example of processed FGMs by this method in our previous studies, Cu-based FGMs with dispersed diamond particles are shown. Graded structures in the Cu-based FGMs are investigated through scanning electron microscope (SEM) observations of microstructures. As the latest processing method for metal-matrix FGMs developed by our research group, centrifugal sintered-casting method is shown. The centrifugal sintered-casting method is a modified processing technique of the centrifugal mixed-powder method. In the centrifugal sintered-casting method, FGMs are processed by the combination of centrifugal sintering and centrifugal casting. Al–Si alloy and Cu-based FGMs with dispersed diamond particles are introduced as examples. Applications of metal-matrix FGMs processed by the centrifugal sintered-casting method are also described. Fabricated metal-matrix FGMs can be used as grinding wheel and applied to carbon fiber-reinforced plastic (CFRP) machining.

Keywords: Functionally graded materials (FGMs), Metal-matrix composite, Powder metallurgy, Centrifugal sintering, Centrifugal casting

1. Introduction

New processing routes for metal-matrix functionally graded materials (FGMs) and structures through combinations of powder metallurgy and casting are described in this chapter. FGMs are well known as a relatively new class of inhomogeneous composite materials having property gradient. The property gradient in the FGMs is caused by a position-dependent chemical composition, microstructure, or atomic order [1]. These FGMs are generally fabricated based on powder metallurgy, melt-processing technique, chemical vapor deposition, physical vapor deposition and so on.
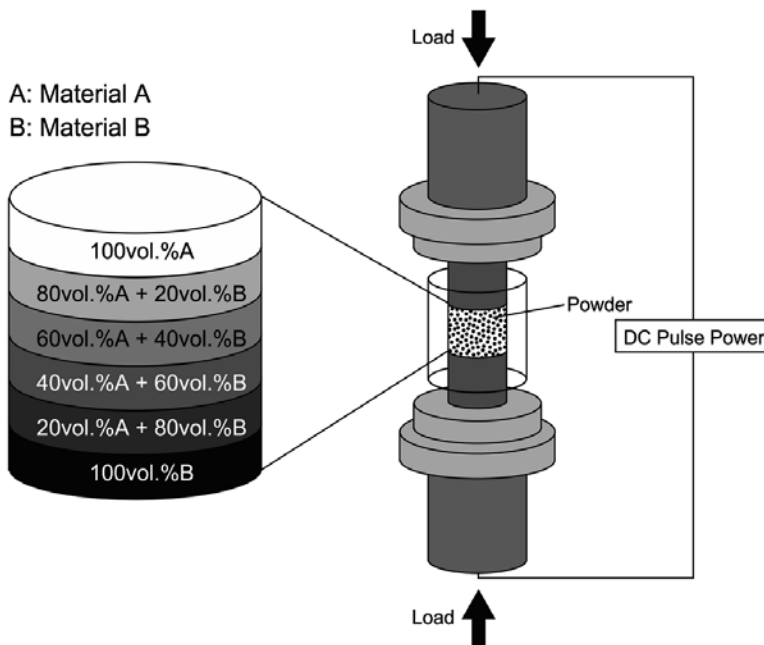
Figure 1. A schematic illustration showing a typical fabrication process of FGMs by the powder metallurgy method through spark plasma sintering (SPS).

Figure 1 shows a schematic illustration of a typical fabrication process of FGMs by the powder metallurgy method through spark plasma sintering (SPS). At first, mixed powders with various ratios of materials A and B are prepared. Predesigned mixed powders are stacked inside a die for the SPS as shown in Figure 1. The case of six-graded composition layers is shown in Figure 1. The number of graded layers can be freely chosen. Then, FGMs with stepwise graded structure can be obtained by sintering these powders with an SPS machine. Ti–ZrO_2 FGMs with stepwise graded structure were fabricated by this method in our previous study [2]. A continuous graded structure can also be obtained by this method with a green body having continuous graded composition. For example, Ti–ZrO_2 FGMs were fabricated by this method in our previous studies [3, 4].

The melt-processing technique is also an effective way to fabricate continuous graded struc-
ture. In terms of melt-processing techniques to fabricate metal-based FGMs, various kinds of
centrifugal method were developed: centrifugal casting [5–7], centrifugal solid-particle
method [8, 9], centrifugal *in situ* method [10, 11], and so on. The centrifugal casting is a
processing method that uses centrifugal force caused by rotation of a mold. By the centrifugal
force in the rotating mold including molten metal and solid particles, compositional gradient
due to the difference of the material densities between the molten metal and the solid particles
is generated. By controlling these phenomena, FGMs can be fabricated. Basically, both the
centrifugal solid-particle method and the centrifugal *in-situ* method are based on the centri-
fugal casting. The centrifugal solid-particle method can be conducted at a temperature of
liquid–solid coexistence in alloy systems, such as Al–Ti [8, 9]. On the other hand, the centrifugal
in-situ method can be made at a temperature of liquid phase in alloy systems, such as Al–Ni
[10] and Al–Cu [11]. By using these processing techniques, various kinds of FGMs having
specific graded distributions of reinforcement can be made.

As new melt processing techniques, centrifugal mixed-powder method [12–15] and centrifugal
sintered-casting method [16, 17] have been recently developed. These two melt processing
techniques are introduced in this chapter. Applications of metal-matrix FGMs processed by
the centrifugal sintered-casting are also described. Fabricated metal-matrix FGMs can be used
as grinding wheel and applied to carbon fiber-reinforced plastic (CFRP) machining [17].

2. Materials processing

2.1. Centrifugal mixed-powder method

Many attempts to fabricate FGMs have been done by the centrifugal casting [5–7]. Generally,
the finer dispersed particle size becomes, the more difficult to disperse them into molten
matrix. The equation for velocity of a solid particle in a viscous liquid can be written as:

$$\frac{dx}{dt} = \frac{\left|\rho_p - \rho_m\right| G g D_p^2}{18\eta} \tag{1}$$

where ρ_p is density of particles, ρ_m density of molten matrix, g gravitational acceleration, D_p
particle diameter, and η viscosity of melt [7]. Since the velocity of a solid particle in a viscous
liquid is dependent on the square of the particle diameter D_p, it is quite difficult to control
graded distributions of dispersion nanoparticles in FGMs in the case of the conventional
centrifugal casting. As a new processing technique for metal-matrix FGMs, the centrifugal
mixed-powder method is proposed by Watanabe et al. [12] for overcoming these problems.
The centrifugal mixed-powder method could give us fine particle-dispersed FGMs by using
a combination of high centrifugal force and mixed powder. This new method is a devel-
oped technique of the centrifugal casting by setting predesigned mixed powder in a mold in
advance [12].
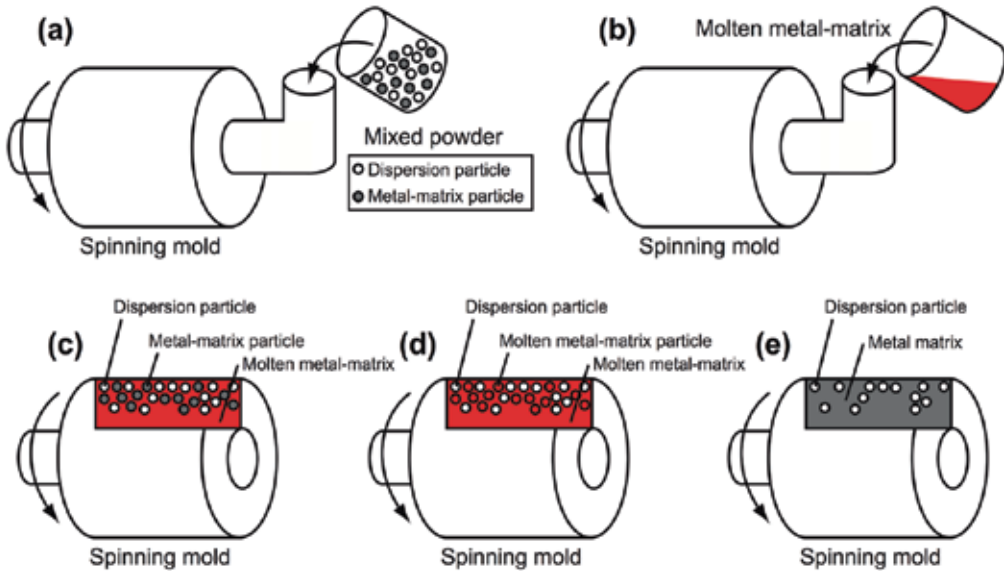
Figure 2. A schematic illustration showing the process of the centrifugal mixed-powder method [12].

Figure 2 shows the experimental procedure of the centrifugal mixed-powder method. At first, a predesigned mixed powder is prepared. This mixed powder consists of metal-matrix particles and dispersion particles. Basically, the melting point of dispersion particles should be higher than that of metal-matrix particles to form FGMs. Particles such as ceramics, metals, and alloys that have higher melting points compared with metal matrix can be chosen as dispersion particles for metal-matrix FGMs. The mixed powder including metal-matrix particles and dispersion particles is inserted into a spinning mold as shown in Figure 2(a). After that, a metal-matrix ingot is melted in a crucible. This molten metal matrix is poured into the spinning mold as shown in Figure 2(b). The poured molten metal matrix penetrates into the space between the particles due to the applied centrifugal force as shown in Figure 2(c). The heat from the poured molten matrix melts the metal-matrix particles as shown in Figure 2(d). Finally, ring- or disc-shaped FGMs or structures having dispersion particles distributed in the outer part of the cast sample can be obtained as shown in Figure 2(e). FGMs, such as Cu/SiC [12], Al/TiO$_2$ [12], and Al/Al$_3$Ti/Ti [15], were obtained with this processing method in our previous studies.

The centrifugal mixed-powder method can also be performed by using centrifugal casting machines which are commercially available. Figure 3 shows a typical appearance of vacuum centrifugal casting machine supplied by Yasui & Co, Japan. This centrifugal casting machine has a heating coil, a straight arm, a crucible, a mold, and a balancer inside the casting chamber [18]. By setting predesigned mixed powder in the mold in advance, FGMs can be obtained. By using this processing method, Cu/diamond [13], Al alloy/diamond [14], and the other FGMs
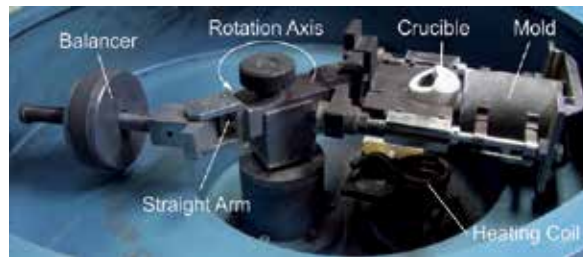
Figure 3. A typical appearance of vacuum centrifugal casting machine.

were fabricated in our previous studies. Detailed processing method and microstructural characterization of fabricated Cu/diamond FGMs are shown below.
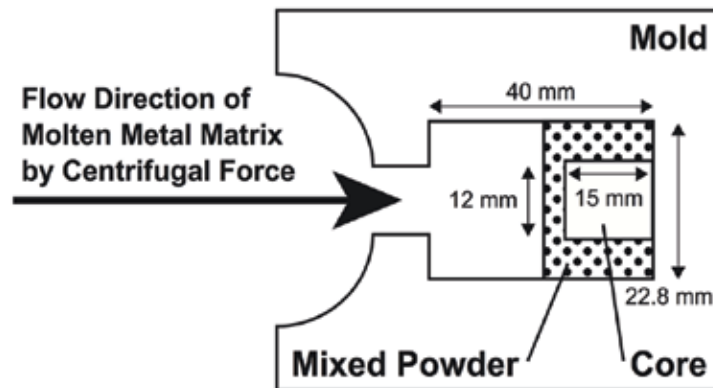

Figure 4. A cross-sectional drawing of a mold for centrifugal casting.

A cross-sectional drawing of a mold for centrifugal casting is shown in Figure 4. The mold has a cylindrical casting pattern with 40 mm width and 22.8 mm diameter. A cylindrical core with 15 mm width and 12 mm diameter is also attached in the mold as shown in Figure 4. Since fabricated FGMs can be applied to grinding wheel for mechanical machining as described in Section 3, these pattern and core are required. Dendritic-shaped Cu particles in the mean particle diameter of approximately 22 μm and 100/120 mesh diamond particles (149 μm in JIS B 4130) were used. Both the particles were mixed in a mortar. The volume fraction of diamond to Cu was chosen as 25 vol.%. The mixed powder was inserted into the mold as shown in Figure 4. Then, molten Cu was cast into the spinning mold by applying centrifugal force with the vacuum centrifugal casting machine in vacuum at 1473 K and 1573 K. The mold was spun for 99 s. The calculated applied G number (ratio of centrifugal force to gravity) at the top of mold along the direction of centrifugal force was about 36 G.

Figure 5 shows Cu/diamond FGMs cast at 1473 K (Fig. 5a) and 1573 K (Fig. 5b) [13]. As these samples were fabricated for an application as grinding wheel, these cast samples have hollows for attaching pulley. It was observed that consolidated mixed-powder area kept leaning to the
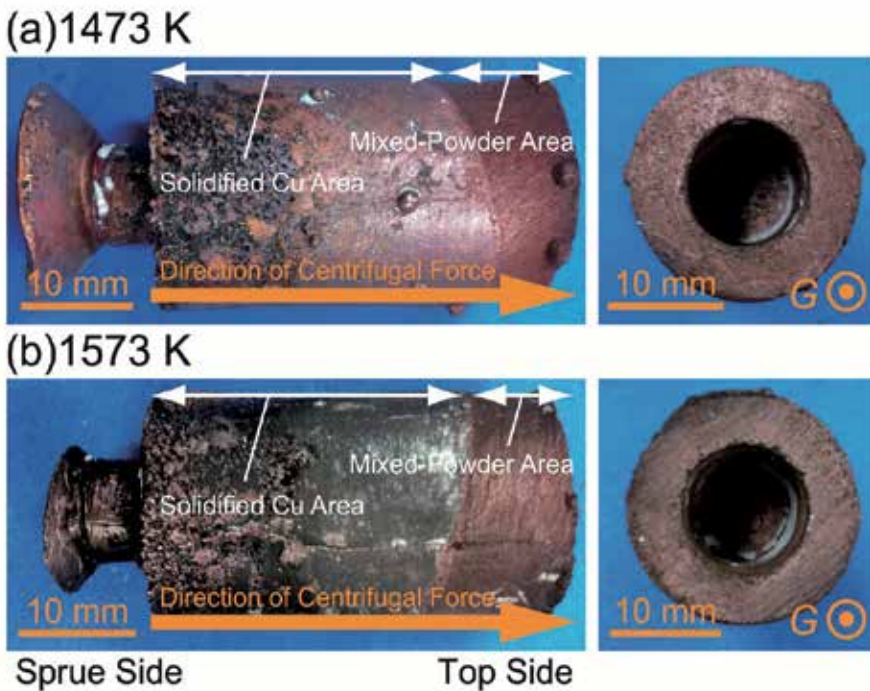
Figure 5. Cu/diamond FGMs fabricated by the centrifugal mixed-powder method. Casting temperatures were 1473 K (a) and 1573 K (b) [13].

right side of the cast sample, that is, the position of maximum centrifugal force as shown in Figure 5. Since density of diamond (3.52 Mg/m^3) was smaller than that of molten Cu (8.00 Mg/m^3), a little amount of diamond particles were distributed around surface at sprue side due to the molten metal flow. A graded structure should be made by this difference of density between diamond and Cu.

Cross-sectional observations were carried out with scanning electron microscope (SEM) to investigate diamond dispersion behavior after casting at 1473 K. Figure 6 shows a backscattered electron compositional image showing a cross section of the Cu-based diamond graded cast sample fabricated without pulley hollow [13]. Diamond particles were distinguished from Cu matrix as black colored area in the sample. It should be noted that the distribution of diamond particles in the inner part of the cast sample also biased to the top side (right side) as shown in Figure 6. It was also confirmed that obvious traces or boundaries of Cu particles were not observed although voids were seen around some diamond particles. Therefore, Cu particles in the predesigned mixed powder were fully melted and fused each other due to heat transfer from the poured molten Cu.

The number of diamond particles and the mean diameter of diamond particles at each divided area along the direction of centrifugal force were measured. The results are shown in Figures 7 and 8, respectively. These data were taken from the cross-sectional image of the cast sample
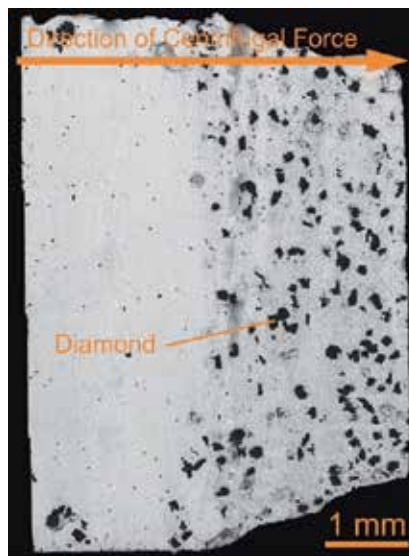
Figure 6. A backscattered electron compositional image showing a cross section of the Cu-based diamond graded cast sample obtained by the centrifugal mixed-powder method [13].
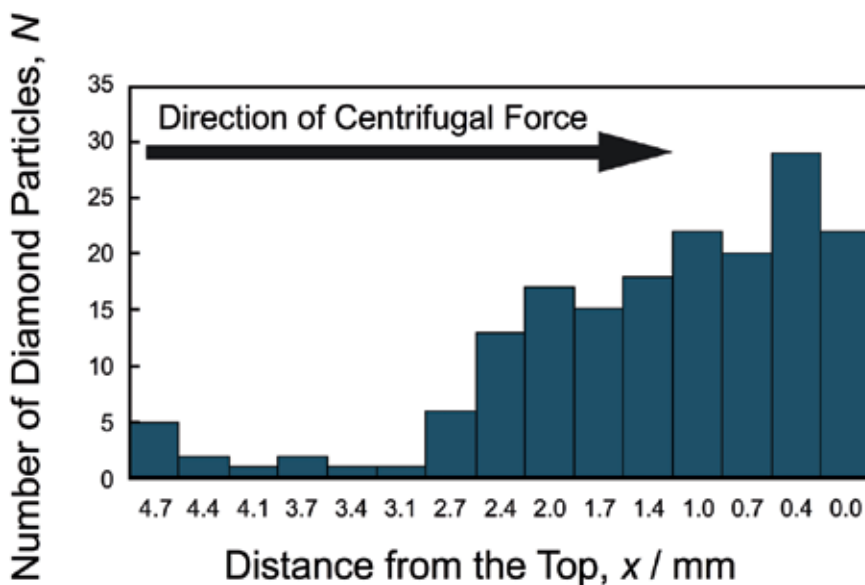
Figure 7. The number of diamond particles as a function of distance from the top of Cu/diamond cast sample [13].

as shown in Figure 6. In Figure 7, the number of diamond particles was drastically decreased at around 3 mm from the top, where the mixed powder was inserted before the centrifugal casting. The result indicates that the mixed powder was compressed and immobilized by pressure of molten metal due to centrifugal force. Whereas diamond particles were sufficiently
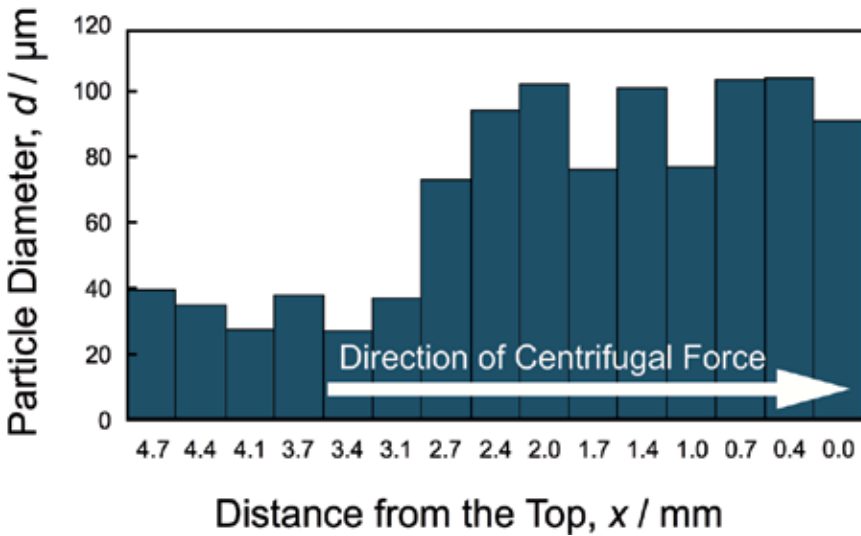
Figure 8. The particle diameter as a function of distance from the top of Cu/diamond cast sample [13].

immobilized by Cu particles between diamond particles, graded distribution of diamond particles was successfully obtained. Within the diamond particles densely dispersed region between 0 and 3 mm from the top of the Cu/diamond cast sample, the number of diamond particles increased with approaching to the top of the Cu/diamond cast sample. Thus, the Cu/ diamond FGMs were successfully fabricated by the centrifugal mixed-powder method. On the other hand, the particle diameter distribution between 0 and 3 mm is almost homogeneous as shown in Figure 8. The mean diameters of diamond particles in this range are 80–100 μm. In the distance from the top, between 3 and 5 mm, particle diameter distribution is also homogeneous. However, the mean diameters of diamond particles in this range are 30–40 μm. These results may suggest that collision of Cu molten metal with the mixed powder at surface of the powder area washed away part of the diamond particles, and molten Cu flow sent it to the surface at the sprue side. This phenomenon is not appropriate for production of FGMs. To overcome this problem, a modified processing method is described in the next section.

2.2. Centrifugal sintered-casting method

As the latest processing method for metal-matrix FGMs developed by our research group, centrifugal sintered-casting method is shown in this section. The centrifugal sintered-casting method is a modified processing technique of the centrifugal mixed-powder method. In the centrifugal sintered-casting method, FGMs are processed by the combination of centrifugal sintering and centrifugal casting [16, 17]. As described in Section 2.1, the centrifugal mixed-powder method enables us to fabricate metal-matrix FGMs. Especially, the centrifugal mixed-powder method is an effective way to fabricate metal-matrix FGMs reinforced with nanoparticles [12]. However, predesigned powder mixtures tended to flow away during the centrifugal casting in the case of some combinations of powders in the centrifugal mixed-

powder method. As an attempt to overcome this problem, the centrifugal sintered-casting method is developed through the combination of centrifugal sintering and centrifugal casting.
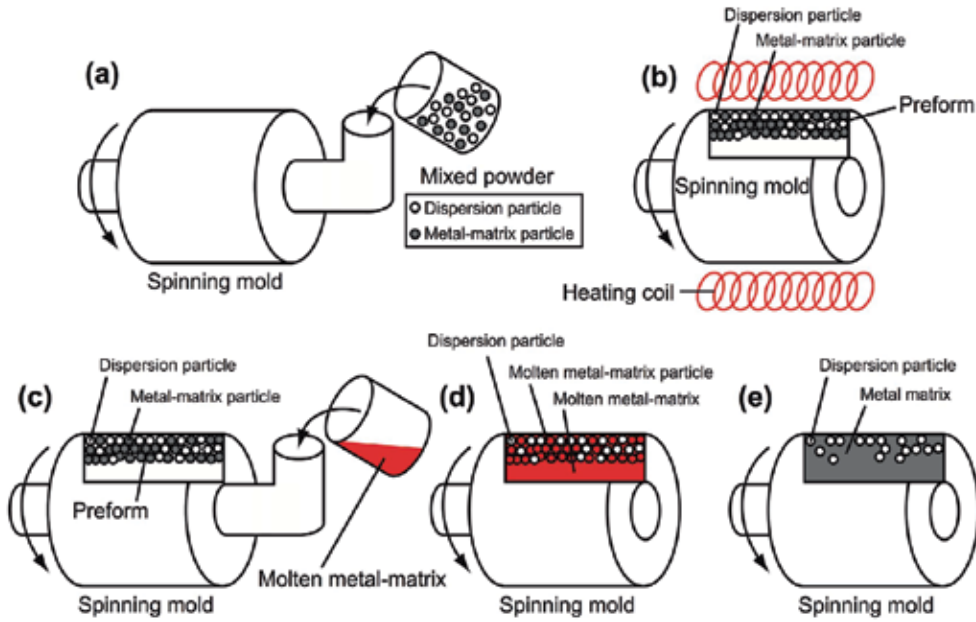
Figure 9. A schematic illustration showing the process of the centrifugal sintered-casting method [17].

Figure 9 shows a schematic illustration of the process of the centrifugal sintered-casting method [17]. In the centrifugal sintered-casting method, a ring-shaped metal-matrix preform with dispersed particles is produced by the centrifugal sintering at first. Predesigned mixed powder of dispersion particles and metal-matrix particles is inserted into a spinning mold as shown in Figure 9(a). Basically, the melting point of dispersion particles should be higher than that of metal-matrix particles to form FGMs in this method as well. Subsequently, the mixed powder is sintered under centrifugal force by heating coils to fabricate a preform as shown in Figure 9(b). Then, molten metal matrix is poured into the fabricated preform by the centrifugal casting to obtain metal-matrix FGMs as shown in Figure 9(c). The molten metal matrix penetrates into the space between the particles by the applied centrifugal force as shown in Figure 9(d). At the same time, the metal matrix particles are melted by the heat from the molten metal matrix. Finally, ring- or disc-shaped FGMs with dispersed particles distributed in the outer part of the samples can be obtained as shown in Figure 9(e).

In our previous studies, Al–Si and Cu were selected as metal matrix to fabricate Al–Si alloy/ diamond and Cu/diamond FGMs, respectively [16, 17]. Al–Si alloy particles and Cu particles were uniformly mixed with diamond particles, respectively. The volume fraction of diamond particles in mixed powder was chosen as 10 vol.%. The predesigned mixed powder

was set in the cylindrical mold having a rotational axis of 20 mm diameter and 30 mm length, respectively. The mixed powders were sintered in the spinning cylindrical mold under the centrifugal force of about 280 G at 843 K in argon atmosphere for Al–Si alloy/diamond particles [16] and 1100 G at 1273 K in vacuum for Cu/diamond particles [17], respectively. Then, the centrifugal casting was performed under the centrifugal force of about 78 G at 1373 K with pouring molten Al in the case of Al–Si alloy/diamond preform [16]. In the same way, molten Cu was poured into the Cu/diamond preform in the mold under the centrifugal force of about 34 G at 1393 K [17].
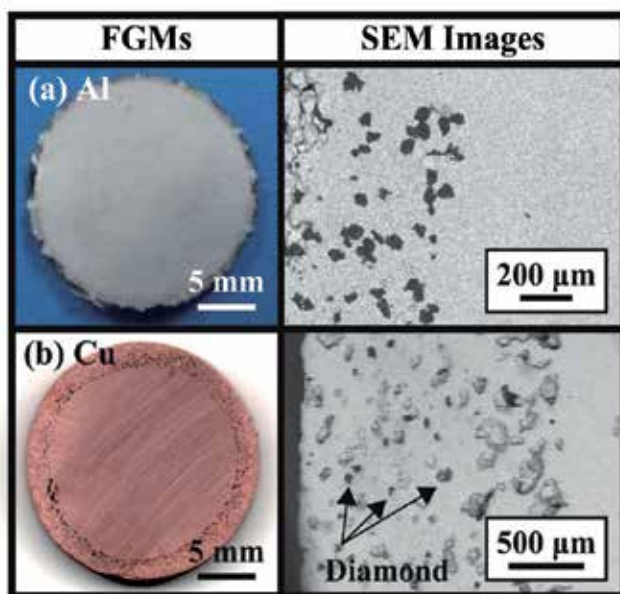
Figure 10. Macrographs of Al–Si alloy based (a) and Cu-based (b) FGMs with dispersed diamond particles fabricated by the centrifugal sintered-casting method and SEM images showing the microstructures of the outer part of the cast samples [16, 17].

Figure 10 shows macrographs of Al–Si alloy and Cu-based FGMs with dispersed diamond particles fabricated by the centrifugal sintered-casting method. SEM images showing the microstructures of the outer part of the Al–Si alloy and Cu-based FGMs are also shown in Figure 10. It should be noted that the diamond particles were distributed at only outer part of the cast samples as shown in Figure 10. The centrifugal sintered-casting method is an effective way to fabricate metal-matrix FGMs.

3. Applications of FGMs processed by the centrifugal sintered-casting

In this section, applications of metal-matrix FGMs processed by the centrifugal sintered-casting method are introduced. As described in Section 2.2, Al–Si alloy/diamond and Cu/

diamond FGMs were fabricated by the centrifugal sintered-casting method. Diamond plays important role as abrasive in the field of mechanical machining. Recently, CFRP is widely used as main structural parts for aircraft due to its high strength, stiffness, and lightweight [19]. However, some issues about occurring defects, such as fiber pullout, delamination, burrs, and splintering, have become problems in machining CFRP by common drills. These technical issues have led numerous researchers to seek solutions for precision machining of CFRP [20–23]. The key issue of precision machining of CFRP has been obtaining good hole quality in the aircraft industry. In addition, tool change is frequently required in drilling CFRP in many practical situations. Therefore, the improvement of tool life for machining CFRP is important subject since high-priced diamond grains have been widely used as abrasive.
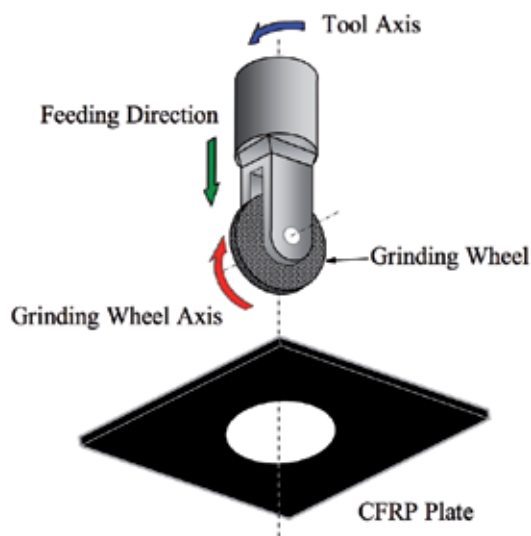
Figure 11. A schematic illustration of the gyro-driving grinding wheel system [24].

A novel CFRP machining equipment, that is, gyro-driving grinding wheel system for machining CFRP was recently developed [24–26]. The gyro-driving grinding wheel system was developed for overcoming problems related to defect issues during mechanical machining. Figure 11 shows a schematic illustration of the gyro-driving grinding wheel system [24]. In the gyro-driving grinding wheel system, a grinding wheel is used instead of drill bits for drilling CFRP. The equipped grinding wheels required toughness as a desirable mechanical property as the grinding wheel was subjected to the torsion force in the gyro-driving grinding wheel system. In the previous studies [17, 24], holes with good quality in CFRP plates have been obtained without defects by this machining system equipped with our fabricated metal-matrix FGMs.

CFRP drilling tests were performed with the gyro-driving grinding wheel system equipped with fabricated Cu/diamond FGMs as a grinding wheel. Cu was selected as metal matrix for its mechanical properties and high thermal conductivity. Diamond particles were used as

abrasive in Cu matrix for machining CFRP. CFRP drilling tests were carried out with feed rate of 5 mm/min, peripheral wheel speed of 7000 rpm, spindle speed of 2800 rpm, and dry machining. Bidirectional CFRP composite laminates having thickness of 5 mm were used as workpiece material. Photographs of a hole having diameter of 20 mm drilled by the gyro-driving grinding wheel system equipped with fabricated Cu/diamond FGMs as a grinding wheel (Fig. 12a) and the one having diameter of 10 mm drilled by a conventional drill bit (Fig. 12b) in CFRP plates are shown in Figure 12. Delamination and burrs were seen in the drilled CFRP plate in the case of the conventional drill bit. It should be noted that precision drilling of CFRP plate without burring and delamination were achieved by the gyro-driving grinding wheel system equipped with fabricated Cu/diamond FGMs as grinding wheel. In this way, FGMs fabricated by the centrifugal sintered-casting method have been attempted to apply for the practical use.
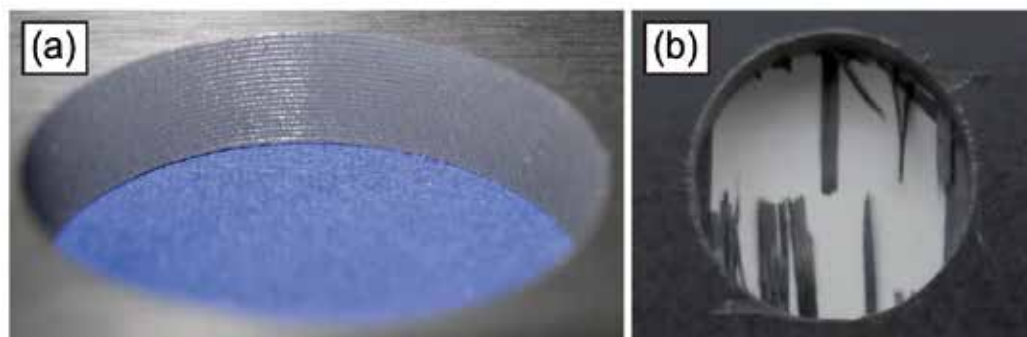
Figure 12. Drilled hole having diameter of 20 mm made by the gyro-driving grinding wheel system equipped with fabricated Cu/diamond FGMs as a grinding wheel (a) and the one having diameter of 10 mm made by a conventional drill bit (b) in CFRP plates [17].

As the other possibilities for application of FGMs, materials for heat sink can be considered as candidate. Nowadays, thermal management materials such as heat sink for microelectronics and semiconductors have been investigated, extensively [27–30]. The materials currently used for heat sinks are Al and Cu due to their high thermal conductivity in metals and alloys. The thermal conductivities of Al and Cu are about 250 and 400 $W\,m^{-1}\,K^{-1}$, respectively. On the other hand, diamond is well known as the material having the highest thermal conductivity in materials. To enhance the thermal conductivity of heat sink materials, Al/diamond and Cu/diamond composites are promising materials. Our Al alloy/diamond and Cu/diamond FGMs fabricated by the centrifugal sintered-casting method might work as well in this field.

4. Summary

Two kinds of new processing routes for metal-matrix FGMs through combinations of powder metallurgy and casting were developed: the centrifugal mixed-powder method and the

centrifugal sintered-casting method. Metal-matrix FGMs were obtained by these two methods. These processing methods enable us to overcome existing problems in the conventional fabrication process of FGMs. Fabricated FGMs were also applied to machining CFRP as an attempt for the practical use. Continued studies for fabrication processes of FGMs and the gyro-driving grinding wheel system are still required to put them into practical use in the future. Further investigations should open up a new field of and a market for FGMs.

Acknowledgements

Author details

Takahiro Kunimine[1,2,3*], Hisashi Sato[1], Eri Miura-Fujiwara[1,4] and Yoshimi Watanabe[1]

*Address all correspondence to: kuniminet9@gmail.com

1 Nagoya Institute of Technology, Nagoya, Japan

2 Kyoto University, Kyoto, Japan

3 Kanazawa University, Kanazawa, Japan

4 University of Hyogo, Himeji, Japan

References

[1] Kieback B, Neubrand A, Riedel H. Processing techniques for functionally graded materials. Materials Science and Engineering A. 2003;362:81–105. DOI:10.1016/S0921-5093(03)00578-1.

[2] Tsukamoto H, Kunimine T, Yamada M, Sato H, Watanabe Y. Microstructure and mechanical properties of Ti-ZrO$_2$ composites fabricated by spark plasma sintering. Key

Engineering Materials. 2012;520:269–275. DOI:10.4028/www.scientific.net/KEM.520.269.

[3] Watanabe Y, Miura-Fujiwara E, Sato H. Fabrication of functionally graded materials by centrifugal slurry-pouring method and centrifugal mixed-powder method. Journal of the Japan Society of Powder and Powder Metallurgy. 2010;57:321–326. DOI:10.2497/jjspm.57.321.

[4] Jayachandran M, Tsukamoto H, Sato H, Watanabe Y. Formation behavior of continuous graded composition in Ti–ZrO$_2$ functionally graded materials fabricated by mixed-powder pouring method. Journal of Nanomaterials. 2013;2013. Article ID: 504681. 8 pages. DOI:10.1155/2013/504631.

[5] Fukui Y. Fundamental investigation of functionally gradient material manufacturing system using centrifugal force. JSME International Journal. Ser. 3, Vibration, Control Engineering, Engineering for Industry. 1991;34:144–148. DOI:10.1299/jsmec1988.34.144.

[6] Fukui Y, Watanabe Y. Analysis of thermal residual stress in a thick-walled ring of duralcan-base Al-SiC functionally graded material. Metallurgical and Materials Transactions A. 1996;27:4145–4151. DOI:10.1007/BF02595662.

[7] Watanabe Y, Yamanaka N, Fukui Y. Control of composition gradient in a metal-ceramic functionally graded material manufactured by the centrifugal method. Composites Part A: Applied Science and Manufacturing. 1998;29:595–601. DOI:10.1016/S1359-835X(97)00121-8.

[8] Watanabe Y, Yamanaka N, Fukui Y. Wear behavior of Al-Al$_3$Ti composite manufactured by a centrifugal method. Metallurgical and Materials Transactions A. 1999;30:3253–3261. DOI:10.1007/s11661-999-0235-1.

[9] Watanabe Y, Eryu H, Matsuura K. Evaluation of three-dimensional orientation of Al$_3$Ti platelet in Al-based functionally graded materials fabricated by a centrifugal casting technique. Acta Materialia. 2001;49:775–783. DOI:10.1016/S1359-6454(00)00384-0.

[10] Watanabe Y, Sato R, Matsuda K, Fukui Y. Evaluation of particle size and particle shape distributions in Al-Al$_3$Ni FGMs fabricated by a centrifugal in-situ method. Science and Engineering of Composite Materials. 2004;11:185–200. DOI:10.1515/SECM.2004.11.2-3.185.

[11] Watanabe Y, Oike S. Formation mechanism of graded composition in Al-Al$_2$Cu functionally graded materials fabricated by a centrifugal in situ method. Acta Materialia. 2005;53:1631–1641. DOI:10.1016/j.actamat.2004.12.013.

[12] Watanabe Y, Inaguma Y, Sato H, Miura-Fujiwara E. A novel fabrication method for functionally graded materials under centrifugal force: The centrifugal mixed-powder method. Materials. 2009;2:2510–2525. DOI:10.3390/ma2042510.

[13] Miura-Fujiwara E, Sato H, Yamada M, Watanabe Y. Fabrication of metal-based functionally graded grinding wheel by a centrifugal mixed-powder method. Materials Science Forum. 2012;706–709:661–666. DOI:10.4028/www.scientific.net/MSF. 706-709.661.

[14] Kunimine T, Yamada M, Sato H, Watanabe Y. Fabrication of aluminum alloy-based diamond grinding wheel by the centrifugal mixed-powder method for novel machining technology of CFRP. In: Proceedings of the 13th International Conference on Aluminum Alloys (ICAA13); 3–7 June 2012; Pittsburgh. New Jersey: Wiley; 2012. pp. 189–194. DOI:10.1002/9781118495292.ch29.

[15] Yamauchi K, Kunimine T, Sato H, Watanabe Y. Grain refinement of Al_3Ti dispersed aluminum matrix composites by reaction centrifugal mixed-powder method. Materials Transactions. 2015;56:99–107. DOI:10.2320/matertrans.L-M2014841.

[16] Watanabe Y, Shibuya M, Sato H. Fabrication of Al/diamond particles functionally graded materials by centrifugal sintered-casting method. Journal of Physics: Conference Series. 2013;419. Article ID: 012002. 4 pages. DOI: 10.1088/1742-6596/419/1/012002.

[17] Kunimine T, Shibuya M, Sato H, Watanabe Y. Fabrication of copper/diamond functionally graded materials for grinding wheels by centrifugal sintered-casting. Journal of Materials Processing Technology. 2015;217:294–301. DOI:10.1016/j.jmatprotec. 2014.11.020.

[18] Watanabe Y, Hattori Y, Sato H. Distribution of microstructure and cooling rate in Al-Al_2Cu functionally graded materials fabricated by a centrifugal method. Journal of Materials Processing Technology. 2015;221:197-204. DOI:10.1016/j.jmatprotec. 2015.01.028.

[19] Pimenta S, Pinho ST. Recycling carbon fibre reinforced polymers for structural applications: Technology review and market outlook. Waste Management. 2011;31:378–392. DOI:10.1016/j.wasman.2010.09.019.

[20] Lin SC, Chen IK. Drilling carbon fiber-reinforced composite material at high speed. Wear. 1996;194:156–162. DOI:10.1016/0043-1648(95)06831-7.

[21] Chen WC. Some experimental investigations in the drilling of carbon fiber-reinforced plastic (CFRP) composite laminates. International Journal of Machine Tools & Manufacture. 1997;37:1097–1108. DOI:10.1016/S0890-6955(96)00095-8.

[22] Faraz A, Biermann D, Weinert K. Cutting edge rounding: An innovative tool wear criterion in drilling CFRP composite laminates. International Journal of Machine Tools & Manufacture. 2009;49:1185–1196. DOI:10.1016/j.ijmachtools.2009.08.002.

[23] Wang X, Kwon PY, Sturtevant C, Kim D, Lantrip J. Tool wear of coated drills in drilling CFRP. Journal of Manufacturing Processes. 2013;15:127–135. DOI:10.1016/j.jmapro.2012.09.019.

[24] Watanabe Y, Miura-Fujiwara E, Sato H, Takekoshi K, Tsuge H, Kaga T, Bando N, Yamagami S, Kurachi K, Yokoyama H. Fabrication of functionally graded grinding wheel by a centrifugal mixed-powder method for CFRP-drilling applications. International Journal of Materials and Product Technology. 2011;42:29–45. DOI:10.1504/IJMPT.2011.044912.

[25] Tsuge H, Takekoshi K, Yamagami S, Kaga T, Bando N, Kamakura M, Watanabe Y. Novel drilling method for CFRP with dual-axes-driving grindstone. Journal of the Japan Society for Abrasive Technology. 2012;56:612–617. DOI:http://doi.org/10.11420/jsat.56.612.

[26] Tsuge H, Ogawa D, Bando N, Kaga T, Watanabe Y. Grinding performance of diamond grinding wheels drilling of CFRP by a dual-axes-driven mechanism. Journal of the Japan Society for Abrasive Technology. 2014;58:168–172. DOI:10.11420/jsat.58.168.

[27] Beffort O, Khalid FA, Weber L, Ruch P, Klotz UE, Meier S, Kleiner S. Interface formation in infiltrated Al(Si)/diamond composites. Diamond & Related Materials. 2006;15:1250–1260. DOI:10.1016/j.diamond.2005.09.036.

[28] Kidalov SV, Shakhov FM. Thermal conductivity of diamond composites. Materials. 2009;2:2467–2495. DOI:10.3390/ma2042467.

[29] Chu K, Liu ZF, Jia CC, Chen H, Liang XB, Gao WJ, Tian WH, Guo H. Thermal conductivity of SPS consolidated Cu/diamond composites with Cr-coated diamond particles. Journal of Alloys and Compounds. 2010;490:453–458. DOI:10.1016/j.jallcom.2009.10.040.

[30] Mańkowski P, Dominiak A, Domański R, Kruszewski MJ, Ciupiński Ł. Thermal conductivity enhancement of copper-diamond composites by sintering with chromium additive. Journal of Thermal Analysis and Calorimetry. 2014;116:881–885. DOI:10.1007/s10973-013-3604-3.

Performance of Functionally Graded Exponential Annular Fins of Constant Weight

Vivek Kumar Gaba, Anil Kumar Tiwari and Shubhankar Bhowmick

Additional information is available at the end of the chapter

Abstract

The present work aims at investigating the performance of exponential annular fins of constant weight made of functionally graded materials (FGM). The work involves computation of efficiency and effectiveness of such fins and compares the fin performances for different exponential profiles and grading parameters, keeping the weight of the fin constant. The functional grading of thermal conductivity is assumed to be a power function of radial co-ordinate which consists of parameters, namely grading parameters, varying which different grading combinations can be investigated. Fin material density is assumed to be constant and temperature gradient exists only along the radial direction. The convective coefficient between the fin surface and the environment is also assumed to be constant. A general second-order governing differential equation has been derived for all the profiles and material grading. The efficiency and effectiveness of the annular fin of different geometry and grading combinations have been calculated and plotted and the results reveal the dependence of thermal behavior on geometry and grading parameter. The effect of variation of grading parameters on fin efficiency and effectiveness is reported. The results are provided in the form of 2-D graphs, which can be used as design monograms for further use.

Keywords: FGM, Annular fin, Exponential profile, Grading parameter, Geometry parameter

1. Introduction

A substantial amount of research endeavors have been carried out to determine the best dimensions of the annular fins so that the rate of heat transfer can be minimized for a given fin volume or the fin volume can be maximized for a specified heat duty. However, the use of fins with optimum profile is restricted due to the associated difficulty of manufacturing.

A detailed review of literature on optimum design of fins was carried out starting with Gardener [1] where upon using a set of idealizing assumptions, the efficiency of various straight fins and spines have been reported. Duffin [2] gave a method for carrying out the minimum weight design of a fin using a rigorous mathematical method based on Variational calculus and assumed constant thermal conductivity of a fin material and a constant heat transfer coefficient along the fin surface. For purely conductive and convective fins, the criterion for the optimal problem was first proposed by Schmidt [3]. Murray [4] presented equations for the temperature gradient and the effectiveness of annular fins with constant thickness with a symmetrical temperature distribution around the base of the fin. Carrier and Anderson [5] discussed straight fins of constant thickness and annular fins of constant cross-sectional area, presenting equations for fin efficiency of each. Duffin and McLain [6] solved the optimization problem of straight-based fins assuming that the minimum weight fin had a linear temperature distribution along its length. Brown [7] reported the optimum dimensions of uniform annular fin by relating fin dimensions to the heat transfer and thermal properties of the fin and heat transfer coefficient between the fin and its surroundings. Smith and Sucec [8] derived analytically the efficiency of circular fins of triangular profile by using Frobenius method.

Maday [9] found the optimum fin thickness variation along the fin. The optimization of fins is generally based on two approaches: one is to minimize the volume or mass for a given amount of heat dissipation and the other is to maximize the heat dissipation for a given volume or mass. Ullmann and Kalman [10] adopted the first way and determined the efficiency and optimum dimensions of annular fins with triangular, exponential, and hyperbolic profiles using numerical techniques. Dhar and Arora [11] described the methods of carrying out the minimum weight design of finned surfaces of specific type by first obtaining the optimum surface profile of a fin required to dissipate a certain amount of heat from the given surface, with no restriction on the fin height and then extended their study for the case when fin height is given. Mikk [12] found the optimum fin thickness variation along the fin. This type of fin shape is complex and involves manufacturing problems. Mikk [13] further worked for convective fins of minimum mass.

In a recent work, Arauzo et al [14] reported a ten-term power series method for predicting the temperature distributions and the heat transfer rates of annular fins of hyperbolic profiles. Assuming fixed fin volume, Arslanturk [15] reported simple correlation equations for optimum design of annular fins with uniform cross sections to obtain the dimensionless geometrical parameters of the fin with maximum heat transfer rates. These simple correlation equations can help the thermal design engineers for carrying out the study on optimum design of annular fins of uniform thickness. In their recent work, Kundu and Das [16] reported the performance analysis and optimization of concentric annular fins with a step change in thickness using Lagrange multiplier. Performance of annular fin of rectangular profile having functionally graded materials (FGM) was reported by Aziz and Rahman [17].

In a recent work, Acosta-Iborra and Campo [18] reported that approximate analytic temperature profiles and heat transfer rates of good quality are easily obtainable without resorting to the exact analytic temperature distribution and heat transfer rate based on modified Bessel

functions. Kang [19] reported the optimum performance and fin length of a rectangular profile annular fin using variations separation method. Theory for FGM for the temperature-dependent material properties with multiobjective optimization was carried out by Goupee and Vel [20]. In this work, the thermal conductivity varies inversely with the square of the radius. Aziz and Fang [21] presented alternative solutions for different tip conditions of longitudinal fins having rectangular, trapezoidal, and concave exponential profiles and reported relationship between dimensionless heat flux, fin parameter, and dimensionless tip temperature for all the geometries. Aziz and Khani [22] presented an analytical solution for thermal performance of annular fins of rectangular and different convex exponential profiles mounted on a rotating shaft, losing heat by convection to its surroundings. In their work, convection heat transfer coefficient was assumed to be a function of radial coordinate and shaft speed.

In an experimental study, heat transfer rate and efficiency for circular and elliptical annular fins were analyzed for different environmental conditions by Nagarani [23] and high efficiency was reported for elliptical fins as compared to circular ones. In a recent work, Aziz and Fang [24] derived analytical expressions for the temperature distribution, tip heat flow, and Biot number at the tip and reported thermal performance of the annular fin under both cooling and heating conditions.

In the present work, investigation has been reported for variation of thickness and thermal conductivity of material along the radius of the fin keeping the weight of the fin equal to that of a standard rectangular fin. The constraint of constant weight is imposed to compare variation in thickness with rectangular profile as there are several applications where weight is a very crucial parameter to decide the fin selection. Also without imposing the constraint of constant weight, there is always a possibility that selection of fin has been done based on larger surface area having higher weight.

It is a well-known fact that the temperature gradient is higher at the base, hence for the maximum heat transfer higher thermal conductivity should be provided at the base as compared to other part of fin; this can be achieved with functional grading of thermal conductivity of fin material. The original concept of functional grading of material was proposed to take the advantage of excellent thermal performance of ceramics with the toughness of metals. This gave way to the idea of gradient-based varying of microstructure from one material to another material. This transition is usually based on power series. Aerospace industry, chip manufactures, engine and energy component manufacturers are most interested in evolution of new graded materials that can withstand high thermal gradients.

2. Mathematical formulation

It is assumed that there are no temperature gradients along the thickness of the fins. It is also assumed that the effect of external environment on the surface convection is negligible and hence a constant convective heat transfer coefficient has been adopted for the fin material. The second-order differential equation for the heat transfer through the fins has to be developed

to find the temperature profile. This correlation equation (second-order differential equation) has been solved using computational algorithm in MATLAB software and the computed information has been analyzed. For calculating the heat balance, the details for a control volume of length 'dr' of a fin is shown in Figure 1. Applying the law of conservation of energy or thermal energy balance:

$$Q_r = Q_{r+dr} + Q_{conv}$$ (1)
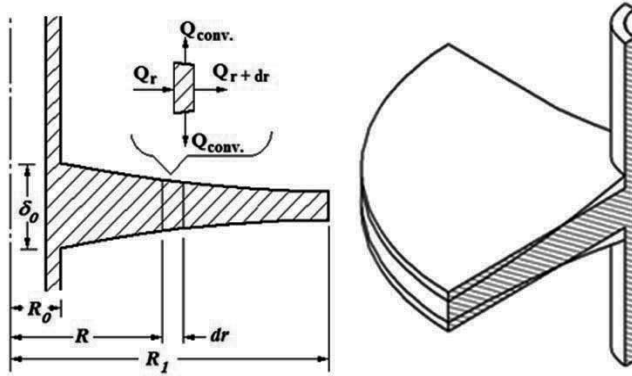
Figure 1. Elemental strip in fin of length 'dr' and a comparison of constant weight uniform and exponential profile.

Normalization of the problem is carried out using the following equations

Using the above equation, the following equation can be arrived at

$$\frac{d}{dr}\left(2\pi.r.k.\delta.\frac{d\theta}{dr}\right)dr = 4\pi.r.h.\theta.dr.\left(1+\left(d\delta/2dr\right)^2\right)^{0.5}$$ (2)

$$\bar{\delta} = \frac{\delta}{\delta_0}, \phi = \frac{\theta}{\theta_0}, x = \frac{R-R_0}{R_1-R_0}, R_f = \frac{R_1}{R_0}$$

and the fin parameter, $m_f = (2h/a\delta_0)^{0.5}$

upon introducing the normalized variables, the governing equation becomes

$$\frac{d^2\phi}{dx^2} + A_1\frac{d\phi}{dx} + A_2\phi = 0$$ (3)

where

$$A_1 = \left[\frac{1}{\bar{\delta}} \cdot \frac{d\bar{\delta}}{dx} + \frac{1}{k} \cdot \frac{dk}{dx} + \frac{L}{R_0 + Lx} \right]$$

Here in A_1, the first term represents the variation in thickness and the second term represents the variation of thermal conductivity along the length of the fin. It means for rectangular profile with isotropic materials only the third term of A_1 exists and that makes equation (3) more generalized for handling complex geometry with FGM.

$$A_2 = -\frac{2hL^2}{k\delta_0\bar{\delta}}\sqrt{1 + \frac{\delta_0^2}{4L^2}(\frac{d\bar{\delta}}{dx})^2}$$

Assuming the geometry variation and thermal conductivity variation of FGM material as follows

$$\delta = \delta_0\left(e^{-nx^m}\right) \text{ or } \delta = \left(e^{-nx^m}\right)$$

and $k = ar^b$

Using the above relation, equation (3) becomes

$$\frac{d^2\phi}{dx^2} + \left[-m.n.x^{m-1} + \frac{L}{(Lx + R_0)}(1+b)\right]\frac{d\phi}{dx}$$
$$- \frac{L^2 m_f^2}{\bar{\delta}.\left(Lx + R_0\right)^b}\left[\sqrt{\frac{\delta_0^2}{4L^2}.\left(m.n.e^{-nx^m}.x^{m-1}\right)^2 + 1}\right]\phi = 0 \tag{4}$$

Equation (4) is solved using the following boundary conditions:

i. $\phi = 1$ at x=0

ii. $\frac{d\phi}{dx} = 0$ at $x = 1$, i.e., tip is insulated

Similarly, efficiency and effectiveness of the fin is obtained from the general equation as follows:

$$\eta = \frac{-\left(\phi'\right)_{x=0}}{\frac{L^2 m_f^2}{R_0^{b+1}}\int_0^1\left[\left(Lx + R_0\right)\sqrt{\left(\frac{\delta_0 mn}{2L}\right)^2 e^{-2nx^m} x^{2m-2} + 1}\right]dx} \tag{5}$$

$$\varepsilon = \frac{-aR_0^b\left(\phi'\right)_{x=0}}{hL} \tag{6}$$

If the temperature distribution or if the first derivative of the temperature $(\phi^{'})_{x=0}$ at the fin base is known, then equations (5) and (6) enable the fin efficiency and effectiveness to be calculated. The first derivative of temperature at the fin base for different shapes of fin has been calculated using the solution of general second-order differential equation (4).

The effect on fin performance has been carried out for the following cases:

Case I: By varying the geometry parameters *n* and *m* and keeping all other parameters constant.

Case II: By varying coefficient of thermal conductivity, *a* is observed with geometry parameters, keeping grading parameter *b* constant.

Case III: The geometry is kept constant with variation in grading parameters *a* and *b*.

3. Results and discussion

The dimensionless temperature ϕ is a function of normalized variables, *n* and *m* due to chosen fin shape, grading parameter, *a* and *b* for thermal conductivity variation, m_f, R_f and *x* due to the fin geometry. Considering *x* as the only independent variable and keeping the other variables constant, equations (4) and (5) have been solved for the various values of *n* ranging between 0 and 0.9, *m* ranging between 0.5 and 1.5, grading parameter *b* ranging between −2 and 2, coefficient of thermal conductivity *a* ranging between 5 and 25, and for all the cases the values of R_f are kept constant, i.e., 3. The numerical values of system properties are *h* = 25 W/m², δ_0 = 0.01 m, and R_0 = 0.1 m.

The first derivative of temperature at the fin base, i.e., ϕ $'_{x=0}$ helps to calculate the fin efficiency and effectiveness and is calculated by solving second-order differential equation in MATLAB. The values of ϕ$'_{x=0}$ can be obtained for different values of R_f, *n*, *m*, and *b*. Temperature variation along the radius is depicted in Figure 2 for the rectangular annular fin, i.e., *n* = 0 for different values of m_f at grading parameter *b* = −1, it has been observed that the results obtained from the numerical coding are having good agreement with the Aziz and Rahman's study [18].

Figure 3 clearly shows the variation of efficiency and effectiveness with the parameter *m* for different values of geometry parameter *n* keeping the other variable constant (i.e., *b* = −1 and m_f = 20). It is evident from Figure 3 that efficiency first decreases and then increases with increase in parameter *m* and a minima has been observed near the value of *m* = 0.6. Effectiveness increases monotonously with the parameter *m* and tends to effectiveness of rectangular fins, i.e., *n* = 0, this is due to the constraint of constant weight. Both efficiency and effectiveness decrease sharply with geometry parameter *n* as shown in Figure 4, and similar trends have also been obtained for different values of geometry parameter *m* as shown in Figure 4.

Variation of efficiency and effectiveness with coefficient of thermal conductivity *a* with different values of *n* keeping other variables constant (i.e., *m* and *b*) is depicted in Figure 5. The efficiency and effectiveness increase sharply with increase in *a*, which is due to the fact that as *a* increases m_f decreases.
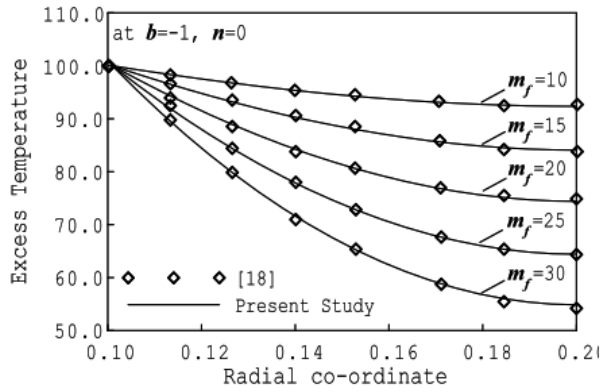
Figure 2. Excess temperature over radial co-ordinate for rectangular annular fin.
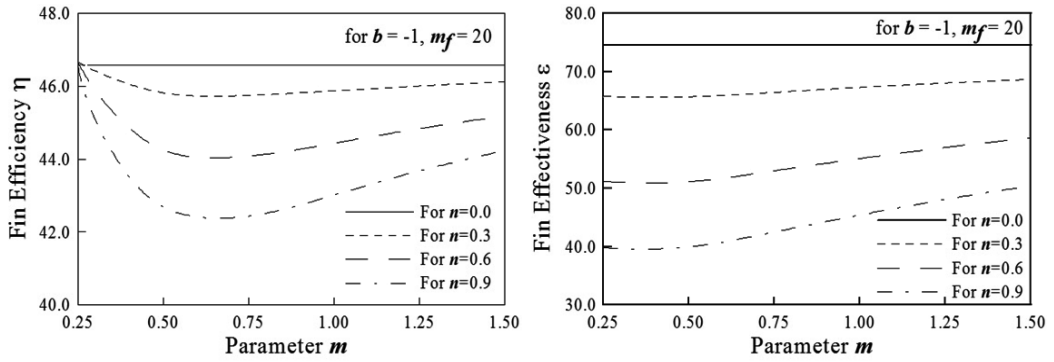
Figure 3. Variation of efficiency and effectiveness with parameter m for different values of n (case I).
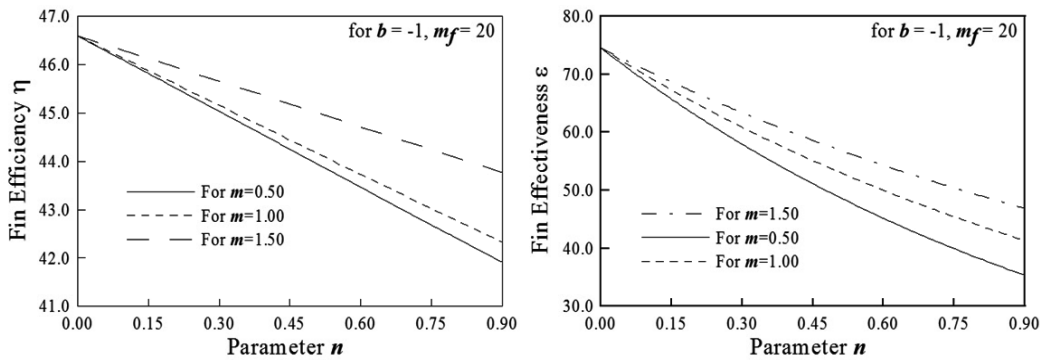
Figure 4. Variation of efficiency and effectiveness with n for different values of m at $m_f = 20$ and $b = -1$ (Case I).
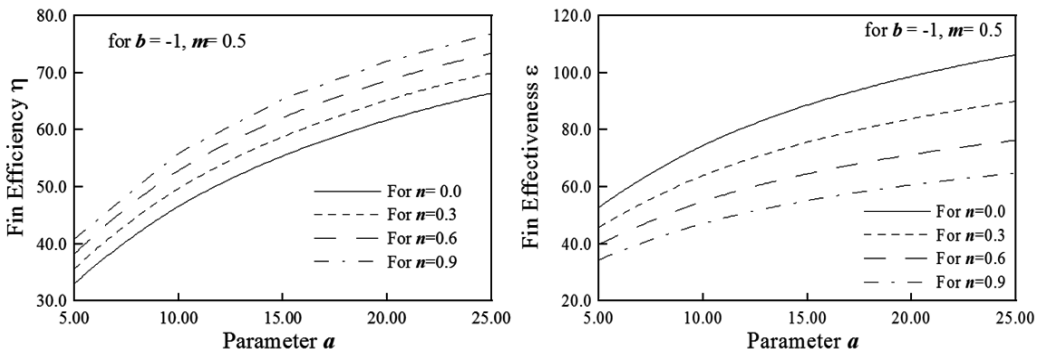
Figure 5. Variation of efficiency and effectiveness with *a* for different values of *n* (Case II).

Similar trends have also been observed for variation of efficiency and effectiveness with coefficient of thermal conductivity *a* with different values of *m*, keeping other variables constant (i.e., *n* and *b*), is depicted in Figure 6 but the effect of variation in parameter *m* is not significant.
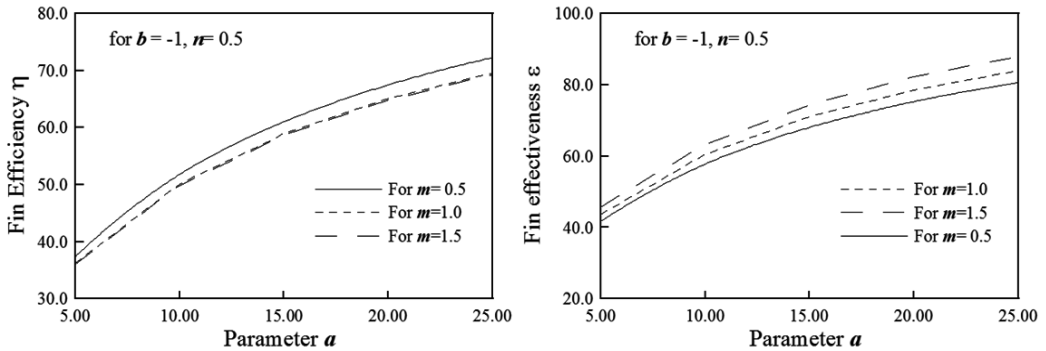
Figure 6. Variation of efficiency and effectiveness with *a* for different values of *m* (Case II).

Variation of excess temperature *θ* along the radial co-ordinate has also been analyzed in Figure 7 and Figure 8 with coefficient of thermal conductivity *a* and grading parameter *b* keeping the geometry of annular fin constant (i.e., *n* = 0.5 and *m* = 0.5). The performance of fin decreases sharply as the grading parameter shifted from negative value to positive value and it is highest for when it has been kept −2. This is because of higher thermal conductivity that is available at the base (as the temperature of base is higher) to dissipate more heat. The variation of temperature along the radius with *a* falls exponentially, and performance of fin increases with increase in *a* value for a fixed geometry of the exponential profile fin.
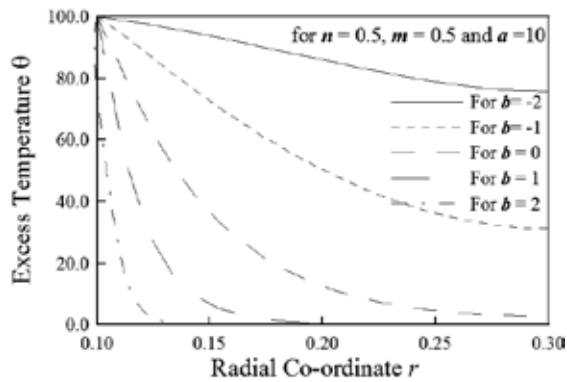
Figure 7. Excess temperature over the radial surface for different grading parameter *b* (Case III).
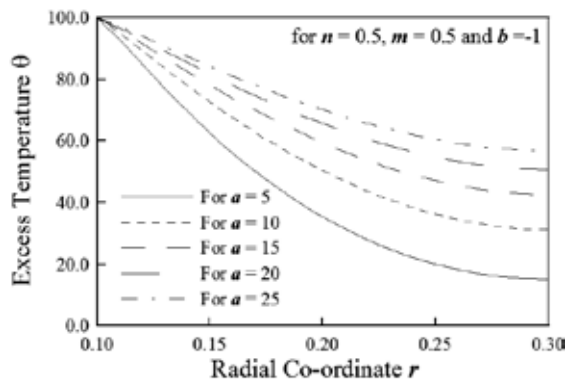
Figure 8. Excess temperature over the radial surface for different grading parameters *a* at *n* = 0.5, *m* = 0.5, and *b* = −1 (Case III).

4. Conclusion

The performance of exponential annular fins made of FGM is reported. During the analysis, the weight of the different geometry fin is kept constant to the rectangular fin. The study is carried out for different values of geometry parameters *n* and *m* and grading parameters *a* and *b*. It is observed that both effectiveness and efficiency decrease as m_f increases for any geometry and grading. Also the variation in efficiency and effectiveness with geometry parameter *m* is almost constant but decreases sharply with *n*, and the effect of variation of *n* on efficiency and effectiveness is direct in nature. The effect of grading parameter *b* on fin performance is also investigated, and it is observed that both efficiency and effectiveness decrease as *b* value shifted from negative to positive and it is highest for *b* = −2. Therefore, it can be concluded that highest

thermal conductivity is required at the base of the fin to dissipate more amount of heat (due to the highest temperature difference available). Also grading of thermal conductivity should provide inversely square of the length from the base of the fin to obtain the highest performance of the fin compared to the isotropic material (i.e., **b** = 0). Performance of the fin increases with increase of coefficient of thermal conductivity **a** due to higher thermal conductivity material of the fin.

5. Nomenclature

a,b Grading parameters for thermal conductivity

h Convection heat transfer coefficient (W/(m^2 °K))

k Thermal conductivity of the fin material (W/m°K)

L Fin length (m)

m Geometry parameter which controls the shape

m_f Convectional fin parameter (($2h/a\delta_0)^{0.5}$)

n Geometry parameter which controls the thickness

Q Heat dissipation (W)

R_f Aspect ratio, constant for fin shape relations (R_1/R_0)

r Fin radius at the start of element (*m*)

R Radius (*m*)

T Temperature (°C)

x Dimensionless radial coordinate

6. Greek symbols

δ Fin thickness (m)

δ Dimensionless fin thickness (δ_1/δ_0)

η Efficiency of fins

ε Effectiveness of fins

θ Temperature excess of fin over ambient fluid (°C) (T – T_0)

Φ Dimension less temperature (θ/θ_0)

7. Subscripts

0 At the base of fin

1 At the tip of fin

Author details

Vivek Kumar Gaba, Anil Kumar Tiwari and Shubhankar Bhowmick[*]

*Address all correspondence to: sbhowmick.mech@nitrr.ac.in

Department of Mechanical Engineering, National Institute of Technology Raipur (CG), India

References

[1] Gardner KA: Efficiency of Extended Surfaces. Transactions of the American Society of Mechanical Engineers 1945;67:621–631.

[2] Duffin RJ: Optimum shape of a cooling fin on a convex cylinder. Journal of Mathematics and Mechanics. 1959;47–56.

[3] Schmidt J: Solution of some boundary problems of heat conduction for cylindrical bodies provided with longitudinal fins. International Journal of Heat and Mass Transfer 1966;10:1305–1326.

[4] Murray WM: Heat dissipation through an annular disk or fin of uniform thickness. Journal of Applied Mechanics – Transactions of the ASME 1938;60:78.

[5] Carrier WH, Anderson SW: The resistance to heat flow through finned tubing. Heat Piping and Air Conditioning. 1944;10:304–320.

[6] Duffin RJ, McLain DT: Optimum shape of a cooling fin on a convex cylinder. Journal of Mathematics and Mechanics 1968;17:769–784.

[7] Brown A: Optimum dimensions of uniform annular fins. International Journal Heat Mass Transfer. 1965;8:655–662.

[8] Smith PJ, Sucec J: Efficiency of circular fins of triangular profile. Trans ASME J Heat Transfer. 1969;181–182.

[9] Maday CJ: The minimum weight one-dimensional straight cooling fin. Journal Engineering Industry. 1974;96:161–165.

[10]   Ullmann A, Kalman H: Efficiency and optimized dimensions of annular fins of different cross-section shapes. International Journal of Heat and Mass Transfer. 1989;32:1105.

[11]   Dhar PL, Arora CP: Optimum design of finned surfaces. J. Franklin Inst. Category: Fluid Mechanics and Heat Transfer. 1976;301:379–392.

[12]   Mikk I: Efficiency of convective round fins with a triangular profile. Journal of Engineering Physics. 1977;32:703–707.

[13]   Mikk I: Convective fin of minimum mass. International Journal of Heat and Mass Transfer 1980;23:707–711.

[14]   Arauzo I, Campo A, Cortes C: Quick estimate of the heat transfer characteristics of annular fins of hyperbolic profile with the power series method. Applied Thermal Engineering 2005;25:623–634.

[15]   Arslanturk C: Simple correlation equations for optimum design of annular fins with uniform thickness. Journal of Applied Thermal Engineering. 2005;25:2463–2468.

[16]   Kundu B, Das PK: Performance analysis and optimization of annular fin with a step change in thickness. ASME Journal of Heat Transfer. 2001;123:601–604.

[17]   Aziz A, Rahman MM: Thermal performance of a functionally graded radial fin. International Journal of Thermophysics 2009;30:1637–1648.

[18]   Acosta-Iborra A, Campo A: Approximate analytic temperature distribution and efficiency for annular fins of uniform thickness. International Journal of Thermal Sciences. 2009;48:773-780(2009).

[19]   Kang HS: Optimization of a rectangular profile annular fin based on fixed fin height. Journal of Mechanical Science and Technology 2009;23:3124–3131.

[20]   Goupee AJ, Vel SS: Multi-objective optimization of functionally graded materials with temperature-dependent material properties. Materials & Design 2007;28:1861–1879.

[21]   Aziz A, Fang T: Alternative solutions for longitudinal fins of rectangular, trapezoidal, and concave parabolic profile. Energy Conversion and Management 2010;51:2188–2194.

[22]   Aziz A, Khani F: Analytic solutions for a rotating radial fin of rectangular and various convex parabolic profiles. Communication in Nonlinear Science and Numerical Simulation. 2010;15:1565–1574.

[23]   Nagarani N. Experimental heat transfer analysis on annular circular and elliptical fins. International Journal of Engineering Sciences and Technology. 2010;2:2839–2845.

[24]   Aziz A, Fang T: Thermal analysis of an annular fin with (a) simultaneously imposed base temperature and base heat flux and (b) fixed base and tip temperatures. Energy Conversion and Management 2011;52:2467-2478(2011).

High-performance Self-lubricating Ceramic Composites with Laminated-graded Structure

Yongsheng Zhang, Yunfeng Su, Yuan Fang, Yae Qi and Litian Hu

Additional information is available at the end of the chapter

Abstract

High-performance ceramic composites are potential candidates for the application of wear-resistance components because of their excellent properties. Nevertheless, many problems, such as high friction coefficient of ceramic material and poor mechanical properties of ceramic-matrix self-lubricating composites, limit a wider range of applications of these composites in tribological areas. Therefore, improving high-toughness ceramic-matrix self-lubricating materials for practical applications is significant. This study proposes a new design for ceramic self-lubricating composites to overcome the conflict between their mechanical and tribological properties. Complying with the design principle of bionic and graded composites, two kinds of self-lubricating ceramic composites with laminated-graded structure were prepared, and their mechanical and tribological properties were studied. The results show that this newly developed ceramic composite has achieved satisfactory strength and tribological properties compared with the traditional ceramic self-lubricating composites. The bending strength reached the same level as the properties of general monolithic ceramics. In the temperature range of 25-800 °C, the friction coefficient of composites was less than 0.55, which was about half of that of monolithic ceramics.

Keywords: Functionally graded material, Laminated structures, Ceramic, High temperature, Self-lubricating

1. Introduction

Ceramic materials are promising candidates for wear-resistance components owing to their excellent properties such as high strength and resistance to corrosion and oxidation stability at high temperature. Nevertheless, both the high coefficient of friction of this kind of material under dry sliding and the brittleness of ceramic-matrix itself limit its practical application in

tribological areas. Generally, incorporating solid lubricants (SLs) in ceramic matrixes solves the friction problems, which can reach a positive effect. Moreover, compound lubricants can exhibit excellent self-lubricating abilities in a wide range of temperatures because the lubricants can promote the formation of well-covered lubricating films on the surfaces of ceramics that can work effectively under different temperature [1-3]. Unfortunately, subsequent studies have shown that these composites are homogenous in terms of mechanical and tribological properties. Thus, the strength of ceramics and the lubrication of SLs cannot be fully utilized. Because the continuity of ceramic phases is destroyed by the layered structural SL phase, the mechanical property of this type of material is reduced [4,5]. In these situations, it is necessary to develop a high-strength and high-toughness self-lubricating ceramic composites.

Lamination is one of the new strategies being used to enhance the mechanical properties of ceramics. The ideas of laminated composites inspired from natural biomaterials, such as shells and teeth, are made of layered architectures combining materials with different properties. During the past decade, there are large amounts of layered ceramic composites that have been fabricated and studied [6-8]. These kinds of materials have non-catastrophic fracture behavior and damage tolerance, which exhibit much higher fracture toughness and work of fracture in them than in monolithic ceramics. Moreover, the unique configurations of the layered material allow design flexibility. Therefore, the combination of the laminated design of ceramic materials and self-lubricating ceramic composites with excellent lubricating property is a promising way to achieve the integration of mechanical and tribological properties [9-12].

For laminated self-lubricating ceramic composites, interfacial residual stress between the adjacent layers may have an important effect on their mechanical properties. Any modification or change of the interfacial structure and composition will be a determining factor in the strength of the interfacial bond and will eventually affect the toughness, strength, and fracture behavior of laminated composites [13]. Therefore, a reasonable residual stress between the adjacent layers is essential to improve the mechanical properties. Previous studies have shown that the graded design of the materials is an effective method to eliminate the interface stress of dissimilar material system [14-16]. This design concept of functionally graded materials (FGMs) was first raised by Japanese scientists in 1987 as reported in reference [14]. That is, components with different properties or structures disperse by a gradient change along with one direction instead of a homogeneous manner. Thus, the composite can exhibit different properties that are mutually exclusive at the same time, and the gradient change can eliminate the interface between components. This new-style and non-uniform composite realized the integration of structure and function, making it to have a wider prospect of application in extreme conditions.

Based on the above background, the authors prepared high-performance structural/lubricating-functional integration ceramic composites using the design of graded laminated structure [4,17,18]. This design is conductive to the combination of mechanical and tribological properties while retaining all the advantages of these materials. The aim of this chapter is to illustrate the design, fabrication, and properties of alumina and zirconia self-lubricating composites with laminated-graded structure and to provide guidance for the optimum design of these materials.

2. Design, fabrication, and properties of laminated ceramic composites

2.1. Design and fabrication of laminated composites

Figure 1 illustrates the schematic and the design concept of laminated composites. The thickness of the A layer and B layer are d_1 and d_2, respectively, where the A layer is the Al_2O_3 or ZrO_2-Al_2O_3 and the B layer is Al_2O_3-ZrO_2 or ZrO_2. Commercially available Al_2O_3, ZrO_2, Y_2O_3, CuO, and TiO_2 were used in this study. The material was manufactured using the following steps [17-20]: (1) ball-milling of powder, (2) sequential stacking of layers in steel mold, and (3) hot-pressing in graphite mold. Hot-pressing was performed at 1350-1400 °C and 25 MPa using graphite die in an argon atmosphere for 100-120 minutes. Monolithic Al_2O_3 and ZrO_2 with sintering aids were also sintered at same condition as comparisons. The micro-structures of the composites were observed using scanning electron microscopy (JSM-5600LV). The sintered specimens were sliced into test bars for bending strength and work of fracture.
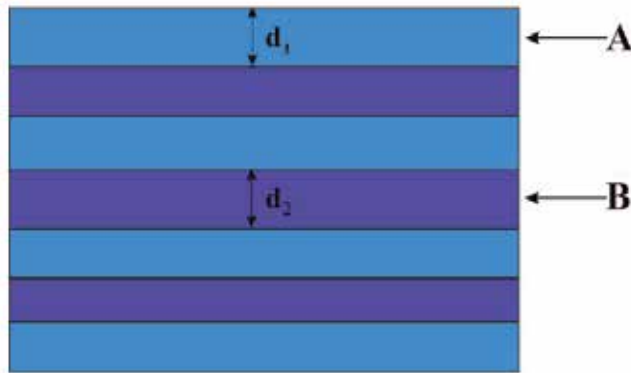
Figure 1. Schematic of laminated composite structure.

An example of the microstructure of the ZrO_2(3Y)-Al_2O_3/ZrO_2(3Y)-laminated composites is shown in Figure 2, where the dark layer is the ZrO_2(3Y)-Al_2O_3 layer and the light layer is the ZrO_2(3Y) layer. The multilayer structure with a relatively straight interface can be observed without clear delamination. It can also be seen from Figure 2 that the ZrO_2(3Y)-Al_2O_3 layer and ZrO_2(3Y) layer have the same thickness of approximately 160 μm.

2.2. The mechanical properties of laminated composites

The geometric parameters of the layered structure are the key factors for the optimal design of laminated composites. These parameters mainly include the layer numbers and thickness ratio of the two layers. The mechanical properties of Al_2O_3/Al_2O_3-10wt.%ZrO_2(3Y)-laminated composites with different layer numbers are shown in Figure 3 [19,20]. As shown in Figure 3, a relatively large number of layers are likely to improve the mechanical properties of the materials. When the number of layers is 41, the bending strength and work of fracture of materials reach the maximum value. The relationship between the mechanical properties and
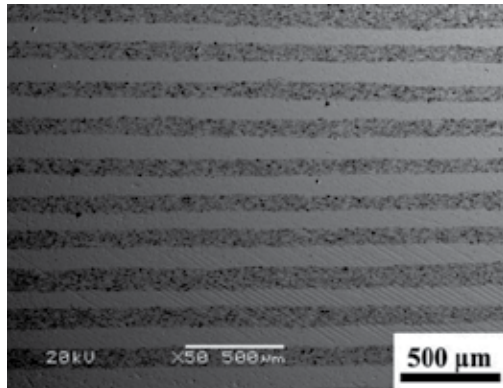
Figure 2. SEM photograph of profile of laminated composites.

layer thickness ratio is displayed in Figure 4 [19,20]. One can see that the layer thickness ratio also has an enormous effect on the mechanical properties of laminated composites. The bending strength and work of fracture of all of the laminated materials are higher than that of the monolithic materials and decrease with the increase of the layer thickness ratio. When the layer thickness ratio is 1:1 and the thickness of each layer is 80 μm, the bending strength and work of fracture of the Al_2O_3/Al_2O_3-ZrO_2(3Y) laminated composites could reach to 740 MPa and 3892 J m^{-2}, respectively [19,20].
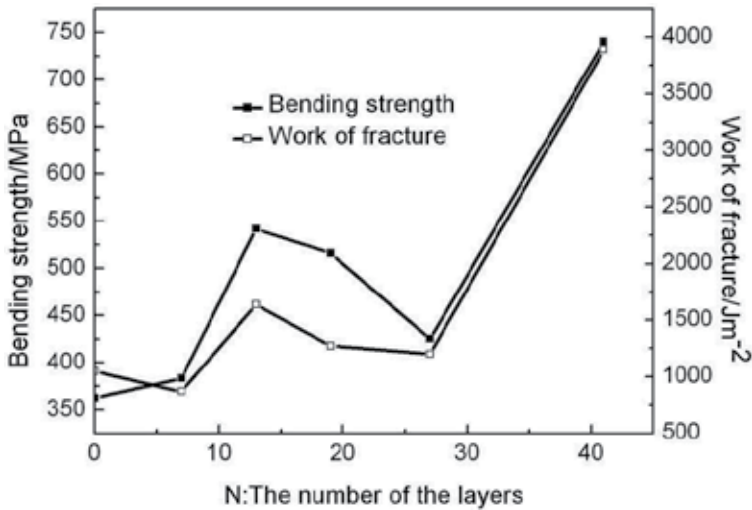
Figure 3. Effect of the layer numbers on the bending strength and work of fracture.

In addition, the compositions of the two layers also have significant effects on the mechanical properties of the laminate composites. The bending strength and work of fracture of Al_2O_3/Al_2O_3-ZrO_2(3Y)-laminated composites with different content of ZrO_2(3Y) in Al_2O_3-ZrO_2(3Y)
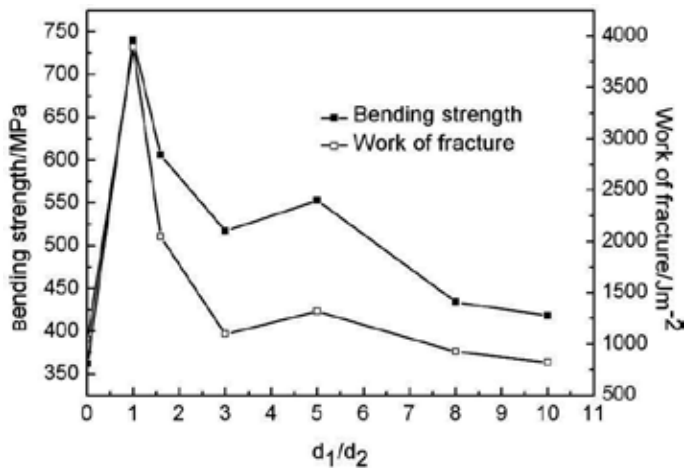
Figure 4. Effect of the thickness ratio on the bending strength and work of fracture.
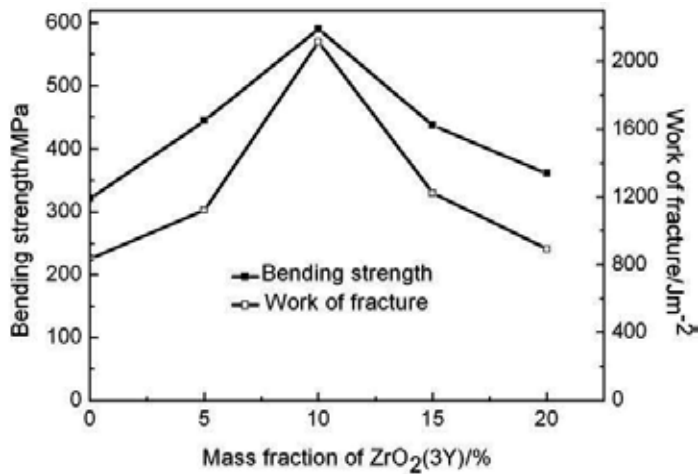
Figure 5. Relationship between mechanical properties of Al_2O_3/Al_2O_3-$ZrO_2(3Y)$-laminated composites and content of $ZrO_2(3Y)$ in the Al_2O_3-$ZrO_2(3Y)$ layers.

layers are shown in Figure 5 [19,20]. As can be seen from the figure, with the increase of the content of $ZrO_2(3Y)$, first, the bending strength and work of fracture of the material increase and then they decrease gradually. When the mass content of $ZrO_2(3Y)$ is 10%, both bending strength and work of fracture reach the optimal value. This is mainly because the variation of content of $ZrO_2(3Y)$ in Al_2O_3-$ZrO_2(3Y)$ layers causes significant changes in the residual stresses between adjacent layers and the contribution of phase transformation toughening to the crack propagation energy of the materials, thus realizing the optimization of the materials [19,20]. The same design principles used for designing Al_2O_3/Al_2O_3-$ZrO_2(3Y)$-laminated composites apply to designing $ZrO_2(3Y)$-$Al_2O_3/ZrO_2(3Y)$ material. When the mass content of Al_2O_3 in

ZrO$_2$(3Y)-Al$_2$O$_3$ layers is 15 %, the bending strength and work of fracture of the ZrO$_2$(3Y)-Al$_2$O$_3$/ZrO$_2$(3Y)-laminated composite reach to 968 MPa and 3751 J m^{-2}, respectively (Fig. 6a and b).
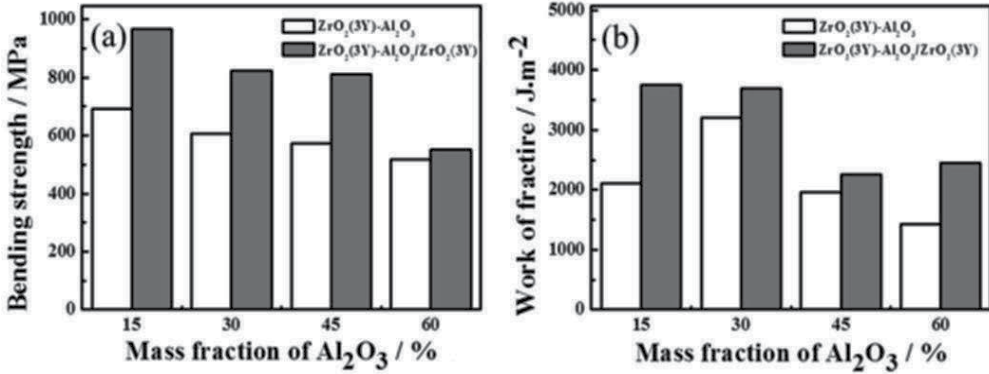
Figure 6. Mechanical properties of ZrO$_2$(3Y)-Al$_2$O$_3$/ZrO$_2$(3Y)-laminated composites and monolithic ceramic.

3. Graded structure and tribology design for optimal lubricating properties in laminated ceramic composites

3.1. Design and preparation of laminated-graded self-lubricating ceramic composites

From the results above, it can be concluded that the layered structure design is a good strategy to enhance the mechanical properties of monolithic ceramics, which can efficiently improve the bending strength and work of fracture. Nevertheless, the friction and wear rate of these materials under dry sliding conditions are still high. To overcome this problem, the laminated-graded structure self-lubricating ceramic composites were designed. Figure 7 shows the schematic of self-lubricating ceramic composites with laminated-graded structure, where d$_1$=d$_2$, the A layer is the Al$_2$O$_3$ or ZrO$_2$-Al$_2$O$_3$, and the B layer is Al$_2$O$_3$-ZrO$_2$ or ZrO$_2$. The center area is composed of laminated composites that are similar to that of in the section 2, which provides high strength for the whole material. The content of SLs is graded, increased from center to two sides, and finally reaches a fixed value on the surface to ensure the excellent lubricating function of the materials. In this study, each couple of ZrO$_2$(3Y)-Al$_2$O$_3$ and ZrO$_2$(3Y) or Al$_2$O$_3$ and Al$_2$O$_3$-ZrO$_2$ has the same SL content. The SL content of each couple $f(x)$ is determined by the following equation [18]:

$$f(x) = (x/m)^p \times f(s) \tag{1}$$

Where x is the number of the couple, m is the total number of the couples in the gradient area, p is the gradient exponent, and $f(s)$ is the content of SLs in surface layers. Commercially

available Al_2O_3, ZrO_2, Y_2O_3, CuO, TiO_2, and SLs (graphite+CaF_2+$BaSO_4$ and graphite+CaF_2 in two kinds of laminated-graded structure self-lubricating ceramic composites, respectively) were used. Experimental details for preparation and characterization are described in these references [17, 18].
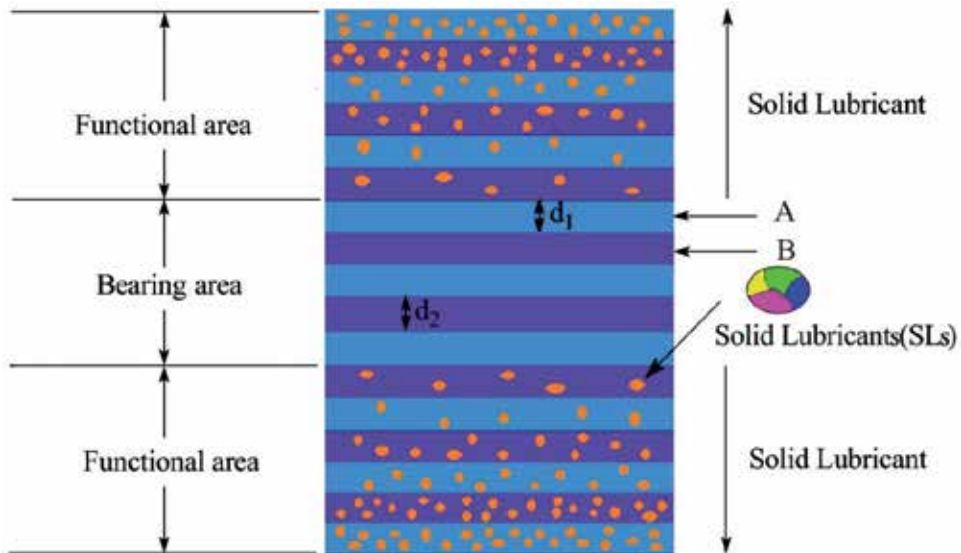
Figure 7. Schematic of the laminated-graded structure self-lubricating composites.

3.2. The mechanical and tribological properties of traditional self-lubricating ceramic composites

For comparison, the mechanical and tribological properties of traditional self-lubricating ceramic composites were first conducted. Figure 8 shows the microstructure of two kinds of traditional self-lubricating ceramic composites. It can be seen that there are lots of tiny pores in the sintered samples. There is no doubt that these defects will greatly degenerate the mechanical properties of the materials. The mechanical properties of two kinds of traditional self-lubricating ceramic composites (Al_2O_3-graphite and Al_2O_3-LaF_3 composites) are given in Figure 9. It can be seen clearly that the bending strength and work of fracture decrease rapidly with the increase of the content of SLs. For the Al_2O_3-LaF_3 composites, when the volume content of lubricants increase to 40%, the bending strength and work of fracture reduced to as low as 67 MPa and 44 J m^{-2}, which were 6.3 and 2.9 times lower than those of monolithic Al_2O_3 ceramic. Therefore, the traditional self-lubricating ceramic composites exhibit poor mechanical properties mainly because of the lots of SLs that destroyed the continuity of ceramic matrix. The ceramic composites may exhibit good lubricating properties when proper amounts of lubricants were added [1,4]. Nevertheless, this kind of ceramics possesses poor anti-destructive and reliability, which is the key obstacle to its practical application. Therefore, as mentioned

earlier, improving high-strength and high-toughness ceramic-matrix self-lubricating materials for practical applications is significant.
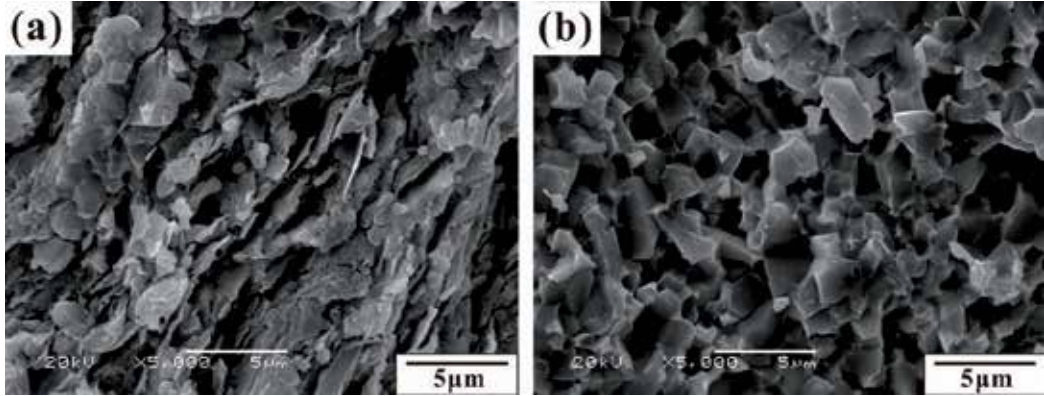
Figure 8. SEM micrographs of fracture surface of traditional Al_2O_3-graphite (a) and Al_2O_3-LaF_3 (b) self-lubricating ceramic composites.
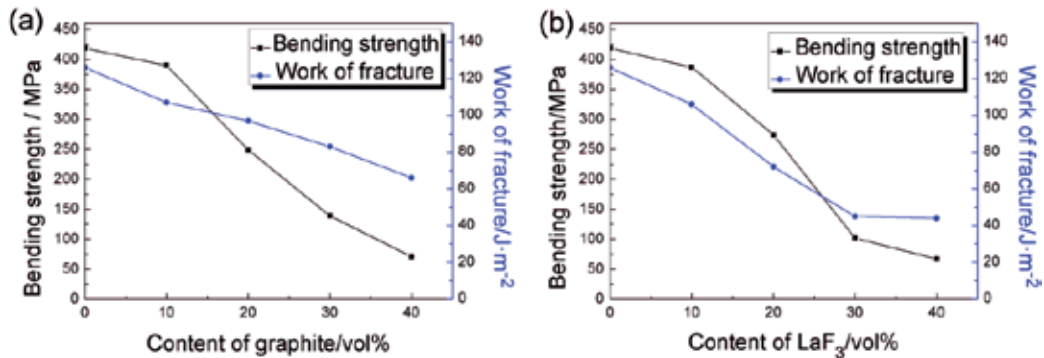
Figure 9. Mechanical properties of Al_2O_3-graphite (a) and Al_2O_3-LaF_3 (b) self-lubricating composites.

3.3. The performance of laminated-graded structure self-lubricating ceramic composites

Compared to the traditional self-lubricating ceramic composites, laminated-graded structure self-lubricating ceramic composites exhibit excellent mechanical properties. Table 1 describes the bending strength of Al_2O_3-laminated-graded structure self-lubricating ceramic composites and of some monolithic self-lubricating ceramic composites. It can be seen from Table 1 that the bending strength of laminated-graded structure self-lubricating ceramic composites are much higher than any one of monolithic materials. The bending strength reached 348 MPa, which is approximately five times higher than that of the traditional monolithic Al_2O_3/SL and Al_2O_3-ZrO_2(3Y)/SL ceramics, and which basically approached the properties of general monolithic Al_2O_3 and Al_2O_3-ZrO_2(3Y) ceramics [17].

Additionally, the gradient exponent p has a remarkable influence on the mechanical properties of laminated-graded structure self-lubricating composites [18]. As shown in Figure 10, the bending strength of the $ZrO_2(3Y)-Al_2O_3/ZrO_2(3Y)/SL$ FGM increased, with the increase of p up to 2.0, and then decreased rapidly when p exceeds 2.0. This phenomenon is caused by the residual stress between the adjacent layers in gradient area. The variation of p causes the change of content of SLs in gradient layers, and then the residual stress that is generated from the thermal mismatch because of the difference in thermal expansion coefficients between the adjacent graded layers (as shown in Figure 11) is influenced. This shows that a reasonable residual stress is essential to adjust the mechanical properties of these materials.

Materials	Bending strength (Mpa)
Al_2O_3/Al_2O_3-10wt.%$ZrO_2(3Y)$/SL FGMs	348
Al_2O_3/SL	68
$ZrO_2(3Y)-Al_2O_3$/SL	69

Table 1. Bending strength of laminated-graded structure self-lubricating ceramic composites [17].
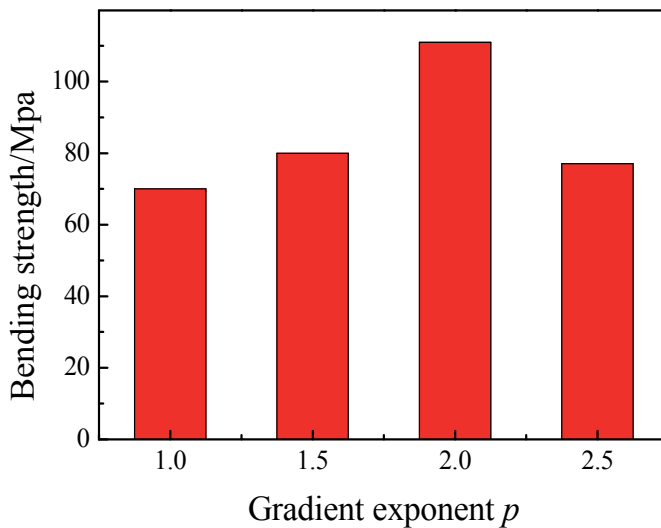
Figure 10. The bending strength of $ZrO_2(3Y)-Al_2O_3/ZrO_2(3Y)$/SL FGMs varies with the gradient exponent.

The laminated-graded structure ceramics not only showed excellent mechanical properties, it also maintained good tribological performance. As shown in Figure 12, in the temperature range of 25–800 °C, the friction coefficient of Al_2O_3 and $ZrO_2(3Y)$ laminated-graded structure composite was less than 0.55, which was approximately half of that of monolithic Al_2O_3 and ZrO_2 ceramics. The decrease of friction coefficients were achieved by the presence of graphite, CaF_2, and $BaSO_4$, which have excellent lubricating property under different temperatures.
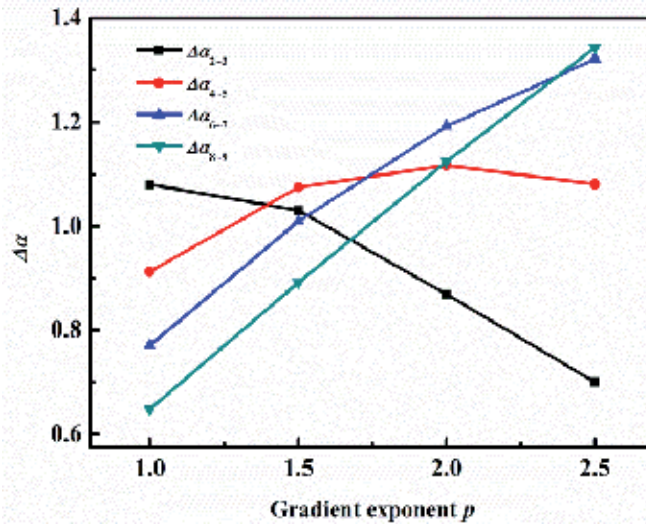
Figure 11. Variation of the difference value of coefficients of thermal expansion between the adjacent layers with the gradient exponent *p* [18].

Graphite has a good lubricating property at room temperature to 300 °C, and CaF$_2$ at 250 °C to 1000 °C. In addition, BaSO$_4$ also possesses excellent self-lubricating performance over a broad temperature range. During the sliding process, these SLs form the self-lubricating film that is helpful to reduce direct contact between the ceramics and further improved the tribological properties of the materials [17,18].
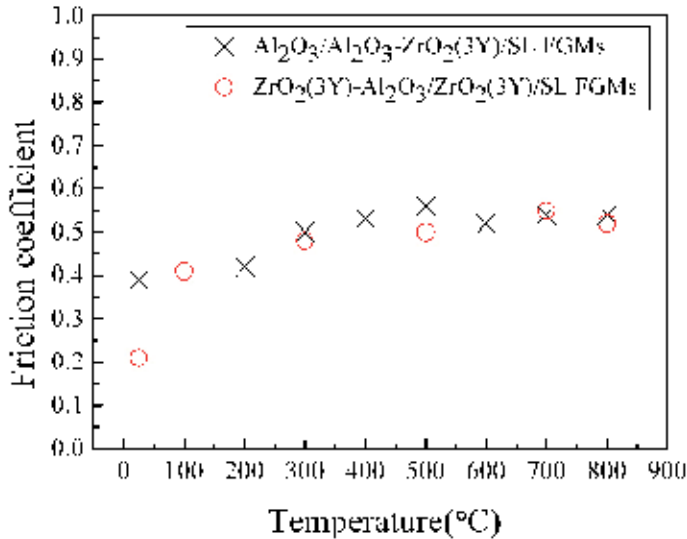
Figure 12. The friction coefficients of two kinds of laminated-graded self-lubricating composites at room temperature to 800 °C.

In conclusion, laminated-graded structure self-lubricating ceramic composites realize the integration of mechanical and tribological properties. Their excellent mechanical and tribological properties indicate that the laminated-graded structure self-lubricating ceramic composites have numerous high-technology applications and promising prospect as structural materials.

Acknowledgements

Author details

Yongsheng Zhang[*], Yunfeng Su, Yuan Fang, Yae Qi and Litian Hu

*Address all correspondence to: zhysh@licp.cas.cn

State Key Laboratory of Solid Lubrication, Lanzhou Institute of Chemical Physics, Chinese Academy of Sciences, Lanzhou, China

References

[1] Liu HW, Xue QJ. The tribological properties of TZP-graphite self-lubricating ceramics. Wear. 1996;198(1-2):143-149. DOI: 10.1016/0043-1648(96)06946-3

[2] Jin Y, Kato K, Umehara N. Further investigation on the tribological behavior of Al_2O_3-20Ag20CaF$_2$ composite at 650 °C. Tribology Letters. 1999;6(3):225-232. DOI: 10.1023/A:1019132328220

[3] Ouyang JH, Sasaki S, Murakami T, Umeda K. Tribological properties of spark-plasma-sintered $ZrO_2(Y_2O_3)$-CaF_2-Ag composites at elevated temperatures. Wear. 2005;258(9):1444-1454. DOI: 10.1016/j.wear.2004.10.007

[4] Zhang YS, Fang Y, Fan HZ, Song JJ, Hu TC, Hu LT. High-performance ceramic lubricating materials. In: Wythers MC, editor, Advances in Materials Science Research, Vol. 17, Nova Science Publishers Inc., 2014, 83-92.

[5] Zhang YS, Hu LT, Chen JM, Liu WM. Lubrication behavior of Y-TZP/Al_2O_3/Mo nanocomposites at high temperature. Wear. 2010;268(9-10):1091-1094. DOI: 10.1016/j.wear.2010.01.009

[6] Vincenzo MS, Massimo B. Design and production of ceramic laminates with high mechanical resistance and reliability. Acta Materialia. 2006;54(18):4929-4937. DOI: 10.1016/j.actamat.2006.06.019

[7] Hassana HA, Lewandowski JJ. Laminated nanostructure composites with improved bend ductility and toughness. Scripta Materialia. 2009;61(11):1072-1074. DOI:c10.1016/j.scriptamat.2009.08.034

[8] Song JJ, Zhang YS, Fang Y, Fan HZ, Hu LT, Qu JM. Influence of structural parameters and transition interface on the fracture property of Al_2O_3/Mo laminated composites. Journal of the European Ceramic Society. 2015;35(5):1581-1591. DOI: 10.1016/j.jeurceramsoc.2014.11.004

[9] Song JJ, Zhang YS, Fan HZ, Fang Y, Hu LT. Design of structure parameters and corrugated interfaces for optimal mechanical properties in alumina/graphite laminated nanocomposites. Materials & Design. 2015;65:1205-1213. DOI: 10.1016/j.matdes.2014.09.084

[10] Song JJ, Zhang YS, Su YF, Fang Y, Hu LT. Influence of structural parameters and compositions on the tribological properties of alumina/graphite laminated composites. Wear. 2015;338-339:351-361. DOI: 10.1016/j.wear.2015.07.017

[11] Qi YE, Zhang YS, Hu LT. High-temperature self-lubricated properties of Al_2O_3/Mo laminated composites. Wear. 2012;280-281:1-4. DOI: 10.1016/j.wear.2012.01.010

[12] Fang Y, Zhang YS, Song JJ, Fan HZ, Hu LT. Influence of structural parameters on the tribological properties of Al_2O_3/Mo laminated nanocomposites. Wear. 2014;320:152-160. DOI: 10.1016/j.wear.2014.09.003

[13] Song JJ, Zhang YS, Fan HZ, Hu TC, Hu LT, Qu JM. Design of interfaces for optimal mechanical properties in Al_2O_3/Mo laminated composites. Journal of the European Ceramic Society. 2015;35(3):1123-1127. DOI: 10.1016/j.jeurceramsoc.2014.09.023

[14] Kawasaki A, Watanabe R. Concept and P/M fabrication of functionally gradient materials. Ceramics International. 1997;23(1):73-83. DOI: 10.1016/0272-8842(95)00143-3

[15] Wang RG, Pan W, Chen J, Fang MH, Jiang MN, Luo YM. Graded machinable Si_3N_4/h-BN and Al_2O_3/$LaPO_4$ ceramic composites. Materials & Design. 2002;23(6):565-570. DOI: 10.1016/S0261-3069(02)00021-3

[16] Wang RG, Pan W, Jiang MN, Chen J, Luo YM. Investigation of the physical and mechanical properties of hot-pressed machinable Si_3N_4/h-BN composites and FGM. Materials Science and Engineering: B. 2002;90(3):261-268. DOI: 10.1016/S0921-5107(01)01048-0

[17] Qi YE, Zhang YS, Fang Y, Hu LT. Design and preparation of high-performance alumina functional graded self-lubricated ceramic composites. Composites Part B: Engineering. 2013;47:145-149. DOI: 10.1016/j.compositesb.2012.09.090

[18] Fang Y, Zhang YS, Song JJ, Fan HZ, Hu LT. Design and fabrication of laminated-graded zirconia self-lubricating composites. Materials & Design. 2013;49:421-425. DOI: 10.1016/j.matdes.2013.01.040

[19] Qi YE, Zhang YS, Hu LT. Preparation and properties optimization of Al_2O_3/Al_2O_3-ZrO_2 laminated nanocomposites. Journal of Materials Engineering. 2013;3(2):17-21. DOI: http://dx.doi.org/10.3969/j.issn.1001-4381.2013.06.001

[20] Qi YE, Zhang YS, Hu LT. Microstructure and bending strength of laminated nano-composites. Journal of the Chinese Ceramic Society. 2011;39(2):228-232.

An Experimental Crack Propagation Analysis of Aluminum Matrix Functionally Graded Material

Arzum Ulukoy, Muzaffer Topcu and Suleyman Tasgetiren

Additional information is available at the end of the chapter

Abstract

In this study, a functionally graded cylindrical specimen was obtained via centrifugal casting and its fatigue crack behavior was investigated. Aluminum 2014 alloy and SiC were used as matrix material and ceramic particle, respectively. The distribution of SiC and the mechanical properties of material through cylinder wall thickness were varied because of the centrifugal force during centrifugal casting. Variations in microstructure and hardness were examined. A cylindrical specimen was cut through its thickness in four sections through vertical slicing. Tensile strength was tested on each section to determine the mechanical properties that can be varied such as Young's modulus, tensile strength, and yielding stress. To investigate the effect of variation in the mechanical properties and distribution of SiC particles on fatigue crack behavior, fatigue crack growth tests were applied under tensile cyclic load with stress ratio $R = 0.1$. The samples were prepared in three separate groups: central notched, single-edge notched on SiC-rich side, and single-edge notched on aluminum-rich side. It was found that SiC distribution affected fatigue crack initiation and propagation. The fatigue life increased up to 350% because of increasing SiC ratio for central notched specimens. Cracks were started out later on the single-edge notched SiC-rich side compared to aluminum-rich side whose fatigue life increased up to 500%. In addition, it was found that unreinforced aluminum material's fatigue life was lower than that of reinforced material.

Keywords: Functionally graded material, Aluminum matrix, Franc2D, Crack propagation, Fatigue

1. Introduction

Material is used to perform a design. The design engineer expects some material properties, either single or combinations of one or more properties, from materials for engineering design such as light weight, strength, fatigue strength, high temperature strength, high fracture

toughness, corrosion resistance, wear resistance, electrical properties, and manufacturability [1, 2]. Although the metallic materials have higher fracture toughness and better thermal shock resistance than the ceramics, their high temperature resistance is lower than of the ceramics. Ceramic materials have low density, good high temperature resistance, and good creep resistance, but their thermal shock resistance is low [2–5]. Man-made polymer materials have been used for the past 100 years because they are lightweight, cheap, highly resistant to corrosion, and wear resistant. Also, the production of polymer materials is much easier than the metallic and ceramic materials. However, their low mechanical strength limits their use in structural design [2]. Composite materials are obtained by combining ceramic, metallic, and/or polymer materials. Thus, the designer can benefit from the superior properties of two different materials simultaneously [2, 4].

Metal matrix composites (MMCs) reinforced with ceramic particles provide the required material properties in many engineering applications. High strength, high corrosion resistance, and stiffness of MMCs have made them suitable for their use in, particularly, aerospace, aviation, automobile, and mineral processing industry [6, 7]. Particulate reinforced MMC materials are cheaper and have higher abrasion resistance and higher temperature stability than that of materials, and they are being used widely in many areas compared to the continuous fiber reinforced composites [6, 7].

Functionally graded materials (FGMs) can be considered as a subcategory of composite materials. The microstructure, mechanical, and thermal properties are changed throughout the thickness or width of the material depending on a function [8–10].

The function type and consequently FGMs' properties are primarily related to mechanical/thermal properties and compatibility of matrix and reinforced materials, FGM thickness or width, and manufacturing method. Function can occur in three different ways depending on the following factors: exponentially, linearly, and according to the rule of force. The mechanical/thermal properties of material such as Young's modulus, yielding stress, tensile stress, fatigue, and thermal/electrical conductivity properties can vary depending on the function type [4, 8–12].

There are some basic manufacturing methods for graded materials, which include powder metallurgy, physical vapor deposition (PVD), chemical vapor deposition (CVD), plasma spray, thermal spray, combustion synthesis (SHS), centrifugal casting, and polymerization [4, 10, 12–29]. Recently developed methods are also available: modified stir casting, centrifugal sintering, gradient slurry disintegration and deposition, and powder cold spray before cold isostatic sintering [30–33].

MMCs reinforced with ceramic particles have been used for a long time because they can be easily manufactured. MMCs are inexpensive than the other composite types and have improvable thermal and mechanical properties [7]. When two different types of materials are combined, it can lead to formation of additional thermal and residual stresses. It is known that discontinuities and thermal stress can be decreased on ceramic–metal interface using FGMs [4, 8, 9].

Crack propagation that causes sudden or stepped fracture occurs when stress concentration at the tip of crack overcomes strength of material [34]. For a linear elastic material, stress concentration at the tip can be represented by K_I, K_{II}, and K_{III}, which are stress intensity factors in opening, sliding, and tearing conditions, respectively. Critical value of stress intensity factor Kc must be equal to K_I for crack propagation under Mode I load.

There are many analytical and numerical studies on fatigue and fracture mechanics of FGMs [34–51]. Theoretical crack propagation analyses of FGMs indicate that the crack tip stress is different from that of the homogeneous material [34, 38–40]. The studies on the subject demonstrate that grading direction and function affect the crack propagation. It is found that FGMs have shown better performance at increasing crack growth compared with homogeneous materials.

Under asymmetric loadings, the crack propagates perpendicularly to grading direction, which changes the direction of crack [43]. However, under symmetric loadings, the crack propagates in parallel to grading direction [42]. Crack propagation experiments in grading materials have been carried out using the following: direction of crack propagation (in parallel to grading direction) under different loading cycles (regularly increasing or decreasing loading [53–54], periodic mechanical loading [50–52], and periodical thermal loading [58–59]). In the experiments where crack propagation was perpendicular to the grading direction, fracture happened quickly [60–62]. Therefore, the effect of grading on the stress concentration factor could not be calculated. Compared to homogeneous material, FGMs' fracture behavior is altered by FGM composition and properties by four of the following [63]:

1. Variable stress region: Crack direction in FGMs is changed by graded mechanical properties (Young's modulus, E, and the Poisson ratio, v), but not in homogeneous materials. As a result, fracture loads and crack path are affected by grading material properties.

2. Crack tip toughness: Since the chemical composition of material changes, internal fracture toughness (K_0) becomes a function ($K_0(a)$) that changes according to the position of the grading.

3. Hardening rate of the crack opening: Change in the microstructure and the chemical composition of graded region changes the characteristics of hardening of the crack opening too. Crack closure as in homogeneous materials depends on not only being on the back of the crack but also the position of the cracks in graded region.

4. Residual and thermal stresses: Thermal and residual stresses in FGMs effect fracture behavior and crack tip stress zone [53–66].

In Equation (1), σ_{ij} represents the crack tip stress, K_α (α = I, II, III) stress intensity factors, θ the angle with respect to the plane of the crack, r the distance from crack tip, δ the Kronecker delta, σ_T the transverse stress, $f_{ij}^{(\alpha)}(\theta)$ angular functions, and $1/\sqrt{r}$ the singularity of crack tip stress. Studies by Delale and Erdogan [35] and Eischen [39] showed that the singularity of crack tip stress of continuous or partially graded materials is similar to that of homogeneous materials.

Jin and Noda [41] verified this situation by determining that the angular distribution function of the elastic and plastic crack tip area ($f_{ij}(\theta)$) is the same.

$$\sigma_{ij} = \frac{K_\alpha}{\sqrt{2\pi r}} f_{ij}^{(\alpha)}(\theta) + \delta_{1i}\delta_{1j}\sigma_T + A_\alpha \sqrt{2\pi r} w_{ij}^{(\alpha)}(\theta) \tag{1}$$

Also, the studies conducted by Eischen [39] and Jin and Noda [41] have shown that FGMs crack tip stress (σ_{ij}) and displacement (u_i) (Eq. (2)) are the same form as homogeneous material. In Equation (2), K_α (α = I, II) represents stress intensity factors, r the distance from crack tip, θ the angle with respect to the plane of the crack, $g_i^{(\alpha)}(\theta)$ angular functions, E_{tip} the Young's modulus at crack tip, and v_{tip} the Poisson ratio at crack tip. These results mean that the stress intensity factor is a determinative fracture parameter for FGMs just like in homogeneous material [67]. Similar results have been found for dynamically propagated cracks by Parameswaran and Shukla [68].

$$u_i \approx \frac{K_\alpha \left(2 + 2v_{\text{tip}}\right)}{E_{\text{tip}}} \sqrt{\frac{8r}{\pi}} g_i^{(\alpha)}(\theta) \tag{2}$$

Continuous or stepped grading prevents the abnormal stress behavior of cracks when the interface of two materials is combined [69]. Moreover, Delale and Erdogan [35] found that the effect of spatial variation of the Poisson ratio on the stress singularity can be neglected.

Fracture behavior depending on orientation in the grading region can be defined by considering two limit states [63]:

1. Crack propagation is parallel to grading direction: crack does not digress although effective fracture toughness changes.

2. Crack propagation is perpendicular to grading direction: asymmetric crack tip zone causes crack to deflect.

In the cracks that are parallel to the direction, stress at the crack tip region becomes symmetric and it is expected that crack opens toward the grading direction. FGM crack tip stresses in graded regions are significantly lower than in materials with combinations of two material properties [37, 70, 71]. Stress intensity factor of FGMs is found to be greater than that of homogeneous materials. Material grading profile and position of the crack effect stress intensity factor too. When grading step increases, its value increases [35, 37, 42, 72]. Grading format also effects the stress intensity factor. If exponential value n is bigger than 1 ($n > 1$), the stress intensity factor is in tendency to decrease compared to $n < 1$ situation [70–72]. Spatial composition changes, which have an important effect on effective fracture toughness of the FGM composites, can effect thermal stress distribution throughout its width. Growing fracture toughness depends on residual stresses partially [53, 64, 73]. As residual stresses change by

composition of FGM, compressive stresses increase the resistance of crack against growing fracture [64].

Critical value of stress intensity factor K_c must be equal to K_I for crack propagation under crack opening mode. In the ongoing process, crack growth rates da/dN in every period can be found by using Paris Equation (Eq. (3)), where N is the number of cycles to failure, c and m are material constants [34].

$$\frac{da}{dN} = c\Delta K^m \qquad\qquad (3)$$

Studies related to FGMs' fatigue and fatigue fracture behaviors have been conducted using numerical and analytical methods and new approaches are developed to date. However, there are hardly enough experimental studies to support this.

In this study, aluminum 2014 matrix reinforced with SiC FGM was manufactured via centrifugal casting. The effect of SiC distribution on the mechanical and fatigue fracture properties was determined and analyzed experimentally.

2. Experimental results and analysis

Two functionally graded aluminum 2014 alloy (1.18% Si, 4.9% Cu, 1.04% Mn, in wt.) matrix materials reinforced with 20% in wt. and 9 μm SiC particles were produced by centrifugal casting. Density of SiC particles is higher than that of aluminum, 3.2 gr/cm^3 and 2.8 gr/cm^3, respectively. As a result of the centrifugal force effect, the distribution of SiC particles was varied through the wall thickness of the cylinder. More SiC particles were dispersed to the outer diameter of the FGM cylinder under these circumstances, as expected. By changing casting wall thicknesses, two cylinders having different mechanical properties were produced. The specimens were named FGM1 and FGM2, and SiC-rich and aluminum-rich regions were formed on both of FGM1 and FGM2. FGM1's wall thickness was higher than FGM2's. This result is compatible with the previous studies on the subject [74–83]. Taking into account the wear, fatigue, and fretting behaviors of FGM from previous studies, an aging process was performed (solutionizing at 500 °C, followed by water quenching and reheating for aging at 145 °C for 10 h, followed by water cooling) [75, 82, 83].

Tensile tests were performed using specimens sliced through the wall thickness and were numbered from 1 to 5 for FGM1 and FGM2 according to their position in the cylinder (from the innermost to the outermost layer). Tensile strength was tested on each section to determine the mechanical properties that can be varied such as Young's modulus (E), tensile strength (R), and yielding stress (R_e) (Figures 1–3). Tensile experiments were conducted using video extensometer at 1 mm/min tensile speed. Obtaining tensile specimens from the cylindrical FGM is shown in Figure 4.
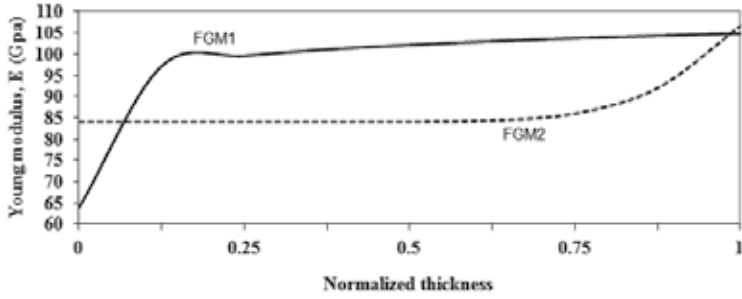
Figure 1. Young's modulus variations of FGM1 and FGM2 [84].
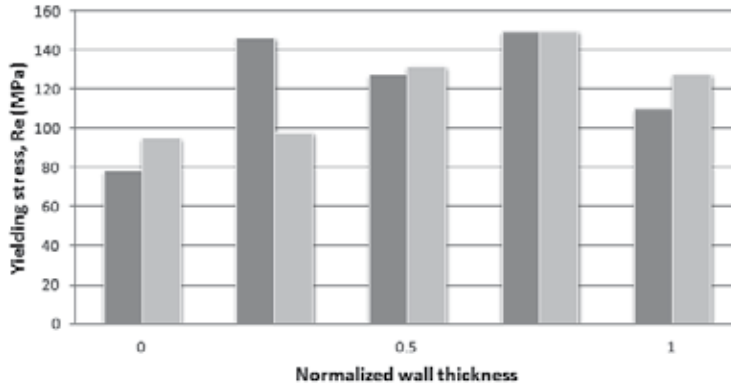
Figure 2. Yielding stress variations of FGM1 and FGM2.
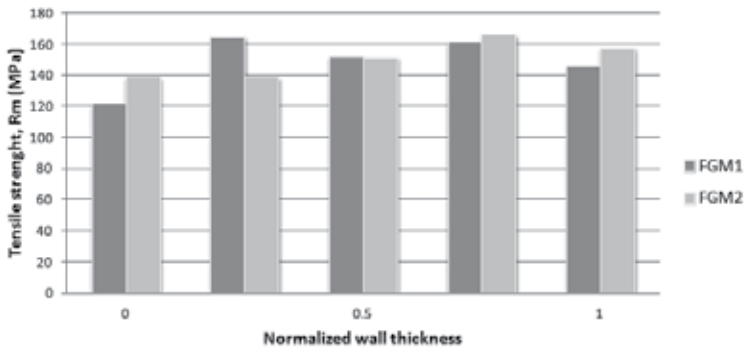
Figure 3. Tensile strength variations of FGM1 and FGM2.
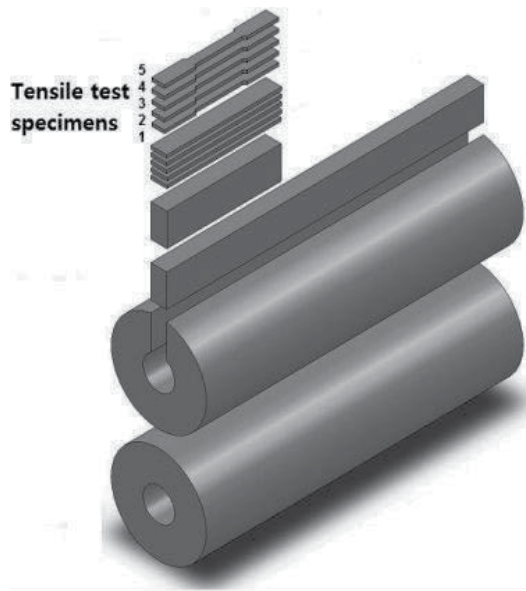
Figure 4. Obtaining tensile test samples from cylindrical FGM.

Due to the higher density of SiC particles (relative to aluminum 2014), many more particles were dispersed to the outer diameter of FGM cylinder during centrifugal casting. This produced a gradient in the Young's modulus, from the inside to the outside layer of cylinder (Figure 1) [84]. It was observed that SiC distribution under centrifugal force and wall thickness of cylinders effected Young's modulus variation. As wall thickness of cylinder decreased, it was observed that Young's modulus value (innermost of cylinder) increased from 65 MPa to 84 MPa. Grading functions of FGMs were differed from each other due to the distribution of SiC. Young's modulus values of the outermost region of cylinders were similar (105–106 MPa). It was observed that wall thickness of FGM and manufacturing process had an impact on the composition and mechanical properties of FGM.

As mentioned above, FGMs' properties can vary exponentially, linearly, and according to the rule of force. In this study, Young's modulus variation was calculated according to the rule of force to compare with experimental results using Equations (4) and (5). In these equations, $E(x)$ represents Young's modulus at x point, E_1 base material Young's modulus, E_2 reinforcing material Young's modulus, t the width/thickness of FGM, x the distance from the starting point, $g(x)$ the distance function, and p the gradient exponent. The gradient exponent (p) was calculated using equations as 0.1 and 7 for FGM1 and FGM2, respectively.

$$g\left(x\right)=\left(\frac{x}{t}\right)^{p} \tag{4}$$

$$E(x) = E_1\left(1 - g(x)\right) + E_2 g(x) \tag{5}$$

Tensile and fatigue crack growth tests were performed with a 5-ton capacity Instron fatigue servo-hydraulic test device. Two cylindrical specimens were cut through their wall thickness in four sections via vertical slicing as shown in Figure 4. Tensile tests were carried out to determine the crack opening properties using video extensometer at 1 mm/min tensile speed.

To investigate the effect of variation in mechanical properties and distribution of SiC particles on fatigue crack behavior, fatigue crack growth tests were applied under tensile cyclic load with stress ratio $R = 0.1$. The samples were prepared according to the ASTM E647 (2011) [85] in three separate groups: central notched (middle tension, M(T)), single-edge notched (SE(T)) on SiC-rich side, and single-edge notched (SE(T)) on aluminum-rich side (Figure 5). The test specimens' dimensions are shown in Figure 6. M(T) and (SE(T)) samples are prepared according to the ASTM E647 (2011) [85]. Samples were processed by laser cutting method. According to the ASTM E647 (2011) [85] standard, crack length to be opened must be at least $0.2W$; sample length $L > 0.3$. W represents width belonging to the sample. Notch length opened on M(T) specimens $2a = 13$ mm, notch length opened on SE(T) $a = 5.5$ mm [86]. Both tensile and fatigue experiments were applied to these samples. Two digital portable microscopes, as shown in Figure 7, were used to determine the crack beginning from notch tip and propagation of that crack. Applied maximum load determined with respect of minimum yielding stress after tensile tests were applied to central and single-edge notched specimens (Eq. (6)).
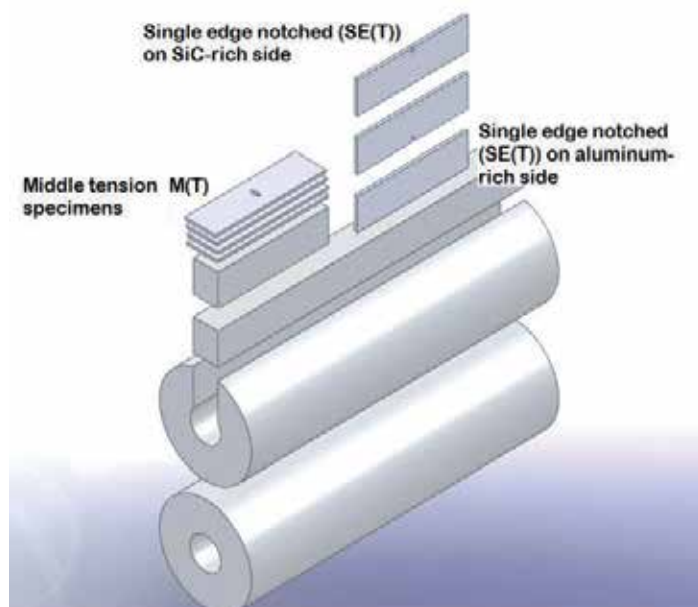
Figure 5. Obtaining fatigue crack growth test samples from cylindrical FGM [84].
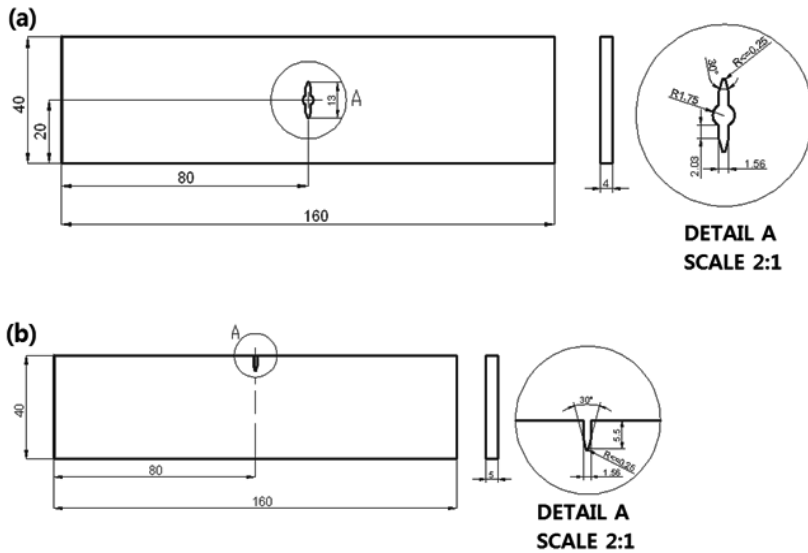
Figure 6. Dimension of fatigue crack growth test samples: (a) middle tension M(T)), (b) single-edge notched (SE(T)) [84].

$$\sigma_{max} = 0.3 Re_{min} \tag{6}$$

Stress ratio (R) is important for calculations of load increment (ΔP) and stress concentration factor increment (ΔK) for homogeneous material according to the ASTM E647 (2011) (Eq. (7–9)) [85].

$$R > 0 \Rightarrow \Delta P = P_{max} - P_{min} \tag{7}$$

$$R \leq 0 \Rightarrow \Delta P = P_{max}$$
$$\frac{2a}{W} < 0.95 \Rightarrow \Delta K = \frac{\Delta P}{B} \sqrt{\frac{\pi \alpha}{2W} \sec \frac{\pi \alpha}{2}} \tag{8}$$

$$R = \frac{P_{min}}{P_{max}} = \frac{\sigma_{min}}{\sigma_{max}} = \frac{K_{min}}{K_{max}} \tag{9}$$

For $2a/W < 0.95$ situation, M(T) specimens were accepted homogeneous and Equations (5) and (6) were used in calculations. a represents crack half-length. If $2a/W$ is greater than or equal to 0.95, it is accepted that crack will be instable and then probably fracture will be occur. The
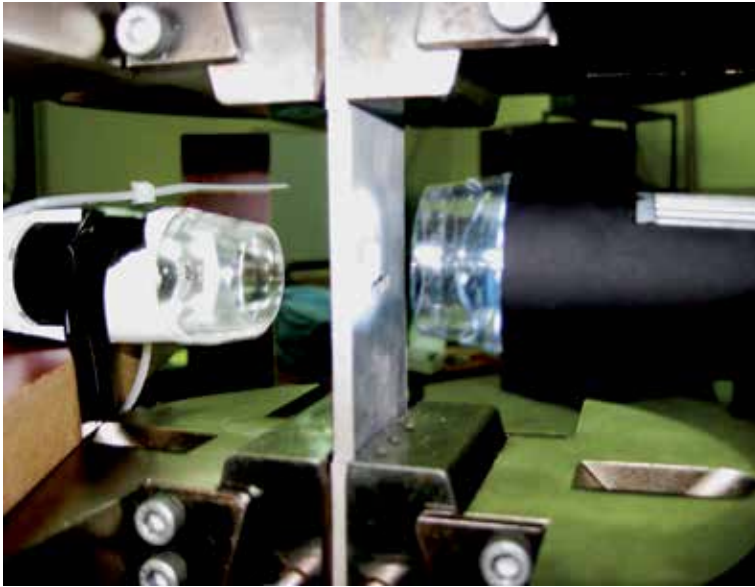
Figure 7. The digital microscopes used in experiments

stress ratio $R = 0.1$ and frequency $f = 5$ Hz were selected as fatigue crack growth experiment parameters. SE(T) specimens' notch was parallel to the grading direction.

Load-crack tip opening diagrams of M(T) specimens obtained from FGM1 after tensile tests are shown in Figure 8. Here, 1–4 refer to specimen numbers from innermost (aluminum-rich side) to outermost (SiC-rich side) regions of cylinder. It can be understood that Al-rich side fractured at a lower load value. Since SiC rate increased, load carrying capacity of specimens increased. SiC-rich side fractured at a higher load value than the others.
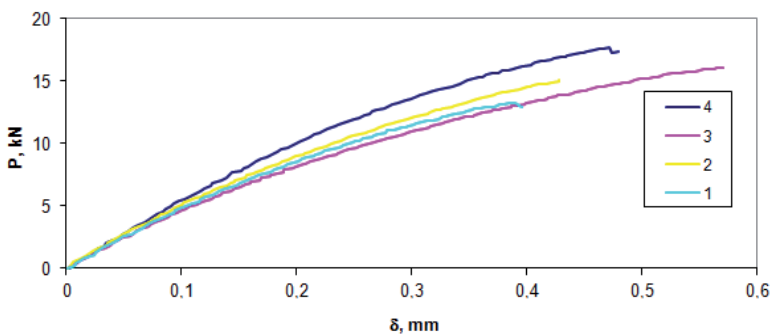
Figure 8. Load-crack tip opening diagrams of M(T) specimens obtained from FGM1.

Load-crack tip opening diagrams of SE(T) specimens obtained from FGM2 after tensile tests can be seen in Figure 9. The specimen (SE(T)) on SiC-rich side was fractured at a higher load

than the (SE(T)) on aluminum-rich side specimen. Curves are almost continued in the same way until opening value is 0.5 mm. However, it is seen that (SE(T)) on aluminum-rich side specimen fractured when load value is up to 12 kN. On the other hand, (SE(T)) on SiC-rich side specimen continues to open till an 1.6 mm opening value at 20 kN load.
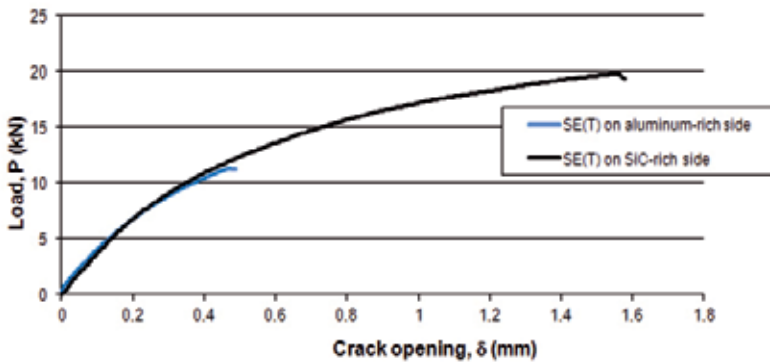
Figure 9. Load-crack tip opening diagrams of SE(T) specimens obtained from FGM2 [84].

Number of cyclic load-crack propagation diagram of M(T) samples obtained from FGM2 with stress ratio $R = 0.1$ condition is shown in Figure 10. Here, 1–4 refer to specimen numbers from innermost (aluminum-rich side) to outermost (SiC-rich side) regions of cylinder, and specimens fractured at 12,880, 27,000, 34,000, and 48,000 number of cyclic loads, respectively. It can be seen that the fatigue life increases to almost 350% because of increase in SiC rate.
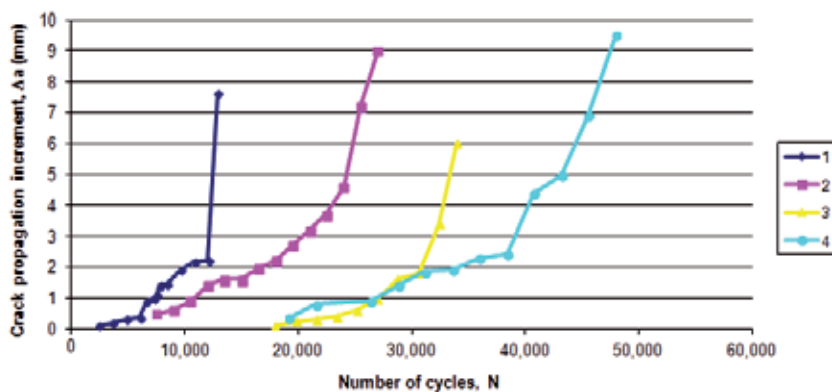
Figure 10. Number of cyclic load-crack propagation diagram of M(T) samples obtained from FGM2: 1–4 refers to specimen numbers from innermost (aluminum-rich side) to outermost (SiC-rich side) [84].

Number of cyclic load-crack propagation diagram of SE(T) samples obtained from FGM1 (both of SiC-rich side and aluminum-rich side) with stress ratio $R = 0.1$ is shown in Figure 11. It was determined that the crack growing rate increased after 14,400 cycles for the aluminum-rich side SE(T) sample. However, after 28,800 cycles, the crack growing rate increased dramatically and after 36,850 cycles, sample fractured in a short time. On the other hand, SiC-rich side SE(T) sample's crack growth rate was very slow up to 13,000 cycles under the same cyclic load and after 13,000 cycles, the growth rate increased gradually. Crack growth rate increased dramatically after 190,000 cycles and sample fractured in a short time after 214,000 cycles. Under the same fatigue load, it was determined that the SiC-rich side SE(T) sample had fatigue life more than 500% compared to the aluminum-rich side SE(T) sample.
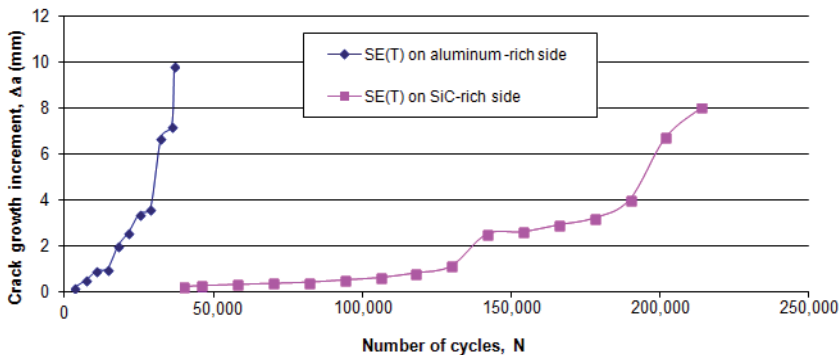
Figure 11. Number of cyclic load-crack propagation diagram of SE(T) samples obtained from FGM1 [84].

Number of cyclic load-crack propagation diagram of SE(T) samples obtained from FGM1 and FGM2 aluminum-rich side with stress ratio $R = 0.1$ condition is shown in Figure 12. A sample belonging to FGM2 displays a quick fracture behavior compared to FGM1. Whereas FGM2 sample fractured at 36,850cycles, FGM1 sample fractured at 238,000 cycles. FGM1's fatigue life was increased 1.5-fold compared to FGM2's fatigue life, which is explained by Young's modulus variation seen in Figure 1. Graphics show differences in variation of Young's modulus. SiC distribution in FGM2 increases from the innermost region to the outermost region till 0.2 times wall thickness, and then the rise slows down. In FGM1's inner region, distributions of SiC and in parallel with Young's modulus are higher than in the FGM2's. The Young's modulus determined as $E = 85$ GPa innermost of cylinder wall thickness does not visually increase by 0.75 times wall thickness.

After the fatigue crack growth experiments finished, c and m, which are material-dependent coefficients of the Paris-Erdogan equation (Eq. (3)), were found for each FGM2 M(T) specimens. The crack propagation behavior of the samples, which were from the inner diameter to the outside diameter of the cylinder numbered from 1 to 4, was observed differently in each of the samples. Therefore, the c and m coefficients were observed different from each other. The FGM's c and m coefficients are shown in Table 1.
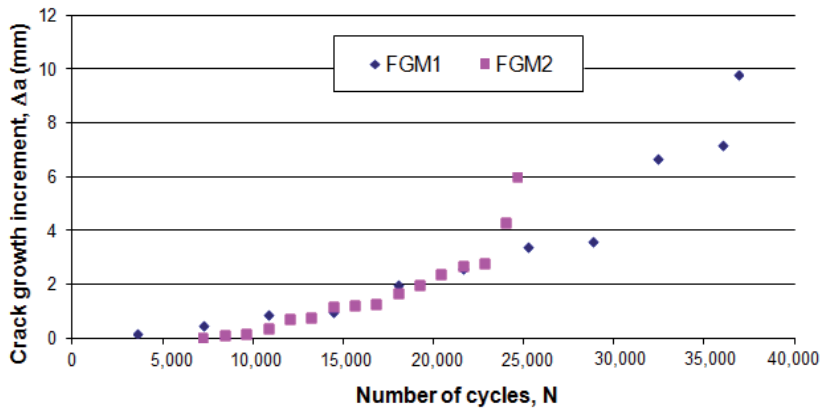
Figure 12. Number of cyclic load-crack propagation diagram of SE(T) samples obtained from FGM1 and FGM2 aluminum-rich side [84].

FRANC2D finite elements program have been developed by the fracture group of Cornell University [87]. The program is usually used for fracture mechanics and fatigue analysis. In this study, FRANC2D analysis was done for FGM2 M(T) specimens. The finite element model can be seen in Figure 13. It was accepted that the M(T) specimen was homogeneous in itself while modeling in FRANC2D. According to the analysis, obtained results from experimental and finite element modeling were similar to each other as seen in Figure 14.

	1	2	3	4
c	10^{-8}	10^{-8}	2×10^{-9}	6×10^{-9}
m	1.3632	1.0801	1.6678	1.2058

Table 1. Calculated c and m coefficients of FGM2 M(T) specimens: 1–4 refer to specimen numbers from innermost (aluminum-rich side) to outermost (SiC-rich side) regions of cylinder
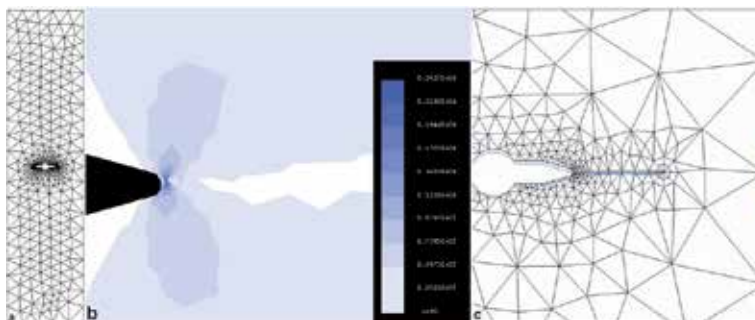
Figure 13. M(T) specimen modeling using FRANC2D program: (a) model, (b) maximum shear stress at crack tip, (c) deformation shape.
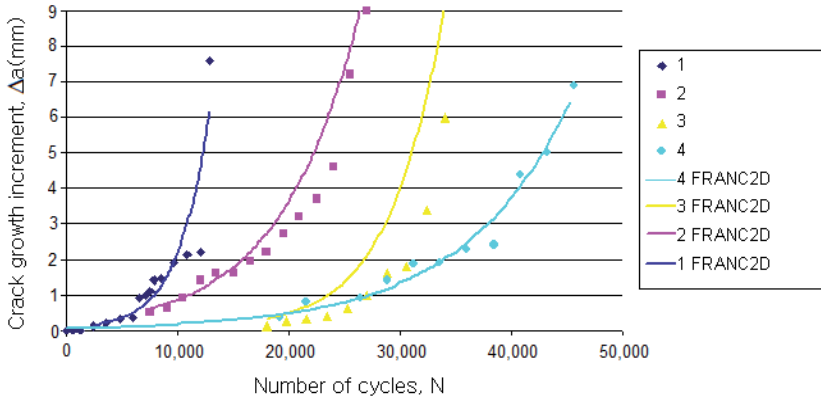
Figure 14. FRANC2D and experimental analysis results for M(T) specimens obtained from FGM2.

3. Conclusions

In the literature, studies related to FGM have mostly focused on determining FGMs' thermal properties using experimental, analytical, and numerical methods. FGMs' fatigue and fatigue fracture behaviors have been tested using numerical and analytical methods and improved new approaches are developed to date. However, there are hardly enough experimental studies to support this.

In conjunction with this study, mechanical properties and fatigue crack propagation behavior were analyzed experimentally. The results can be summarized as follows:

1. FGMs can be manufactured easily by centrifugal casting. It is possible to obtain FGM having different properties by changing casting parameters, FGM thickness, and casting weight from reinforced mixture.

2. Since SiC density is higher than aluminum, it is dispersed mostly to the outer region of material because of the centrifugal force during centrifugal casting. Therefore, hardness, composition, and mechanical properties change throughout the FGM thickness.

3. Crack propagation behaviors of single-edge notched (SE(T)) on SiC-rich side and single-edge notched (SE(T)) on aluminum-rich side specimens are different from each other under the same fatigue load. Fatigue crack propagation both begins later and has long fatigue life on SiC-rich side.

4. Each middle tension M(T) specimen obtained by slicing wall thickness as four sections shows different crack propagation behaviors. As SiC rate increases, crack begins and propagations are delayed under the same experimental conditions. After all, fatigue life increases to approximately 350%.

5. $p < 1$ seems to be more advantageous than $p > 1$ condition after crack propagation experiments of FGM when crack propagation starts from single-edge notched (SE(T)) aluminum-rich side considering the gradient exponent.

Acknowledgements

Author details

Arzum Ulukoy[1*], Muzaffer Topcu[2] and Suleyman Tasgetiren[3]

*Address all correspondence to: aulukoy@pau.edu.tr

1 Manufacturing Engineering Department, Faculty of Technology, Pamukkale University, Denizli, Turkey

2 Mechanical Engineering Department, Faculty of Engineering, Pamukkale University, Denizli, Turkey

3 Mechanical Engineering Department, Faculty of Engineering, Bursa Orhangazi University, Bursa, Turkey

References

[1] Ashby MF. Materials Selection in Mechanical Design. Burlington: Butterworth-Heinemann Linacre House, Jordan Hill, Oxford OX28DP30 Corporate Drive; 2004. pp. 80–81.

[2] Wojciechowski S. New trends in the development of mechanical engineering materials. J Mater Process Technol. 2000; 106(1): 230–235.

[3] Mukerji J. Ceramic matrix composites. Defence Sci J. 2013; 43(4): 385–395.

[4] Cirakoglu M. Processing and characterization of functionally graded titanium/titanium boride/titanium diboride composites by combustion synthesis/compaction and microwaves [thesis]. University of Idaho; 2001.

[5] Yamamoto G and Hashida T. Carbon nanotube reinforced alumina composite materials. In: Hu N, editor. Composites and Their Properties. p. 483. InTech, Rijeka, Cro-

atia, DOI: 10.5772/48667; 2012. Available from: www.intechopen.com/books/composites-and-their-properties/carbon-nanotube-reinforced-alumina-composite-materials.

[6] Ahmad Z and Aleem JA. Corrosion behavior of aluminium metal matrix composite. In: Ahmad Z, editor. Recent Trends in Processing and Degradation of Aluminium Alloys. p. 385. InTech, Rijeka, Croatia, DOI: 10.5772/23631; 2011. Available from: www.intechopen.com/books/recent-trends-in-processing-and-degradation-of-aluminium-alloys/corrosion-behavior-of-aluminium-metal-matrix-composite.

[7] Chawla N and Chawla KK. Metal Matrix Composites. New York: Springer Science + Business Media; 2006.

[8] Tilbrook MT, Moon RJ, and Hoffman M. Crack propagation in graded composite. Compos Sci Technol 2005;65: 201–220.

[9] Cho JR and Oden JT. Functionally graded material: a parametric study on thermal-stress characteristics using the crank-nicolson-galerkin scheme. Comput Meth Appl Mech Eng. 2000;188: 17–38.

[10] Reimanis IE. Functionally graded materials. In: Wessel JK, editor. Handbook of Advanced Materials: Enabling New Designs. Wiley-Interscience, Hoboken, New Jersey; 2004. pp. 465–487.

[11] Koizumi M. The concept of FGM. Ceram Trans Funct Gradient Mater. 1993; 34: 3–10.

[12] Rassbach S and Lehnert W. Investigations of deformation of FGM. Comp Mater Sci. 2000; 19: 298–303.

[13] Xu FM, Zhu SJ, Zhao J, Qi M, Wang FG, Li SX, and Wang ZG. Effect of stress ratio on fatigue crack propagation in a functionally graded metal matrix composite. Compos Sci Technol. 2004; 64: 1795–1803.

[14] Oyelayo AO and Haselkorn MH. Modified boron containing coating for improved wear and pitting resistance. U.S.A. Patent. 2002; patent number: 6432480.

[15] Cetinel H, Uyulgan B, Tekmen C, Ozdemir I, and Celik E.. Wear properties of functionally gradient layers on stainless steel substrates for high temperature applications. Surf Coat Technol. 2003; 174–175: 1089–1094.

[16] Demirkiran AS, Celik E, Yargan M, and Avcı E. Oxidation behaviour of functionally gradient coatings including different composition of cermets. Surf Coat Technol. 2001; 142–144: 551–556.

[17] Burris KW, Beardsley MB, and Chuzhoy L. Process for applying a functionally gradient coating to a component for improved performance. U.S.A. Patent. 2000; patent number: 6048586

[18] Ichikawa K Functionally Graded Materials in the 21st Century: A Workshop on Trends and Forecasts. Boston: Kluwer Academic Publishers; 2001.

[19] Biesheuvel MP and Verweij H. Calculation of the composition profile of a functionally graded material produced by centrifugal casting. J Am Ceram Soc. 2000; 83: 743–749.

[20] Qin XH, Han WX, Fan CG, Rong LJ, and Li YY. Research on distribution of SiC particles in aluminum-alloy matrix functionally graded composite tube manufactured by centrifugal casting. J Mater Sci Lett. 2002; 21: 665–667.

[21] Zhang J, Wang YQ, Zhou BL, and Wu XQ. Functionally graded Al/Mg2Si in-situ composites prepared by centrifugal casting. J Mater Sci Lett. 1998; 17: 1677–1679.

[22] Sivakumar R, Nishikawa T, Honda S, Awaj H, and Gnanam FD. Processing of mullite-molybdenum graded hollow cylinders by centrifugal molding technique. J Eur Ceram Soc. 2003; 23: 765–772.

[23] Watanabe Y, Yamanaka N, and Fukui Y. Control of composition gradient in a metal-ceramic functionally graded material manufactured by the centrifugal method. Compos Part A Appl Sci Manuf. 1998; 29: 595–601.

[24] Watanabe Y, Yamanaka N, and Fukui Y. Wear behavior of Al-Al3Ti composite manufactured by a centrifugal method. Metall Mater Trans A. 1999; 30(12): 3253–3261.

[25] Watanabe Y, Kawamoto A, and Matsuda K. Particle size distributions in functionally graded materials fabricated by the centrifugal solid-particle method. Compos Sci Technol. 2002; 62: 881–888.

[26] Lee NJ, Jang J, Park M, and Choe CR. Characterization of functionally gradient epoxy/carbon fibre composite prepared under centrifugal force. J Mater Sci. 1997; 32: 2013–2020.

[27] Kim JK and Rohatgi PK. Formation of a graphite-rich zone in centrifugally cast copper alloy graphite composites. J Mater Sci. 1998; 33: 2039–2045.

[28] Chen W, Wang Q, Zai C, Ma C, Zhu Y, and He W. Functionally graded Zn-Al-Si in-situ composites fabricated by centrifugal casting. J Mater Sci Lett. 2001; 20: 823–826.

[29] Duque NB, Melgarejo ZH, and Suarez OM. Functionally graded aluminum matrix composites produced by centrifugal casting. Mater Charact. 2005;55:167-171.

[30] Ahmad SNAS, Hashim J, and Ghazali MI. Effect of porosity on tensile properties of cast particle reinforced MMC. J Compos Mater. 2005; 39(5): 451–466.

[31] Kinemuchi Y, Wataria K, and Uchimurab K. Centrifugal sintering of ceramics. J Eur Ceram Soc. 2004; 24: 2061–2066.

[32] Gupta M. Functionally gradient materials and the manufacture thereof. U.S.A. Patent. 2002; patent number: 6495212

[33] Groza JR, and Kodash V. Methods for production of FGM net shaped body for various applications. U.S.A. Patent. 2006; patent number: 0172073.

[34]   Paris PC and ErdoganA critical analysis of crack propagation lawsJ Basic Eng196385(4)528–533.

[35]   Delale F and Erdogan F. The crack problem for a nonhomogeneous plane. J Appl Mech. 1983; 50: 609–614.

[36]   Erdogan F. The crack problem for bonded nonhomogeneous materials under anti-plane shear loading. J Appl Mech. 1985; 52: 823–828.

[37]   Erdogan F. Fracture mechanics of functionally graded materials. Compos Eng. 1995; 5(7): 753–770.

[38]   Erdogan F. Fracture mechanics of functionally graded materials. U.S. Air Force Office of Scientific Research Final Technical Report. October 1996.

[39]   Eischen JW. Fracture of nonhomogeneous materials. Int J Fract. 1987; 34: 3–22.

[40]   Konda N and Erdogan F. The mixed mode crack problem in a nonhomogeneous elastic medium. Eng Fract Mech. 1994; 47(4): 533–545.

[41]   Jin ZH and Noda N. Crack-tip singular fields in nonhomogeneous materials. J Appl Mech. 1994; 61: 738–740.

[42]   Jin ZH and Batra RC. Some basic fracture mechanics concepts in functionally graded materials. J Mech Phys Solids. 1996; 44(8): 1221–12234.

[43]   Gu P and Asaro RJ. Cracks in functionally graded materials. Int J Solids Struct. 1997; 34(1): 1–17.

[44]   Lee YL and Erdogan F. Interface cracking of FGM coatings under steady-state heat flow. Eng Fract Mech. 1998;59(3):361-380.

[45]   Xu FM, Zhu SJ, Zhao J, Qi M, Wang FG, Li SX and Wang ZG. Effect of stress ratio on fatigue crack propagation in a functionally graded metal matrix composite. Composites Science and Technology. 2004;64:1795-1803.

[46]   Guler MA and Erdogan F. The frictional sliding formulations upon which subsequent analysis of the contact problems of rigid parabolic and cylindrical tangential loading problem will be performed in stamps on graded coatings. Int. J. Mech. Sci. 2007;49:161-182.

[47]   Chen J, Wu L and Du S. A modified J integral for functionally graded materials. Mechanics Research Communications. 2000;27(3):301-306.

[48]   Weichen S. On the dynamic energy release rate in functionally graded materials. International Journal of Fracture. 2005;131(3):31-35.

[49]   Kolednik O. The yield stress gradient effect in inhomogeneous materials. Int J Solids Struct. 2000; 37: 781–808.

[50] Konda N and Erdogan F. The mixed mode crack problem in a nonhomogeneous elastic medium. Eng Fract Mech. 1994; 47(4): 533–545.

[51] Oral A, Çopur IH, and Anlas G. Özellikleri fonksiyonel olarak değişen malzemelerde karışık mod yükleme altında çatlak başlama açıları ve gerilim şiddet çarpanları. In: 8. Ulusal Kırılma Konferansı Bildiriler Kitabı; November 7–9 2007; Istanbul, Turkey; 2007. pp. 10–19.

[52] Yıldırım B, Dag S, and Erdogan F. Three dimensional fracture analysis of FGM coatings under thermomechanical loading. Int J Fract. 2005; 132: 369–395.

[53] Chung TJ, Neubrand A, Rödel J, and Fett T. Fracture toughness and r-curve behaviour of Al_2O_3/Al FGMs. Ceram Trans. 2001; 114: 789–796.

[54] Moon RJ, Hoffman M, Hilden J, Bowman KJ, Trumble KP, and Rödel. R-Curve behaviour in alumina-zirconia composites with repeating graded layers. J. Eng Fract Mech. 2002; 69: 1647–1665.

[55] Forth SC, Favrow LH, Keat WD, and Newman JA. Three-dimensional mixed-mode fatigue crack growth in a functionally graded titanium alloy. Eng Fract Mech. 2003; 70: 2175–2185.

[56] Xu FM, Zhu SJ, Zhao J, Qi M, Wang FG, Li SX, and Wang ZG. Fatigue crack growth in SiC particulate-reinforced Al matrix graded composite. Mater Sci Eng A. 2003; 360: 191–196.

[57] Xu FM, Zhu SJ, Zhao J, Qi M, Wang FG, Li SX, and Wang ZG. Comparison of the fatigue growth behaviour in homogeneous and graded SiC particulate reinforced Al composite. J Mater Sci Lett. 2003; 22: 899–901.

[58] Balke H, Bahr HA, Semenov AS, Hofinger I, Häusler C, Kirchhoff G, and Weiss HJ. Graded thermal barrier coatings: Cracking due to laser irradiation and determining of fracture toughness. Ceram Trans. 2001; 114: 205–212.

[59] Hofinger I, Bahr HA, Balke H, Kirchhoff G, Häusler C, and Weiß HJ. Fracture mechanical modelling and damage characterisation of functionally graded thermal barrier coatings by means of laser irradiation. Mater Sci Forum. 1999; 308(311): 450–456.

[60] Rousseau CE and Tippur HV. Compositionally graded materials with cracks normal to the elastic gradient. Acta mat. 2000; 48: 4021–4033.

[61] Hoffman M, Kidson L, Kelly D, and Deneke C. Effect of crack growth resistance upon fracture of ceramic/polymer graded interfaces. In: Ravi-Chandar K, Karihaloo BL, Kishi T, Ritchie RO, Yokobori AT, Yokobori T, editors. Advances in Fracture Research, Proc. ICF10; Pergamon2001.

[62] Chapa-Cabrera JG and Reimanis IE. Effects of residual stress and geometry on predicted crack paths in graded composites. Eng Fract Mech. 2002; 69: 1667–1678.

[63] Tilbrook MT. Fatigue crack propagation in functionally graded materials [thesis]. University of New South Wales; 2005.

[64] Lin JS and Miyamoto Y. Internal stress and fracture behaviour of symmetric Al2O3/TiC/Ni FGMs. Mater Sci Forum. 1999; 308(311): 855–860.

[65] Freund LB. Stress distribution and curvature of a general compositionally graded semiconductor layer. J Crystal Growth. 1993; 132(1–2): 341–344.

[66] Shabana YM and Noda N. Thermo-elastic-plastic stresses in functionally graded materials subjected to thermal loading taking residual stresses of the fabrication process into consideration. Composites: B. 2001; 32: 111–121.

[67] Anderson TL. Fracture Mechanics: Fundamentals & Applications. Boca Raton: CRC Press; 1995.

[68] Parameswaran V and Shukla A. Crack-tip stress fields for dynamic fracture in functionally graded materials. Mech Mater. 1999; 31: 579–596.

[69] Chen YF and Erdogan F. The interface crack problem for a nonhomogeneous coating bonded to a homogeneous substrate. J Mech Phys Solids. 1996; 44: 771–787.

[70] Bao G and Wang L. Multiple cracking in functionally graded ceramic/metal coatings. Int J Solids Struct. 1995; 32(19): 2853–2871.

[71] Bleek O, Munz D, Schaller W, and Yang YY. Effect of a graded interlayer on the stress intensity factor of cracks in a joint under thermal loading. Eng Fract Mech. 1998; 60(5–6): 615–623.

[72] Wang YS and Gross D. Analysis of a crack in a functionally gradient interface layer under static and dynamic loading. Key Eng Mater. 2000; 187(183): 331–336.

[73] Chung TJ, Neubrand A, and Rödel J. Effect of residual stress on the fracture toughness of Al_2O_3/Al gradient materials. Key Eng Mater. 2002; 206(213): 965–968.

[74] Duque NB, Melgarejo ZH, and Suarez OM. Functionally graded aluminum matrix composites produced by centrifugal casting. Mater Charact. 2005; 55: 167–171.

[75] Quadrini E. Microstructural characterization of a silicon carbide whisker reinforced 2014 aluminum metal matrix composite. Journal De Physique, IV Colloque C7, SupplBment au Journal de Physique. 1993; 111(3): 1741–1744.

[76] Melgarejo ZH, Sua´ rez OM, and Sridharan K. Wear resistance of a functionally-graded aluminum matrix composite. Scr Mater. 2005; 55: 95–98.

[77] Rajan TPD, Pillai RM, and Pai BC. Characterization of centrifugal cast functionally graded aluminum-silicon carbide metal matrix composites. Mater Charact. 2010; 61: 923–928.

[78] Vieira AC, Sequeira PD, Gomes JR, and Rocha LA. Dry sliding wear of Al alloy/SiC functionally graded composites: Influence of processing conditions. Wear. 2009; 267: 585–592.

[79] Watanabe Y and Nakamura T. Microstructures and wear resistances of hybrid Al-(Al3TişAl3Ni) FGMs fabricated by a centrifugal method. Intermetallics. 2001; 9: 33–43.

[80] Kai W, Xue HS, Zou MH, Liu CM. Microstructural characteristics and properties in centrifugal casting of SiCp/Zl104 composite. Trans Nonferrous Met Soc China. 2009; 19: 1410–1415.

[81] Tokaji K. Effect of stress ratio on fatigue behaviour in SiC particulate-reinforced aluminium alloy composite. Fatigue Fract Eng Mater Struct. 2005; 28: 539–545.

[82] Ulukoy A, Topcu M, and Tasgetiren S. The effect of aging treatments on wear behavior of aluminum matrix functionally graded material under wet and dry sliding conditions. Mat wiss u Werkstofftech. 2011; 42: 806–811.

[83] Ulukoy A, Topcu M, and Tasgetiren S. Experimental investigation of aluminum matrix functionally graded material: Microstructural and hardness analyses, fretting, fatigue, and mechanical properties.. Proceedings of the Institution of Mechanical Engineers, Part J: Journal of Engineering Tribology. DOI: 10.1177/1350650115594405

[84] Uluköy A, Topçu M, and Taşgetiren S. Experimental investigation of crack propagation in aluminum matrix functionally graded material. In: UMTIK-2014 16th International Conference on Machine Design and Production; June 30–July 3, Izmir, Turkey, 2014.

[85] ASTM E647. Standard Test Method for Measurement of Fatigue Crack Growth Rates. ASTM International, 100 Barr Harbor Drive, PO Box C700, West Conshohocken, PA 19428-2959; 2011.

[86] Ergun E. Fracture and fatigue analysis of repaired cracks in aluminum plates with composite patch under temperature and moisture [thesis]. Pamukkale University; 2009.

[87] www.cfg.cornell.edu/software.html, Cornell Fracture Group, 02/04/2016 [Internet].

[88] Ulukoy A. Experimental and numerical analysis of fretting fatigue behavior of functionally graded material manufactured by centrifugal casting [thesis]. Pamukkale University; 2011.

A Unified Accurate Solution for Three-dimensional Vibration Analysis of Functionally Graded Plates and Cylindrical Shells with General Boundary Conditions

Guoyong Jin, Zhu Su and Tiangui Ye

Additional information is available at the end of the chapter

Abstract

Three-dimensional (3-D) vibration analysis of thick functionally graded plates and cylindrical shells with arbitrary boundary conditions is presented in this chapter. The effective material properties of functionally graded structures vary continuously in the thickness direction according to the simple power-law distributions in terms of volume fraction of constituents and are estimated by Voigt's rule of mixture. By using the artificial spring boundary technique, the general boundary conditions can be obtained by setting proper spring stiffness. All displacements of the functionally graded plates and shells are expanded in the form of the linear superposition of standard 3-D cosine series and several supplementary functions, which are introduced to remove potential discontinuity problems with the original displacements along the edge. The Rayleigh-Ritz procedure is used to yield the accurate solutions. The convergence, accuracy and reliability of the current formulation are verified by numerical examples and by comparing the current results with those in published literature. Furthermore, the influence of the geometrical parameters and elastic foundation on the frequencies of rectangular plates and cylindrical shells is investigated.

Keywords: Three-dimensional elasticity theory, functional graded materials, plate and cylindrical shell, general boundary conditions

1. Introduction

Functionally graded materials (FGMs) are a new type of composite materials with smooth and continuous variation in material properties in desired directions. This is achieved by gradually varying the volume fraction of the constituent materials. Such materials possess various advantages over conventional composite laminates, such as smaller stress concentration,

higher fracture toughness and improved residual stress distribution. Recently, the FGMs have been used to build plate and shell components in various engineering applications, especially mechanical, aerospace, marine and civil engineering. In some cases, those FGM plates and shells are frequently subjected to dynamic loads, which leads to the vibration behaviours, which may cause fatigue damage and result in severe reduction in the strength and stability of the whole structures. Therefore, the vibration analysis of the FGM plates and shells is required and it is important to provide insight into dynamic behaviours and optimal design.

It is well known that vibration problems deal with two main concepts: plate and shell theories and computational approaches. The development of plate and shell theories has been subjected to significant research interest for many years, and many plate and shell theories have been proposed and developed. The main plate and shell theories can be classified into two categories: two-dimensional (2-D) plate and shell theories, including classic plate and shell theory (CPT) [1–4], the first-order shear deformation theory (FSDT) [5–16], and the higher order shear deformation theory (HSDT) [17–26], and three-dimensional (3-D) theory of elasticity [27–35]. However, all 2-D theories are approximate because they were developed based on certain kinematic assumptions that result in relatively simple expression and derivation of solutions. Actually, 3-D elasticity theory, which does not rely on any hypotheses about the distribution field of deformations and stress, not only provides realistic results but also allows for further physical insight. More attempts have been made for 3-D vibration analysis of plates and shells in the recent decades. Furthermore, many analytical, semi-analytical and numerical computational methods have also been developed, such as Ritz method, state-space method, differential quadrature method (DQM), Galerkin method, meshless method, finite element method (FEM) and discrete singular convolution (DSC) approach.

However, a close scrutiny of the literature in this field reveals that most investigations were carried out based on 2-D plate and shell theories, and a general 3-D solution for this subject seems to be limited. Moreover, the review also reveals that most of previous research efforts were restricted to vibration problems of FGM plates and shells with limited sets of classical boundary conditions. It is well recognized that there exist various possible boundary restraint cases for plates and shells in practical assembly and engineering applications. Consequently, it is necessary and of great significance to develop a unified, efficient and accurate method that is capable of universally dealing with FGM plates and shells with general boundary conditions.

In view of these apparent voids, the aim of this chapter is to develop an accurate semi-analysis method that is capable of dealing with vibrations of FGM plates and shells with general boundary conditions, including classical boundaries, elastic supports and their combinations and to provide a summary of known 3-D results of plates and shells with general boundary conditions, which may serve as benchmark solutions for future researches in this field.

In this chapter, 3-D vibration analysis of thick functionally graded plates and cylindrical shells with arbitrary elastic restraints is presented. The effective material properties of functionally graded structures vary continuously in the thickness direction according to the simple power-law distributions in terms of volume fraction of constituents and are estimated by Voigt's rule

of mixture. By using the artificial spring boundary technique, the general boundary conditions can be obtained by setting proper spring stiffness. All displacements of the functionally graded plates and shells are expanded in the form of the linear superposition of standard 3-D cosine series and several supplementary functions, which are introduced to remove potential discontinuity problems with the original displacements along the edge. The RayleighRitz procedure is used to yield the accurate solutions.

2. Theoretical formulations

2.1. Preliminaries

A differential element of a shell with uniform thickness h is considered, as shown in Fig. 1. An orthogonal curvilinear coordinate system composed of coordinates α, β and z coordinates is located on the bottom surface. The u, v and w denote the displacement components of an arbitrary point in the α, β and z directions, respectively. Within the context of 3-D elasticity theory, the linear strain-displacement relations can be expressed as follows [36]:

$$\varepsilon_{\alpha\alpha} = \frac{1}{h_\alpha}\frac{\partial u}{\partial \alpha} + \frac{1}{h_\alpha h_\beta}\frac{\partial h_\alpha}{\partial \beta}v + \frac{1}{h_\alpha h_z}\frac{\partial h_\alpha}{\partial z}w \tag{1}$$

$$\varepsilon_{\beta\beta} = \frac{1}{h_\beta}\frac{\partial v}{\partial \beta} + \frac{1}{h_\beta h_z}\frac{\partial h_\beta}{\partial z}w + \frac{1}{h_\beta h_\alpha}\frac{\partial h_\beta}{\partial \alpha}u \tag{2}$$

$$\varepsilon_{zz} = \frac{1}{h_z}\frac{\partial w}{\partial z} + \frac{1}{h_z h_\alpha}\frac{\partial h_z}{\partial \alpha}u + \frac{1}{h_z h_\beta}\frac{\partial h_z}{\partial \beta}v \tag{3}$$

$$\gamma_{\beta z} = \frac{1}{h_\beta h_z}\left(h_\beta \frac{\partial v}{\partial z} + h_z \frac{\partial w}{\partial \beta} - \frac{\partial h_\beta}{\partial z}v - \frac{\partial h_z}{\partial \beta}w \right) \tag{4}$$

$$\gamma_{\alpha z} = \frac{1}{h_\alpha h_z}\left(h_\alpha \frac{\partial u}{\partial z} + h_z \frac{\partial w}{\partial \alpha} - \frac{\partial h_\alpha}{\partial z}u - \frac{\partial h_z}{\partial \alpha}w \right) \tag{5}$$

$$\gamma_{\alpha\beta} = \frac{1}{h_\alpha h_\beta}\left(h_\alpha \frac{\partial u}{\partial \beta} + h_\beta \frac{\partial v}{\partial \alpha} - \frac{\partial h_\beta}{\partial \alpha}v - \frac{\partial h_\alpha}{\partial \beta}u \right) \tag{6}$$

where ε_α, ε_β, ε_z, $\varepsilon_{\beta z}$, $\varepsilon_{\alpha z}$ and $\varepsilon_{\alpha\beta}$ are the normal and shear strain components, and h_α, h_β and h_z are Lame coefficients.
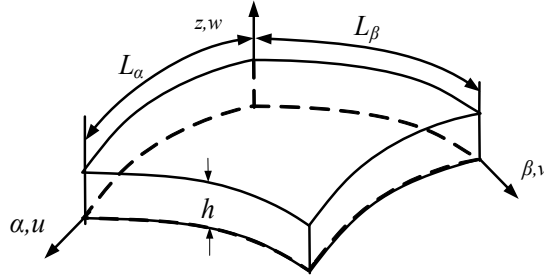
Figure 1. Geometry of differential element of shells
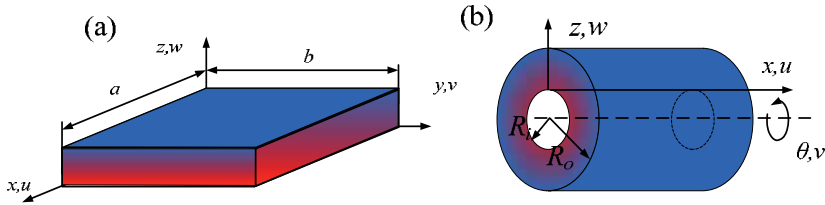
Figure 2. Definition of coordinate systems: (a) plate and (b) cylindrical shell.

In engineering applications, plates and shells are the basic structural elements. For the sake of brevity, this chapter will be confined to rectangular plates and cylindrical shells. According to Fig. 2, the coordinate systems and Lame coefficients are given as follows [36]: for rectangular plates, $\alpha = x$, $\beta = y$, $z = z$, $h_\alpha = h_\beta = h_\gamma = 1$ and   for   cylindrical   shells, $\alpha = x$, $\beta = \theta$, $z = r$, $h_\alpha = h_\gamma = 1$, $h_\beta = R_i + r$. The explicit expressions of strains can be obtained by substituting above quantities into Eqs. (1–6). The 3-D linear constitutive relations for the plates and shells can be written as follows:

$$
\begin{bmatrix} \sigma_{\alpha\alpha} \\ \sigma_{\beta\beta} \\ \sigma_{zz} \\ \sigma_{\beta z} \\ \sigma_{\alpha z} \\ \sigma_{\alpha\beta} \end{bmatrix} = \begin{bmatrix} Q_{11} & Q_{12} & Q_{13} & 0 & 0 & 0 \\ Q_{12} & Q_{22} & Q_{23} & 0 & 0 & 0 \\ Q_{13} & Q_{23} & Q_{33} & 0 & 0 & 0 \\ 0 & 0 & 0 & Q_{44} & 0 & 0 \\ 0 & 0 & 0 & 0 & Q_{55} & 0 \\ 0 & 0 & 0 & 0 & 0 & Q_{66} \end{bmatrix} \begin{bmatrix} \varepsilon_{\alpha\alpha} \\ \varepsilon_{\beta\beta} \\ \varepsilon_{zz} \\ \gamma_{\beta z} \\ \gamma_{\alpha z} \\ \gamma_{\alpha\beta} \end{bmatrix} \tag{7}
$$

where Q_{ij} ($i, j = 1$–6) are the elastic coefficients and are given as:

$$Q_{11} = Q_{22} = Q_{33} = \frac{E(r)[1 - \mu(r)]}{[1 + \mu(r)][1 - 2\mu(r)]},$$

$$Q_{12} = Q_{13} = Q_{23} = \frac{\mu(r)E(r)}{[1 + \mu(r)][1 - 2\mu(r)]}, \tag{8}$$

$$Q_{44} = Q_{55} = Q_{66} = \frac{E(r)}{[2(1 + \mu(r)]},$$

where $E(r)$ and $\mu(r)$ are the effective Young's modulus and Poisson's ratio of a FGMs, respectively. In this chapter, it is assumed that the FGMs are manufactured by ceramic and metallic constituents, and the effective material properties of FGMs can be expressed as follows [37]:

$$E(r) = (E_c - E_m)V_c + E_m$$

$$\mu(r) = (\mu_c - \mu_m)V_c + \mu_m \tag{9}$$

$$\rho(r) = (\rho_c - \rho_m)V_c + \rho_m$$

where E, μ, ρ and V are Young's modulus, Poisson's ratio, density and volume fraction, respectively. The subscripts c and m donate the ceramic and metallic constituents, respectively. The ceramic volume fraction follows simple power-law distribution:

$$V_c = (\frac{z}{h})^p, V_m = 1 - (\frac{z}{h})^p \qquad (0 \le z \le h) \tag{10}$$

where z is the thickness coordinate, and p is the power-law index that takes only positive values. The value of p equal to zero represents a fully ceramic plate, whereas infinite p indicates a fully metallic plate.

In this work, the general boundary conditions can be described in terms of three groups of springs (k_u, k_v, k_w). Taking edge α = constant, for example, the boundary conditions can be given as follows:

$$k_u^{\alpha 1} u = \sigma_{\alpha\alpha}, k_v^{\alpha 1} v = \sigma_{\alpha\beta}, k_w^{\alpha 1} w = \sigma_{\alpha z} \tag{11}$$

$$k_u^{\alpha 2} u = \sigma_{\alpha\alpha}, k_v^{\alpha 2} v = \sigma_{\alpha\beta}, k_w^{\alpha 2} w = \sigma_{\alpha z} \tag{12}$$

where the superscripts $\alpha 1$ and $\alpha 2$ denote the edges of $\alpha = 0$ and $\alpha = L_1$, respectively. For the rectangular plates, the similar conditions exist for the edges of β = constant. The classical boundary conditions and elastic restrains can be obtained by easily changing the values of boundary spring.

2.2. Energy functional

The energy functional of plates or shells can be expressed as follows:

$$\Pi = T - U - P \tag{13}$$

where T is kinetic energy, U is elastic strain energy, and P denotes the potential energy stored in boundary springs.

The kinetic energy T can be written as follows:

$$T = \frac{1}{2} \iiint \rho(z)\left(\dot{u}^2 + \dot{v}^2 + \dot{w}^2\right) \mathrm{d}\alpha\mathrm{d}\beta\mathrm{d}z \tag{14}$$

where the over dot represents the differentiation with respect to time.

The strain energy U can be written in an integral form as follows:

$$U = \frac{1}{2} \iiint \left(\sigma_{\alpha\alpha}\varepsilon_{\alpha\alpha} + \sigma_{\beta\beta}\varepsilon_{\beta\beta} + \sigma_{zz}\varepsilon_{zz} + \sigma_{\beta z}\gamma_{\beta z} + \sigma_{\alpha z}\gamma_{\alpha z} + \sigma_{\alpha\beta}\gamma_{\alpha\beta}\right) \mathrm{d}\alpha\mathrm{d}\beta\mathrm{d}z \tag{15}$$

Substituting Eqs. (1–16) into Eq. (15) together with Lame coefficients, one can obtain the explicit expressions of strain energy for rectangular plates and cylindrical shells.

The potential energy (P) stored in the boundary springs is given as follows:

$$P = \frac{1}{2}\left[\int_{S_{\alpha i}} \left(k_u^{\alpha i}u^2 + k_v^{\alpha i}v^2 + k_w^{\alpha i}w^2\right)\mathrm{d}S_{\alpha i} + \int_{S_{\beta i}} \left(k_u^{\beta i}u^2 + k_v^{\beta i}v^2 + k_w^{\beta i}w^2\right)\mathrm{d}S_{\beta i} \right] \tag{16}$$

where $S_{\alpha i}$ and $S_{\beta i}$ denote the area of boundary surfaces.

2.3. Admissible functions

It is crucially important to construct the appropriate admissible displacement functions in the Rayleigh–Ritz method. Beam functions, orthogonal polynomials and Fourier series are often used as displacement functions of plates and shells. However, the use of beam function will lead to at least a very tedious solution process [38]. The problem with using a complete set of orthogonal polynomials is that the higher-order polynomials tend to become numerically unstable because of the computer round-off errors [38, 39]. These numerical difficulties can be avoided by the Fourier series because the Fourier series constitute a complete set and exhibit an excellent numerical stability. However, when the displacements are expressed in terms of conventional Fourier series, discontinuities potentially exist in the original displacements and

their derivatives. In this chapter, a modified Fourier series defined as the linear superposition of a 3-D Fourier cosine series and some auxiliary polynomial functions is used to express the displacement components, which are given as follows [40–43]:

$$
u(\alpha,\beta,z,t) = \left\{
\begin{array}{l}
\displaystyle\sum_{m=0}^{M}\sum_{n=0}^{N}\sum_{q=0}^{Q} A_{mnq}\cos\lambda_m\alpha\cos\lambda_n\beta\cos\lambda_q z + \\[2ex]
\displaystyle\sum_{l=1}^{2}\sum_{n=0}^{N}\sum_{q=0}^{Q} a_{lnq}\xi_{l\alpha}(\alpha)\cos\lambda_n\beta\cos\lambda_q z + \\[2ex]
\displaystyle\sum_{m=0}^{M}\sum_{l=1}^{2}\sum_{q=0}^{Q} \bar{a}_{lmq}\cos\lambda_m\alpha\,\xi_{l\beta}(\beta)\cos\lambda_q z + \\[2ex]
\displaystyle\sum_{m=0}^{M}\sum_{n=0}^{N}\sum_{l=1}^{2} \tilde{a}_{lmn}\cos\lambda_m\alpha\cos\lambda_n\beta\,\xi_{lz}(z) +
\end{array}
\right\} e^{j\omega t}
\tag{17}
$$

$$
v(\alpha,\beta,z,t) = \left\{
\begin{array}{l}
\displaystyle\sum_{m=0}^{M}\sum_{n=0}^{N}\sum_{q=0}^{Q} B_{mnq}\cos\lambda_m\alpha\cos\lambda_n\beta\cos\lambda_q z + \\[2ex]
\displaystyle\sum_{l=1}^{2}\sum_{n=0}^{N}\sum_{q=0}^{Q} b_{lnq}\xi_{l\alpha}(\alpha)\cos\lambda_n\beta\cos\lambda_q z + \\[2ex]
\displaystyle\sum_{m=0}^{M}\sum_{l=1}^{2}\sum_{q=0}^{Q} \bar{b}_{lmq}\cos\lambda_m\alpha\,\xi_{l\beta}(\beta)\cos\lambda_q z + \\[2ex]
\displaystyle\sum_{m=0}^{M}\sum_{n=0}^{N}\sum_{l=1}^{2} \tilde{b}_{lmn}\cos\lambda_m\alpha\cos\lambda_n\beta\,\xi_{lz}(z) +
\end{array}
\right\} e^{j\omega t}
\tag{18}
$$

$$
w(\alpha,\beta,z,t) = \left\{
\begin{array}{l}
\displaystyle\sum_{m=0}^{M}\sum_{n=0}^{N}\sum_{q=0}^{Q} C_{mnq}\cos\lambda_m\alpha\cos\lambda_n\beta\cos\lambda_q z + \\[2ex]
\displaystyle\sum_{l=1}^{2}\sum_{n=0}^{N}\sum_{q=0}^{Q} c_{lnq}\xi_{l\alpha}(\alpha)\cos\lambda_n\beta\cos\lambda_q z + \\[2ex]
\displaystyle\sum_{m=0}^{M}\sum_{l=1}^{2}\sum_{q=0}^{Q} \bar{c}_{lmq}\cos\lambda_m\alpha\,\xi_{l\beta}(\beta)\cos\lambda_q z + \\[2ex]
\displaystyle\sum_{m=0}^{M}\sum_{n=0}^{N}\sum_{l=1}^{2} \tilde{c}_{lmn}\cos\lambda_m\alpha\cos\lambda_n\beta\,\xi_{lz}(z) +
\end{array}
\right\} e^{j\omega t}
\tag{19}
$$

where $\lambda_m = m\pi/L_\alpha$, $\lambda_n = n\pi/L_\beta$, $\lambda_q = q\pi/L_z$. A_{mnq}, a_{lnq}, $\bar{a}_{lmq}$, $\tilde{a}_{lmn}$, B_{mnq}, b_{lnq}, $\bar{b}_{lmq}$, $\tilde{b}_{lmn}$, C_{mnq}, c_{lnq}, $\bar{c}_{lmq}$ and $\tilde{c}_{lmn}$ are the unknown coefficients that need to be determined in future. ω is the circular frequency and t is the time variable. $\xi_{l\alpha}$, $\xi_{l\beta}$ and ξ_{lz} represent a set of closed-form sufficiently smooth functions introduced to remove the discontinuities of the original displacement functions and their derivatives at edges and then to accelerate the convergence of the series representations. According to the 3-D elasticity theory, it is required that at least two-order

derivatives of the displacement functions exist and continuous at any point. Consequently, two auxiliary functions in every direction are supplemented, as shown in Eqs. (17–19). The auxiliary functions are given as follows:

$$\xi_{1\alpha} = \alpha\left(\frac{\alpha}{L_\alpha} - 1\right)^2, \xi_{2\alpha} = \frac{\alpha^2}{L_\alpha}\left(\frac{\alpha}{L_\alpha} - 1\right) \tag{20}$$

$$\xi_{1\beta} = \beta\left(\frac{\beta}{L_\beta} - 1\right)^2, \xi_{2\beta} = \frac{\beta^2}{L_\beta}\left(\frac{\beta}{L_\beta} - 1\right) \tag{21}$$

$$\xi_{1z} = z\left(\frac{z}{L_z} - 1\right)^2, \xi_{2z} = \frac{z^2}{L_z}\left(\frac{z}{L_z} - 1\right) \tag{22}$$

It is easy to verify that

$$\xi_{1\alpha}(0) = \xi_{1\alpha}(L_\alpha) = \xi'_{1\alpha}(L_\alpha) = 0, \ \xi'_{1\alpha}(0) = 1 \tag{23}$$

$$\xi_{2\alpha}(0) = \xi_{2\alpha}(L_\alpha) = \xi'_{2\alpha}(0) = 0, \ \xi'_{2\alpha}(L_\alpha) = 1 \tag{24}$$

The similar conditions exist for the β- and z-related polynomials. It should be mentioned that as the circumferential symmetry of the cylindrical shells in the coordinate θ, the 3-D problem of the cylindrical shell can be transformed to 2-D analysis by using the Fourier series in circumferential direction.

2.4. Solution procedure

Substituting Eqs. (14–16) into Eq. (13) together with the displacement functions defined in Eqs. (17–19) and performing the Rayleigh–Ritz operation, a set of linear algebraic equation against the unknown coefficients can be obtained as follows:

$$\left\{\mathbf{K} - \omega^2\mathbf{M}\right\}\mathbf{X} = \mathbf{0} \tag{25}$$

where $\mathbf{K}$ is the total stiffness matrix for the structure and $\mathbf{M}$ is the total mass matrix. Both of them are symmetric matrices. $\mathbf{X}$ is the column matrix composed of unknown coefficients expressed in the following form:

$$\mathbf{X} = [\mathbf{X}_u, \mathbf{X}_v, \mathbf{X}_w]^T \tag{26}$$

where

$$\mathbf{X}_u = \left\{ \begin{array}{l} A_{000}, \cdots, A_{mnq}, \cdots, A_{MNQ}, a_{100}, \cdots, a_{lnq}, \cdots, a_{2NQ}, \\ \overline{a}_{100}, \cdots, \overline{a}_{lmq}, \cdots \overline{a}_{2MQ}, \tilde{a}_{100}, \cdots, \tilde{a}_{lmn}, \cdots \tilde{a}_{2MN} \end{array} \right\} \tag{27}$$

$$\mathbf{X}_v = \left\{ \begin{array}{l} B_{000}, \cdots, B_{mnq}, \cdots, B_{MNQ}, b_{100}, \cdots, b_{lnq}, \cdots, b_{2NQ}, \\ \overline{b}_{100}, \cdots, \overline{b}_{lmq}, \cdots \overline{b}_{2MQ}, \tilde{b}_{100}, \cdots, \tilde{b}_{lmn}, \cdots \tilde{b}_{2MN} \end{array} \right\} \tag{28}$$

$$\mathbf{X}_w = \left\{ \begin{array}{l} C_{000}, \cdots, C_{mnq}, \cdots, C_{MNQ}, c_{100}, \cdots, c_{lnq}, \cdots, c_{2NQ}, \\ \overline{c}_{100}, \cdots, \overline{c}_{lmq}, \cdots \overline{c}_{2MQ}, \tilde{c}_{100}, \cdots, \tilde{c}_{lmn}, \cdots \tilde{c}_{2MN} \end{array} \right\} \tag{29}$$

The frequencies can be determined by solving Eq. (25) via the eigenfunction of MATLAB program. The mode shape corresponding to each frequency can be obtained by back substituting the eigenvector to the displacement functions in Eqs. (17–19).

3. Numerical examples and discussion

In this section, several vibration results of FGM plates and cylindrical shells with general boundary conditions are presented to illustrate the accuracy and reliability of the current formulation. To simplify presentation, C, S, F and E denote the clamped, simply supported, free and elastic restraints. Three types of elastic boundary conditions designated by symbols E_1, E_2 and E_3 are considered. E_1-type edge is considered to be elastic in normal direction; the support type E_2 only allows elastically restrained displacement in both tangential directions; when all of three displacements along the edges are elastically restrained, the edge support is defined by E_3. The expressions of the different boundary conditions along the edge $\alpha = 0$ are given as follows:

Free boundary condition (F):

$$\sigma_{\alpha\alpha} = \sigma_{\alpha\beta} = \sigma_{\alpha z} = 0$$

Clamped boundary condition (C):

$$u = v = w = 0$$

Simply supported boundary condition (S):

$$\sigma_{\alpha\alpha} = v = w = 0$$

First type of elastic restraint (E$_1$):

$$u \neq 0, v = w = 0$$

Second type of elastic restraint (E$_1$):

$$u = 0, v \neq 0, w \neq 0$$

Three type of elastic restraint (E$_1$):

$$u \neq 0, v \neq 0, w \neq 0$$

A simple letter is used to describe the boundary conditions of structure. For example, SFCE denotes a plate having simply supported boundary condition at $\alpha = 0$, free boundary condition at $\beta = 0$, clamped boundary condition at $\alpha = L_\alpha$, and elastic restraint at $\beta = L_\beta$; CS denotes a cylindrical shell having clamped boundary condition at $\alpha = 0$ and simply supported boundary condition at $\alpha = L_\alpha$.

3.1. Rectangular plates

In this section, several numerical examples concerning the free vibration of FGM rectangular plates with different geometrical parameters and boundary conditions have been investigated to verify the convergence, accuracy and reliability of the present method. Some new vibration results of rectangular plates with elastic boundary conditions are given. Unless stated otherwise, the material properties for ceramic and metallic constituents of FGM plates are given as follows: $E_c = 380$ GPa, $\mu_c = 0.3$ and $\rho_c = 3800$ kg/m^3 and $E_m = 70$ GPa, $\mu_m = 0.3$ and $\rho_m = 2702$ kg/m^3.

3.1.1. Convergence study

Theoretically, there are infinite terms in the modified Fourier series solution. However, the series is numerically truncated, and only finite terms are counted in actual calculations. The convergence of this method will be checked. Table 1 presents the first seven frequency parameters Ω of completely free FGM square plates. The frequency parameter Ω is defined as follows:

$$\Omega = \omega a^2 / h\sqrt{\rho_c / E_c}$$

The geometrical parameters are given as follows: $a/b = 1$ and $h/b = 0.1$, 0.2 and 0.5. The power-law index p is taken to be $p = 1$. It is obvious that the results of this study show a monotonic trend, and the solutions converge quite rapidly as the truncated number increases. In the following examples, the truncated numbers of the displacement expressions will be uniformly selected as $M \times N \times Q = 13 \times 13 \times 8$.

h/b	$M \times N \times Q$	Ω_1	Ω_2	Ω_3	Ω_4	Ω_5	Ω_6	Ω_7
	$9 \times 9 \times 4$	2.9579	4.3853	5.4058	7.4361	7.4361	12.903	12.903
	$11 \times 11 \times 4$	2.9558	4.3851	5.4054	7.4293	7.4293	12.901	12.901
0.1	$11 \times 11 \times 8$	2.9524	4.3802	5.4018	7.4256	7.4256	12.898	12.898
	$13 \times 13 \times 8$	2.9514	4.3802	5.4016	7.4225	7.4225	12.897	12.897
	$13 \times 13 \times 10$	2.9513	4.3800	5.4015	7.4223	7.4223	12.897	12.897
	$9 \times 9 \times 4$	2.7261	4.0298	4.9324	6.4506	6.4506	10.093	10.642
	$11 \times 11 \times 4$	2.7257	4.0297	4.9322	6.4492	6.4492	10.093	10.640
0.2	$11 \times 11 \times 8$	2.7250	4.0287	4.9315	6.4485	6.4485	10.093	10.639
	$13 \times 13 \times 8$	2.7247	4.0286	4.9314	6.4479	6.4479	10.093	10.637
	$13 \times 13 \times 10$	2.7247	4.0286	4.9313	6.4478	6.4478	10.093	10.637
	$9 \times 9 \times 4$	2.0442	2.8571	3.4668	3.9777	3.9777	4.0369	4.3056
	$11 \times 11 \times 4$	2.0442	2.8571	3.4667	3.9776	3.9776	4.0369	4.3055
0.5	$11 \times 11 \times 8$	2.0441	2.8568	3.4665	3.9773	3.9773	4.0368	4.3053
	$13 \times 13 \times 8$	2.0440	2.8568	3.4665	3.9772	3.9772	4.0368	4.3052
	$13 \times 13 \times 10$	2.0440	2.8568	3.4664	3.9772	3.9772	4.0368	4.3052

Table 1. Convergence of frequency parameters of completely free FGM square plates with different thickness-to-width ratios h/b ($p = 1$).

As aforementioned, the boundary conditions can be easily obtained via changing the value of boundary springs. Therefore, the accuracy of the current method is strongly influenced by the values of springs' stiffness. To determine the appropriate values of spring's stiffness, the effects of elastic parameters on the frequencies of the FGM plate are investigated. The elastic parameter Γ is defined as ratios of corresponding spring's stiffness to bending stiffness $D_c = E_c h^3/12(1 - \mu_c^2)$. The plates are free at y = constant and restrained by only one kind of spring whose stiffness parameter ranges from 10^{-1} to 10^{10} at x = constant. The first three frequency parameters of the FGM square plates with $h/b = 0.2$ and $p = 1$ are presented in Table 2. It is obvious that the increase of the elastic parameter leads to increase of the frequency parameters. When $\Gamma \geq 10^7$, the influence of the elastic parameters on the frequencies of the plates can be neglected. The clamped boundary conditions can be simulated by assuming the elastic parameters equal to 10^9. The elastic boundary conditions can be obtained by assuming the elastic parameters equal to 100.

Γ	$k_u = \Gamma D, k_v = k_w = 0$			$K_v = \Gamma D, k_u = k_w = 0$			$K_w = \Gamma D, k_u = k_v = 0$		
	Ω_1	Ω_2	Ω_3	Ω_1	Ω_2	Ω_3	Ω_1	Ω_2	Ω_3
10^{-1}	0.0167	0.0464	0.0654	0.0167	0.0654	0.0802	0.0650	0.0654	0.1117
10^0	0.0419	0.1463	0.2069	0.0419	0.2069	0.2533	0.2028	0.2061	0.3514
10^1	0.1285	0.4615	0.6536	0.1286	0.6513	0.7985	0.6294	0.6301	1.1044
10^2	0.3984	1.4270	2.0440	0.3996	1.9750	2.4251	1.5056	1.7178	3.2905
10^3	1.0903	2.8583	3.7961	1.1184	3.0710	4.2125	2.0002	2.7732	5.9372
10^4	1.8471	3.1625	4.5503	2.0317	3.8426	4.3529	2.0785	3.0227	6.4327
10^5	2.0625	3.2758	4.5745	2.3675	4.2459	4.3815	2.0880	3.0600	6.5168
10^6	2.0904	3.2915	4.5774	2.4305	4.3436	4.3859	2.0891	3.0657	6.5299
10^7	2.0934	3.2932	4.5777	2.4464	4.3740	4.3870	2.0893	3.0664	6.5316
10^8	2.0937	3.2934	4.5778	2.4490	4.3790	4.3871	2.0893	3.0665	6.5318
10^9	2.0937	3.2934	4.5778	2.4493	4.3796	4.3871	2.0893	3.0665	6.5319
10^{10}	2.0937	3.2934	4.5778	2.4493	4.3796	4.3871	2.0893	3.0665	6.5319

Table 2. The first three frequency parameters Ω of the FGM square plates with different elastic parameters Γ (p=1).

3.1.2. Plate with general boundary conditions

To illustrate the accuracy of the present method, the comparisons of the current results with those in the published literature are presented. Table 3 presents the first two frequency parameters of the FGM square plates with different boundary conditions. The results are compared with those presented by Huang et al. [32] using the Ritz method on the basis of 3-D elasticity theory. Table 4 presents the fundamental frequency parameters of the FGM square plates with SSSS boundary conditions. Numerical vibration results for the same problems have been reported by Hosseini-Hashemi et al. [18] and Matsunaga [20] using HSDTs, showing that excellent agreement of the results is achieved.

	SSSS			CFFF			CFCF		
	Ref. []	Present	Diff%	Ref. []	Present	Diff%	Ref. []	Present	Diff%
Ω_1	3.406	3.406	0.000	0.6637	0.6657	0.347	3.400	3.421	0.618
Ω_2	6.296	6.296	0.000	1.432	1.434	0.140	3.820	3.840	0.524
Ω_3	6.296	6.296	0.000	2.154	2.158	0.186	5.774	5.787	0.225
Ω_4	7.347	7.345	0.027	3.396	3.405	0.265	5.976	5.989	0.218
Ω_5	7.347	7.345	0.027	4.347	4.348	0.023	7.609	7.657	0.631

Table 3. First five frequency parameters of FGM square plates with different boundary conditions (h/b = 0.2, p = 5).

h/b		p = 0	p = 0.5	p = 1	p = 4	p = 10	p = ∞
0.1	Ref. [18]	0.0577	0.0490	0.0443	0.0381	0.0364	0.0293
	Ref. [20]	0.0577	0.0492	0.0442	0.0381	0.0364	0.0293
	Present	0.0578	0.0491	0.0443	0.0381	0.0364	0.0294
0.2	Ref. [18]	0.2113	0.1807	0.1631	0.1378	0.1301	0.1076
	Ref. [20]	0.2121	0.1819	0.1640	0.1383	0.1306	0.1077
	Present	0.2122	0.1816	0.1640	0.1383	0.1306	0.1080

Table 4. Fundamental frequency parameters of FGM square plates with SSSS boundary conditions ($a/b = 1$).

BC	h/b	a/b = 1				a/b = 2			
		p = 0.6	p = 1	p = 5	p = 10	p = 0.6	p = 1	p = 5	p = 10
CSSS	0.1	5.660	5.235	4.434	4.272	12.66	11.71	10.01	9.671
	0.3	4.415	4.096	3.263	3.083	11.01	10.20	8.354	7.676
	0.5	3.391	3.156	2.435	2.265	6.866	6.464	5.023	4.591
CCSS	0.1	6.416	5.936	5.008	4.819	17.17	15.88	13.48	13.00
	0.3	4.807	4.464	3.520	3.313	13.68	12.69	10.12	9.566
	0.5	3.582	3.336	2.549	2.366	10.54	9.807	7.548	7.037
CCCS	0.1	7.437	6.884	5.772	5.544	17.71	16.38	13.90	13.40
	0.3	5.264	4.894	3.815	3.572	14.01	13.00	10.36	9.782
	0.5	3.797	3.540	2.681	2.479	10.75	10.00	7.679	7.153
CFFF	0.1	0.864	0.799	0.687	0.664	0.862	0.797	0.687	0.665
	0.3	0.816	0.755	0.637	0.613	0.845	0.781	0.669	0.647
	0.5	0.746	0.690	0.568	0.543	0.821	0.759	0.645	0.622
CCFF	0.1	1.684	1.558	1.330	1.285	4.230	3.911	3.356	3.246
	0.3	1.473	1.363	1.125	1.076	3.900	3.608	3.021	2.902
	0.5	1.253	1.160	0.932	0.885	3.479	3.220	2.627	2.506
CCCF	0.1	5.643	5.223	4.393	4.222	7.628	7.056	6.031	5.825
	0.3	4.074	3.785	2.956	2.774	6.594	6.107	5.009	4.781
	0.5	2.944	2.738	2.080	1.932	5.503	5.102	4.053	3.831

Table 5. Foundational frequency parameters Ω of FGM rectangular plates with different classical boundary conditions.

Several new numerical results for free vibration of FGM plates with general boundary conditions, including classical and elastic boundary conditions, are presented in Tables 5 and 6. The geometrical parameters are given as: $a/b = 1$ and 2, $h/b = 0.1$, 0.3 and 0.5. The different

boundary conditions, including CSSSS, CCSS, CCCS, CFFF, CCFF, CCCF, $E_1E_1E_1E_1$, $E_2E_2E_2E_2$ and $E_3E_3E_3E_3$, are studied. The power-law exponent is taken to be p = 0.6, 1, 5 and 10. From tables, it is obvious that the fundamental frequency of the plate strongly depends on the values of geometrical parameters, power-law index and boundary conditions. For the plates with classic boundary conditions, the foundational frequency parameters decrease with increase in the thickness-to-width ratio h/b. Except for plates with CFFF boundary conditions, the fundamental frequency parameters of the square plate (a/b = 1) are smaller than those of the plates with a/b = 2. The increase of the power-law index leads to decrease of the fundamental frequency parameter for all cases considered. For the plates with elastic restraints, the foundational frequency parameters increase as the length-to-width ratio a/b increases. Except for plates with h/b = 0.1 subjected to $E_2E_2E_2E_2$ and $E_3E_3E_3E_3$ boundary conditions, the foundational frequency parameters decrease with increase in the power-law index p. The effects of the thickness-to-width ratio h/b on the foundational frequency parameters are more complex. Some 3-D mode shapes for FGM plates with different boundary conditions are shown in Figs. 3 and 4.

BC	h/b	a/b = 1				a/b = 2			
		p = 0.6	*p = 1*	*p = 5*	*p = 10*	*p = 0.6*	*p = 1*	*p = 5*	*p = 10*
$E_1E_1E_1E_1$	0.1	4.798	4.437	3.786	3.655	12.138	11.228	9.626	9.303
	0.3	4.113	3.837	3.142	2.983	11.145	10.426	8.736	8.339
	0.5	3.444	3.236	2.522	2.352	10.019	9.439	7.495	7.035
$E_2E_2E_2E_2$	0.1	1.975	2.006	2.090	2.109	6.541	6.592	6.748	6.780
	0.3	3.043	3.025	2.844	2.773	9.601	9.476	8.804	8.569
	0.5	3.083	2.979	2.487	2.343	9.597	9.238	7.680	7.238
$E_3E_3E_3E_3$	0.1	1.823	1.823	1.828	1.826	5.690	5.649	5.586	5.563
	0.3	2.594	2.541	2.357	2.298	7.867	7.670	7.063	6.874
	0.5	2.724	2.634	2.234	2.123	8.308	8.014	6.799	6.471

Table 6. Foundational frequency parameters Ω of FGM rectangular plates with different elasticity boundary conditions.

3.2. Cylindrical shells

This section is concerned with the free vibration of FGM cylindrical shells with different boundary conditions. The convergence, accuracy and reliability of the present method are demonstrated by numerical examples and comparisons. New numerical results for the FGM cylindrical shells with the elastic boundary conditions are also presented. Unless stated otherwise the material properties for ceramic and metallic constituents of FGM cylindrical shells are given as follows: E_c = 168 GPa, μ_c = 0.3 and ρ_c = 5700 kg/m³ and E_m = 70 GPa, μ_m = 0.3 and ρ_m = 2707 kg/m³.

Mode shape 1   Mode shape 2

Mode shape 3   Mode shape 4
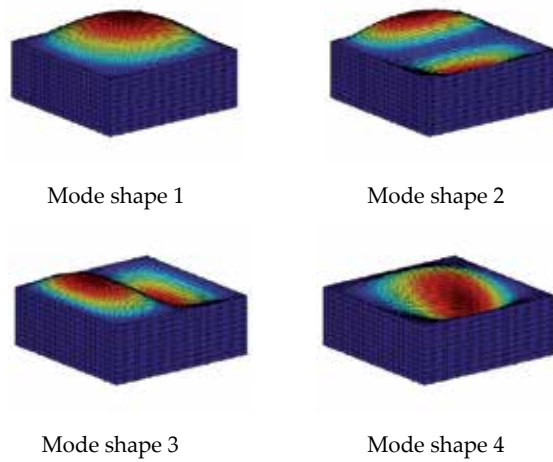
Figure 3. Mode shapes of FGM square plate with CCCC boundary conditions with h/a = 0.5 and p = 1.

Mode shape 1   Mode shape 2

Mode shape 3   Mode shape 4
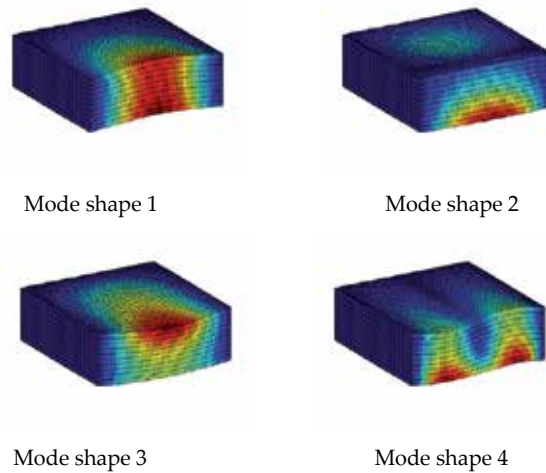
Figure 4. Mode shapes of FGM square plate with CCCF boundary conditions with h/a = 0.5 and p = 1.

3.2.1. Convergence study

The convergence studies of the first two frequencies for the completely free cylindrical shells with different circumferential wave numbers n are presented in Table 7. The different thickness-to-radius ratios (i.e., h/R_0 = 0.1, 0.2 and 0.5) and circumferential wave numbers (i.e., n = 1, 2, 3 and 4) are considered. The power-law exponent is taken to be p = 1. From Table 7, it is evident that the present method has a good convergence, and the truncated numbers of the displacement expressions will be uniformly selected as $M \times Q$ = 13 × 13.

h/R_0	$M \times Q$	n = 1		n = 2		n = 3		n = 4	
		f_1	f_2	f_1	f_2	f_1	f_2	f_1	f_2
	10 × 10	675.95	775.84	72.216	93.963	202.45	236.49	383.66	422.39
	11 × 11	675.95	775.84	72.213	93.900	202.44	236.37	383.64	422.20
0.1	12 × 12	675.95	775.82	72.211	93.898	202.43	236.36	383.61	422.19
	13 × 13	675.95	775.82	72.209	93.859	202.42	236.28	383.60	422.07
	14 × 14	675.95	775.81	72.208	93.858	202.42	236.28	383.58	422.06
	10 × 10	702.69	829.15	156.06	195.32	426.43	484.16	782.43	843.50
	11 × 11	702.69	829.14	156.06	195.27	426.42	484.05	782.41	843.32
0.2	12 × 12	702.69	829.12	156.05	195.27	426.41	484.04	782.37	843.29
	13 × 13	702.68	829.12	156.05	195.24	426.40	483.98	782.36	843.19
	14 × 14	702.68	829.11	156.05	195.24	426.39	483.97	782.34	843.18
	10 × 10	813.89	990.82	472.71	513.27	1119.84	1157.84	1798.22	1821.60
	11 × 11	813.88	990.82	472.71	513.25	1119.82	1157.80	1798.18	1821.52
0.5	12 × 12	813.88	990.81	472.70	513.25	1119.81	1157.78	1798.15	1821.49
	13 × 13	813.88	990.81	472.70	513.24	1119.80	1157.76	1798.13	1821.45
	14 × 14	813.88	990.81	472.70	513.24	1119.80	1157.75	1798.12	1821.43

Table 7. Convergence of the first two frequencies for the completely free cylindrical shells with different circumferential wave numbers n ($R_0 = 1$ m, $L/R_0 = 2$, $p = 1$).

Γ	$k_u = \Gamma D, k_v = k_w = 0$			$K_v = \Gamma D, k_u = k_w = 0$			$K_w = \Gamma D, k_u = k_v = 0$		
	n = 1	n = 2	n = 3	n = 1	n = 2	n = 3	n = 1	n = 2	n = 3
10^{-1}	6.0482	156.26	426.50	6.0495	156.10	426.42	6.3136	156.05	426.40
10^0	19.080	158.13	427.41	19.120	156.58	426.54	19.945	156.05	426.41
10^1	58.929	174.72	435.81	60.159	161.25	427.76	62.811	156.06	426.42
10^2	153.57	251.42	482.58	181.20	197.82	438.59	190.65	156.13	426.59
10^3	233.55	318.79	529.79	404.21	306.64	485.62	424.98	156.65	427.85
10^4	250.70	330.93	538.16	506.09	361.57	523.38	510.67	157.86	430.84
10^5	253.21	332.47	539.14	519.80	369.75	532.12	521.32	158.32	432.03
10^6	253.55	332.66	539.26	521.22	370.71	533.44	522.45	158.38	432.19
10^7	253.62	332.69	539.28	521.37	370.89	533.83	522.56	158.39	432.20
10^8	253.65	332.70	539.29	521.38	370.94	533.98	522.58	158.39	432.21

Γ	$k_u = \Gamma D, k_v = k_w = 0$			$K_v = \Gamma D, k_u = k_w = 0$			$K_w = \Gamma D, k_u = k_v = 0$		
	$n = 1$	$n = 2$	$n = 3$	$n = 1$	$n = 2$	$n = 3$	$n = 1$	$n = 2$	$n = 3$
10^9	253.66	332.71	539.29	521.38	370.95	534.00	522.58	158.39	432.21
10^{10}	253.66	332.71	539.29	521.38	370.95	534.00	522.58	158.39	432.21

Table 8. The frequencies of the FGM cylindrical shells with different elastic parameters Γ ($p = 1$).

It is significant to investigate the effects of elastic parameters on the frequencies of the cylindrical shells. The cylindrical shells are restrained by only one kind of spring whose stiffness parameter ranges from 10^{-1} to 10^{10} at x = constant. The frequencies of the cylindrical shells with different circumferential wave numbers n are presented in Table 8. The geometrical parameters are used as $R_0 = 1$ m, $L/R_0 = 2$ and $h/R_0 = 0.2$. The power-law index is taken to be p = 1. It is obvious that the increase of the elastic parameter leads to the increase of the frequency parameters. When $\Gamma \geq 10^7$, the influence of the elastic parameters on the frequencies of the plates can be neglected. The clamped boundary conditions can be simulated by assuming the elastic parameters equal to 10^9. The elastic boundary conditions can be obtained by assuming the elastic parameters equal to 100.

3.2.2. Cylindrical shells with general boundary conditions

To illustrate the accuracy of the present method, the comparisons of the current results with those in published literature are presented. Table 9 presents the first three frequency parameters $\lambda = \omega L \sqrt{\rho(1 + \mu)/E}$ for the cylindrical shells with CC, CF and FF boundary conditions. The geometrical parameters are given as follows: $h/R = 0.3$, $L/R = 2$, $R = R_0 - R_i$. The results are compared with exact 3-D elasticity results by Malekzadeh et al. [31] using Layerwise theory and DQM (LW-DQ) and FEM. Table 10 presents first 10 frequencies of FGM cylindrical shells with CF boundary conditions. The geometrical parameters are given as follows: $R_i = 0.95$ m, $R_0 = 1.05$ m, $h = 0.1$ m, $L = 2$ m. Numerical vibration results of the same problems have been reported by Tornabene et al. [13] using FSDT and generalized DQM. It is noted that the V_c is defined as $V_c = (1-z/h)^p$. It is obvious that the results show very good agreement. The slight discrepancies may be due to the different solution strategies in the studies.

Several new numerical results for free vibration of FGM cylindrical shells with general boundary conditions, including classical and elastic boundary conditions, are presented in Tables 11 and 12. The geometrical parameters are given as follows: $R_0 = 1$ m, $L/R_0 = 2$, $h/R_0 = 0.1$, 0.3 and 0.5. The different boundary conditions, including CC, CS, SS, CF, SF, E_1E_1, E_2E_2 and E_3E_3, are studied. The power-law exponent is taken to be p = 0, 0.6, 1, 2, 5, 10 and 20. It is observed from Table 11 that the boundary conditions have a significant effect on the frequencies of cylindrical shells. The higher constraints at edges may increase the flexural rigidity of the shell leading to higher frequency response. It is obvious that the increase of the thickness-to-radius ratio h/R_0 leads to the increase of the frequency parameters. It is also seen that the fundamental frequencies decrease as the power-law index increases. From Table 12, the frequencies of shells also increase as thickness-to-radius ratio h/R_0 increases. However, the effects of the power-law index on the frequencies of shells became more complex. Some 3-D mode shapes for FGM cylindrical shells with different boundary conditions are shown in Figs. 5 and 6.

BC	n	λ_1			λ_2			λ_3		
		LW-DQ [31]	FEM [31]	Present	LW-DQ [31]	FEM [31]	Present	LW-DQ [31]	FEM [31]	Present
CC	1	1.7860	1.7972	1.7905	2.6043	2.6222	2.6050	3.4148	3.4192	3.4245
	2	1.7452	1.7573	1.7500	3.2942	3.3114	3.2949	3.4921	3.5150	3.5012
	3	1.8867	1.8862	1.8912	3.6024	3.6320	3.6099	3.9416	3.9257	3.9447
	4	2.1966	2.2072	2.2004	3.8126	3.8228	3.8193	4.2757	4.3215	4.2783
	5	2.6385	2.6617	2.6415	4.1302	4.1327	4.1364	4.7010	4.7322	4.7031
CF	1	0.7514	0.7546	0.7516	1.7563	1.7692	1.7568	1.8800	1.8996	1.8812
	2	0.6620	0.6713	0.6622	1.8962	1.9256	1.8980	2.1305	2.1557	2.1324
	3	0.9246	0.9301	0.9247	2.0610	2.0668	2.0630	2.5165	2.5482	2.5179
	4	1.4021	1.4282	1.4021	2.4030	2.4646	2.4049	2.9919	3.0342	2.9930
	5	1.9814	2.0228	1.9814	2.8666	2.8571	2.8684	3.5251	3.5628	3.5258
FF	1	0.0000	0.0000	0.0000	0.0001	0.0001	0.0003	1.0710	1.0734	1.0709
	2	0.2576	0.2608	0.2576	0.3800	0.3831	0.3799	1.3533	1.3594	1.3532
	3	0.6884	0.6890	0.6884	0.9253	0.9377	0.9252	1.8689	1.8794	1.8689
	4	1.2302	1.2525	1.2302	1.5160	1.5307	1.5158	2.4754	2.4917	2.4753
	5	1.8427	1.8694	1.8426	2.1343	2.1532	2.1341	3.1169	3.1417	3.1169

Table 9. First three frequency parameters of the cylindrical shells with different boundary conditions ($\mu = 0.3$).

	p = 0		p = 0.6		p = 1		p = 5	
	Ref. [13]	Present	Ref. [13]	Present	Ref. [13]	Present	Ref. [13]	Present
f_1	152.93	152.13	150.03	148.67	149.29	147.76	148.75	147.10
f_2	152.93	152.13	150.03	148.67	149.29	147.76	148.75	147.10
f_3	220.06	219.31	212.94	211.89	212.22	211.00	219.49	218.00
f_4	220.06	219.31	212.94	211.89	212.22	211.00	219.49	218.00
f_5	253.78	254.30	250.74	250.36	249.31	248.68	243.43	242.86
f_6	253.78	254.30	250.74	250.36	249.31	248.68	243.43	242.86
f_7	383.55	384.04	370.63	370.69	369.46	369.21	383.71	382.79
f_8	383.55	384.04	370.63	370.69	369.46	369.21	383.71	382.79
f_9	420.51	420.86	415.47	414.68	412.97	411.88	402.56	401.57
f_{10}	431.45	428.75	420.39	416.91	418.46	414.66	423.57	419.16

Table 10. First 10 frequencies (Hz) of the FGM cylindrical shells with F–C boundary conditions.

BC	h/R_0	$p = 0$	$p = 0.6$	$p = 1$	$p = 2$	$p = 5$	$p = 10$	$p = 20$
	0.1	390.33	377.23	374.78	375.39	379.94	379.62	376.24
CC	0.3	621.15	599.34	594.11	591.68	594.96	595.70	593.23
	0.5	701.10	686.38	681.10	674.46	668.80	666.26	663.96
	0.1	378.25	365.82	363.43	363.82	367.81	367.48	364.19
CS	0.3	567.55	548.06	543.23	540.49	542.33	542.55	540.43
	0.5	648.20	634.72	629.77	623.22	617.07	614.23	612.09
	0.1	367.68	355.76	353.44	353.68	357.26	356.85	353.71
SS	0.3	528.69	510.67	506.15	503.35	504.53	504.51	502.59
	0.5	608.85	596.84	592.29	585.94	579.40	576.22	574.05
	0.1	153.27	149.63	148.75	148.30	148.46	147.80	146.56
CF	0.3	257.65	254.87	253.62	251.58	248.56	246.32	244.47
	0.5	263.06	261.04	260.07	258.44	255.66	253.17	250.86
	0.1	149.92	146.38	145.51	145.06	145.17	144.51	143.30
SF	0.3	247.41	245.02	243.86	241.81	238.61	236.30	234.48
	0.5	248.50	246.92	246.06	244.45	241.51	238.95	236.67

Table 11. Fundamental frequencies of FGM cylindrical shells with different classical boundary conditions.

Mode shapes 1–2


Mode shapes 3–4

Mode shape 5
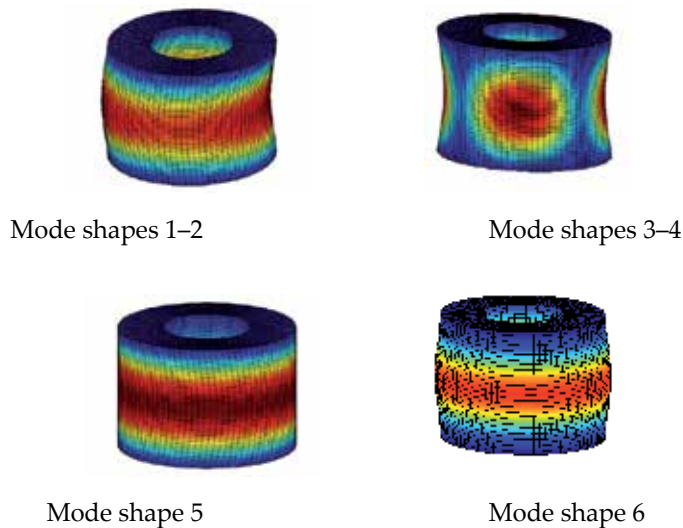
Mode shape 6

Figure 5. Mode shapes of FGM cylindrical shells with CC boundary conditions with $h/R_0 = 0.5$, $L/R_0 = 2$ and $p=1$.

BC	h/R_0	$p = 0$	$p = 0.6$	$p = 1$	$p = 2$	$p = 5$	$p = 10$	$p = 20$
	0.1	368.31	356.53	354.28	354.66	358.44	358.13	355.04
E_1E_1	0.3	558.81	545.07	542.41	542.83	548.35	550.42	549.32
	0.5	669.03	660.42	657.10	652.86	649.27	647.64	645.98
	0.1	82.564	91.860	95.778	101.94	109.61	113.78	116.41
E_2E_2	0.3	381.14	384.20	386.62	392.04	400.91	405.96	408.78
	0.5	539.57	539.80	540.83	544.12	551.17	556.07	559.18
	0.1	80.874	89.444	93.013	98.592	105.46	109.13	111.41
E_3E_3	0.3	331.30	347.67	354.18	364.51	377.62	384.51	388.49
	0.5	515.44	522.81	525.80	531.29	539.88	545.19	548.45

Table 12. Fundamental frequencies of FGM cylindrical shells with different elasticity boundary conditions.

Mode shapes 1–2

Mode shape 3

Mode shapes 4–5
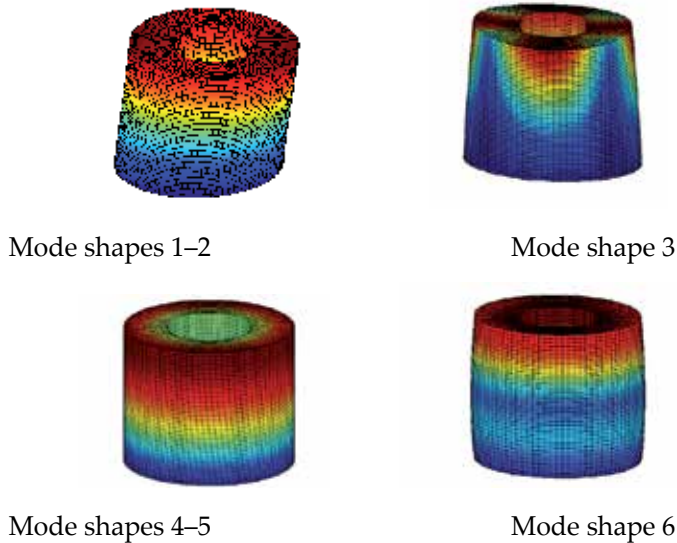
Mode shape 6

Figure 6. Mode shapes of FGM cylindrical shells with CF boundary conditions with $h/R_0 = 0.5$, $L/R_0 = 2$ and $p = 1$.

4. Conclusions

A new 3-D exact solution for free vibration analysis of thick functionally graded plates and cylindrical shells with arbitrary boundary conditions is presented in this chapter. The effective material properties of functionally graded structures vary continuously in the thickness direction according to the simple power-law distributions in terms of volume fraction of constituents and are estimated by Voigt's rule of mixture. By using the artificial spring

boundary technique, the general boundary conditions can be obtained by setting proper spring stiffness. All displacements of the functionally graded plates and shells are expanded in the form of the linear superposition of standard 3-D cosine series and several supplementary functions, which are introduced to remove potential discontinuity problems with the original displacements along the edge. The Rayleigh-Ritz procedure is used to yield the accurate solutions. The convergence, accuracy and reliability of this formulation are verified by numerical examples and by comparng the current results with those in published literature. The influence of the geometrical parameters and elastic foundation on the frequencies of rectangular plates and cylindrical shells is investigated.

Acknowledgements

Author details

Guoyong Jin, Zhu Su* and Tiangui Ye

*Address all correspondence to: xiuzhu0403@163.com

College of Power and Energy Engineering, Harbin Engineering University, Harbin, P.R. China

References

[1] Zhang D., Zhou Y. A theoretical analysis of FGM thin plates based on physical neutral surface. Computational Material Science. 2008; 44: 716–20.

[2] Chi S., Chung Y. Mechanical behavior of functionally graded material plates under transverse load – Part ◎: Analysis. International Journal of Solids and Structures. 2006; 43: 3657–74.

[3] Chi S., Chung Y. Mechanical behavior of functionally graded material plates under transverse load – Part ◎: Numerical results. International Journal of Solids and Structures. 2006; 43: 3675–91.

[4] Latifi M., Farhatnia F., Kadkhodaei M. Bucking analysis of rectangular functionally graded plates under various edge conditions using Fourier series expansion. European Journal of Mechanics – A/Solids. 2013; 41: 16–27.

[5]   Zhao X., Lee Y.Y., Liew K.M. Free vibration analysis of functionally graded plates using the element-free kp-Ritz method. Journal of Sound and Vibration. 2009; 319: 918–39.

[6]   Hosseini-Hashemi S., Rokni Damavandi Taher H., Akhavan H., Omidi M. Free vibration of functionally graded rectangular plates using first-order shear deformation plate theory. Applied Mathematical Modelling. 2010; 34: 1276–91.

[7]   Hosseini-Hashemi S., Fadaee M., Atashipour S.R. A new exact analytical approach for free vibration of Reissner-Mindlin functionally graded rectangular plates. International Journal of Mechanical Sciences. 2011; 53: 11–22.

[8]   Ferreira A.J.M., Batra R.C., Roque C.M.C., Qian L.F., Jorge R.M.N. Natural frequencies of functionally graded plates by a meshless method. Composite Structures. 2006; 75: 593–600.

[9]   Fallah A., Aghdam M.M., Kargarnovin M.H. Free vibration analysis of moderately thick functionally graded plates on elastic foundation using extended Kantorovich method. Archive of Applied Mechanics. 2013; 83: 177–91.

[10]   Croce L.D., Venini P. Finite elements for functionally graded Reissner-Mindlin plates. Compute Methods in Applied Mechanics and Engineering. 2004; 193: 705–25.

[11]   Kadoli R., Ganesan N. Buckling and free vibration analysis of functionally graded cylindrical shells subjected to a temperature-specified boundary condition. Journal of Sound and Vibration. 2006; 289(3): 450–80.

[12]   Tornabene F. Free vibration analysis of functionally graded conical, cylindrical shell and annular plate structures with a four-parameter power-law distribution. Computer Methods in Applied Mechanics and Engineering. 2009; 198(37): 2911–35.

[13]   Tornabene F., Viola E., Inman D.J. 2-D differential quadrature solution for vibration analysis of functionally graded conical, cylindrical shell and annular plate structures. Journal of Sound and Vibration. 2009; 328(3): 259–90.

[14]   Sheng G.G., Wang X. Thermomechanical vibration analysis of a functionally graded shell with flowing fluid. European Journal of Mechanics – A/Solids. 2008; 27(6): 1075–87.

[15]   Jin G.Y., Xie X., Liu Z.G. The Haar wavelet method for free vibration analysis of functionally graded cylindrical shells based on the shear deformation theory. Composite Structures. 2014; 108: 435–48.

[16]   Qu Y.G., Long X.H., Yuan G.Q., Meng G. A unified formulation for vibration analysis of functionally graded shells of revolution with arbitrary boundary conditions. Composites Part B: Engineering. 2013; 50: 381–402.

[17]   Reddy J.N. Analysis of functionally graded plates. International Journal of Numerical Methods in Engineering. 2000; 47: 663–84.

[18] Hosseini-Hashemi S., Fadaee M., Atashipour S.R. Study on the free vibration of thick functionally graded rectangular plates according to a new exact closed-form procedure. Composite Structures. 2011; 93: 722–35.

[19] Baferani A.H., Saidi A.R., Ehteshami H. Accurate solution for free vibration analysis of functionally graded thick rectangular plates resting on elastic foundation. Composite Structures. 2011; 93: 1842–53.

[20] Matsunaga H. Free vibration and stability of functionally graded plates according to a 2-D higher-order deformation theory. Composite Structures. 2008; 82: 499–512.

[21] Ferreira A.J.M., Batra R.C., Roque C.M.C., Qian L.F., Martins P.A.L.S. Static analysis of functionally graded plates using third-order shear deformation theory and a meshless method. Composite Structures. 2005; 69: 449–57.

[22] Qian L.F., Batra R.C., Chen L.M. Static and dynamic deformations of thick functionally graded elastic plates by using higher-order shear and normal deformable plate theory and meshless local Petrov-Galerkin method. Composites Part B: Engineering. 2004; 35: 685–97.

[23] Najafizadeh M.M., Isvandzibaei M.R. Vibration of functionally graded cylindrical shells based on higher order shear deformation plate theory with ring support. Acta Mechanica. 2007; 191(1–2): 75–91.

[24] Matsunaga H. Free vibration and stability of functionally graded circular cylindrical shells according to a 2D higher-order deformation theory. Composite Structures. 2009; 88(4): 519–31.

[25] Viola E., Rossetti L., Fantuzzi N. Numerical investigation of functionally graded cylindrical shells and panels using the generalized unconstrained third order theory coupled with the stress recovery. Composite Structures. 2012; 94(12): 3736–58.

[26] Zozulya V.V., Zhang C. A high order theory for functionally graded axisymmetric cylindrical shells. International Journal of Mechanical Sciences. 2012; 60(1): 12–22.

[27] Vel S.S., Batra R.C. Three-dimensional exact solution for the vibration of functionally graded rectangular plates. Journal of Sound and Vibration. 2004; 272: 703–30.

[28] Reddy J.N., Cheng Z.Q. Three-dimensional thermoelastic deformations of a functionally graded elliptic plate. Composites Part B: Engineering. 2000; 31: 97–106.

[29] Amini M.H., Soleimani M., Rastgoo A. Three-dimensional free vibration analysis of functionally graded material plates resting on an elastic foundation. Smart Materials and Structure. 2009; 18: 1–9.

[30] Malekzadeh P. Three-dimensional free vibration analysis of thick functionally graded plates on elastic foundations. Composite Structures. 2009; 89: 367–73.

[31] Malekzadeha P., Faridb M., Zahedinejadc P., Karamid G. Three-dimensional free vibration analysis of thick cylindrical shells resting on two-parameter elastic supports. Journal of Sound and Vibration. 2008; 313: 655–75.

[32] Huang C.S., Yang P.J., Chang M.J. Three-dimensional vibration analyses of functionally graded material rectangular plates with through internal cracks. Composite Structures. 2012; 94(9): 2764–76.

[33] Santos H., Mota Soares C.M., Mota Soares C.A., Reddy J.N. A semi-analytical finite element model for the analysis of cylindrical shells made of functionally graded materials. Composite Structures. 2009; 91(4): 427–32.

[34] Qu Y.G., Meng G. Three-dimensional elasticity solution for vibration analysis of functionally graded hollow and solid bodies of revolution. Part I: Theory. European Journal of Mechanics – A/Solids. 2014; 44: 222–33.

[35] Qu Y.G., Meng G. Three-dimensional elasticity solution for vibration analysis of functionally graded hollow and solid bodies of revolution. Part II: Application. European Journal of Mechanics – A/Solids. 2014; 44: 234–48.

[36] Saada A.S. Elasticity: Theory and applications. 2nd ed. Florida: Ross Publishing, Inc; 2009.

[37] Shen H.S. Functionally graded materials: Nonlinear analysis of plates and shells. Florida: CRC Press; 2009.

[38] Li W.L. Vibration analysis of rectangular plates with general elastic boundary supports. Journal of Sound and Vibration. 2004; 273(3): 619–35.

[39] Beslin O., Nicolas J. A hierarchical functions set for predicting very high order plate bending modes with any boundary conditions. Journal of Sound and Vibration. 1997; 202(5): 633–55.

[40] Ye T.G., Jin G.Y., Shi S.X., Ma X.L. Three-dimensional free vibration analysis of thick cylindrical shells with general end conditions and resting on elastic foundations. International Journal of Mechanical Sciences. 2014; 84: 120–37.

[41] Jin G.Y., Su Z., Shi S.X., Ye T.G., Gao S.Y. Three-dimensional exact solution for the free vibration of arbitrarily thick functionally graded rectangular plates with general boundary conditions. Composite Structures. 2014; 108: 565–77.

[42] Su Z., Jin G.Y., Ye T.G. Three-dimensional vibration analysis of thick functionally graded conical, cylindrical shell and annular plate structures with arbitrary elastic restraints. Composite Structures. 2014; 118: 432–47.

[43] Jin G.Y., Su Z., Ye T.G., Jia X.Z. Three-dimensional vibration analysis of isotropic and orthotropic conical shells with elastic boundary restraints. International Journal of Mechanical Sciences. 2014; 89: 207–21.

Edited by Farzad Ebrahimi

Functionally graded materials (FGMs) were initially designed as thermal barrier materials for aerospace structures and fusion reactors and now they are also considered as potential structural materials for future high-speed spacecraft and recently are being increasingly considered in various applications to maximize strengths and integrities of many engineering structures. This book is a result of contributions of experts from international scientific community working in different aspects of FGMs and structures and reports on the state of the art research and development findings on this topic through original and innovative research studies. Through its six chapters the reader will have access to works related to processing, sintering properties and applications of functionally graded ceramics and new processing routes for FGMs while it introduces some specific applications, such as functionally graded annular fins and the high-performance self-lubricating ceramic composites with laminated graded structure. Besides, it presents an experimental crack propagation analysis of aluminum matrix FGMs and a unified accurate solution for three-dimensional vibration analysis of functionally graded plates and cylindrical shells with general boundary conditions.

IntechOpen